POSITIVE GAGING SYSTEM

FEASIBILITY STUDY

INTERIM REPORT

PERIOD, May 15, 1967 to November 15, 1967

Contract No. NAS 9-6751

Prepared for

NASA - MANNED SPACECRAFT CENTER
Houston, Texas

by

THE BENDIX CORPORATION
INSTRUMENTS & LIFE SUPPORT DIVISION
Davenport, Iowa

PUBLICATION NO. 3914.1-68-1
February 15, 1968

NASA CR 102062

TABLE OF CONTENTS

TABLE OF CONTENTS

LIST OF FIGURES

LIST OF FIGURES

LIST OF FIGURES

LIST OF TABLES

FOREWORD

This Interim Report was prepared by the Instruments and Life Support Division of the Bendix Corporation under Contract NAS 9-6751, "To Investigate and Design a Radio Frequency (RF) Mass Gaging Technique Independent of Gravity". The work was administered under the direction of the National Aeronautics and Space Administration Manned Spacecraft Center.

This report covers work conducted from May 15, 1967 to November 15, 1967.

Prepared by T. A. Loftus
T. A. Loftus
Project Engineer

Reviewed by R. E. Resh
R. E. Resh
Manager Fluid Measurements

D. A. Paustian
Administrative Engineer

Approved by N. F. Hosford
N. F. Hosford
Director of Engineering

Publication No. 3914.1-68-1

ABSTRACT

This report documents the work performed in a positive gaging system feasibility study. Three RF techniques of mass gaging were studied, both theoretically and experimentally, to determine their capability to gage the propellants, N_2O_4, Aerozine 50 and MMH, in Apollo or LEM spacecraft tanks.

The theoretical work predicts the response of each technique relative to the propellants and tanks. The experimental evaluation of this theory was performed using a scale model SPS tank, and a N_2O_4 simulant. A study was also made of the dielectric properties of the propellants over the expected range of operating conditions. Finally, a preliminary specification was made of the system's expected characteristics and components needed for the flight implementation of each of the techniques.

SECTION I

INTRODUCTION

The Bendix Corporation, Instruments & Life Support Division, respectively submits this Interim Report to the Manned Spacecraft Center (MSC) to document the progress made during the period May 15, 1967 to November 15, 1967, on NASA Contract NAS 9-6751, "To Investigate and Design a Radio Frequency (RF) Mass Gaging Technique Independent of Gravity". The work performed under this contract is based on the proposed program plan submitted as a portion of Bendix Publication No. 3564-66, Revision A, "Technical Proposal for Positive Gaging System Feasibility Study", Option A, as modified by letter dated February 3, 1967.

The work was divided into two phases within the proposed program. During the first phase, a theoretical analysis was performed detailing the measurement of fuel dielectric properties, and the performance of several RF Measurement Systems relative to a "worst" Apollo or LEM Spacecraft fuel and tank configuration. Experimental work was then conducted on a limited basis to verify the theoretical predictions or to evaluate measurement techniques. The experiments to determine system performance were performed using scale model SPS tanks, propellent simulants and laboratory type test hardware.

This report indicates that predictions of full-scale system performance can be made by scaling the results obtained from the model tank and simulated fuel study to the actual tank. The performance of the system with other fuels in the particular tank configuration is included to enable a choice of a best gaging technique for a particular tank and fuel combination.

During the second phase, an analysis was made of potential failure areas and their effect on the system performance. This analysis was of a limited scope because of the theoretical nature of this study. As such, it is concerned with only the major sources of failure predicted for a system component of a particular class or principle of operation.

Conclusions on the performance of a proposed RF gaging system based on the concepts investigated, and recommendations for design, development and future evaluation, are made in this report based on the results of the analysis and experiments conducted during the investigation.

SECTION II

PROGRAM OBJECTIVES

Performance requirements and design objectives for the propellant mass gaging system studied during this program were based on the design goals listed below:

a) The system will have a mass gaging accuracy of ± 0.5% of full scale, varying linearly to 0.25% of full scale at the 10% full condition maintaining 0.25% of full scale down to zero. The system's maximum response time (for a single measurement) will be 0.2 second and the system will have a resolution of ± 0.1% of full scale. This accuracy will be maintained under Zero "G" as well as normal gravity conditions, and under all filling and operating conditions.

b) The system will be compatible with Apollo or LEM propellants, which are N_2O_4-oxidizer, 50% UDMH/50% Hydrazine and MMH fuels.

c) The system will be designed to be capable of easy tank installation, requiring a minimum of modification in existing Apollo or LEM tank hardware.

d) The system accuracy will be maintained independent of tank pressure and fluid temperatures of 0 to 300 psia and +40 to +90°F respectively.

e) To make the system compatible with man-rated applications, the system will have a design goal of meeting the following vibration and acceleration requirements:

Vibration	Acceleration
0 - 14 cps @ 1 g	0 - 12 g's in any direction
14 - 40 cps @ 10 g's	
40 - 100 cps @ 20 g's	
100 - 2500 cps @ 40 g's	

Only an analysis showing compatability will be performed to show that these goals can be met. Testing of the prototypes will not be performed for this purpose.

f) The system will have a maximum weight of fifty (50) pounds, excluding interconnecting cables. Every effort will be made to reduce the system weight below fifty (50) pounds.

g) The system power requirements will be 28 volts DC, 1 ampere continuous and will be limited to 5-second,5-amp surges.

h) The system output will be parallel and serial binary signals.

i) The system will be adaptable to a variety of cylindrical and/or spherical tanks or other tank geometries as specified by the contracting agency. Where the proposed gaging technique does not satisfy these specified requirements, the effects of the deficiencies will be detailed.

j) The system will include the capability of providing mass gaging for up to four separate tanks.

Additional program objectives are covered in the proposal referenced in Section 1.

SECTION III

THEORETICAL STUDIES

3.1 INTRODUCTION

The operational theory of techniques used to measure propellant mass content in spacecraft tanks is covered in this section. Also included is a discussion of analytical techniques used to determine the electrical properties of spacecraft propellants. The mass gaging techniques that are investigated have as a common characteristic, excitation (by illumination) of the fuel or oxidizer tanks with energy in the RF region of the electro-magnetic spectrum. Each technique investigated, has been shown to have advantages and disadvantages for a particular fuel or oxidizer because the characteristic response of each proposed gaging system depends in a different way on the dielectric and loss tangent properties. Thus for a particular propellant, where one technique for mass measurement may show a poor sensitivity, another may have a good sensitivity. An understanding of these differences can be used to isolate techniques which give the best sensitivity for each fuel or oxidizer.

Also outlined in this section are the propellants and tank configurations considered in this study. The results of experiments that were performed to supplement the theoretical analysis and evaluate proposed gaging techniques are presented in Section IV.

3.2 PROPELLANT TANKS AND FUELS STUDIED

The propellant tanks studied were those used on the Apollo or LEM spacecraft. A particular tank configuration, that of the SPS tanks, was chosen as a "worst" type, containing the elements shown in Figure 3-1. The tank configuration was termed worst because of the presence of pipes, screens and the sump region, which electrically isolated regions of the tank. Another structure included as a possible tank element, was a bladder used for positive propellant expulsion. A representative portion of bladder material was obtained from the contracting agency for evaluation of its effect on the system performance.

The fluids to be used in the tanks were N_2O_4-oxidizer, 50% UDMH/50% Hydrazine and MMH fuels. Because of the handling problems associated with these fluids, the physical and electrical properties of these fluids were simulated using mixtures of hydrocarbon fluids. The simulant fluids were selected to have electrical properties similar to the actual fuels and oxidizer.

A tank operating region from 0 to 300 psia and $+40^0$ to $+90^0$F, was given by MSC as representative of the thermodynamic environment of the oxidizer and fuels. A pressure range of 1 ATM to 10^{-7} torr and temperatures of $+40^0$ to $+90^0$F, was taken as the environment in the equipment bay region.

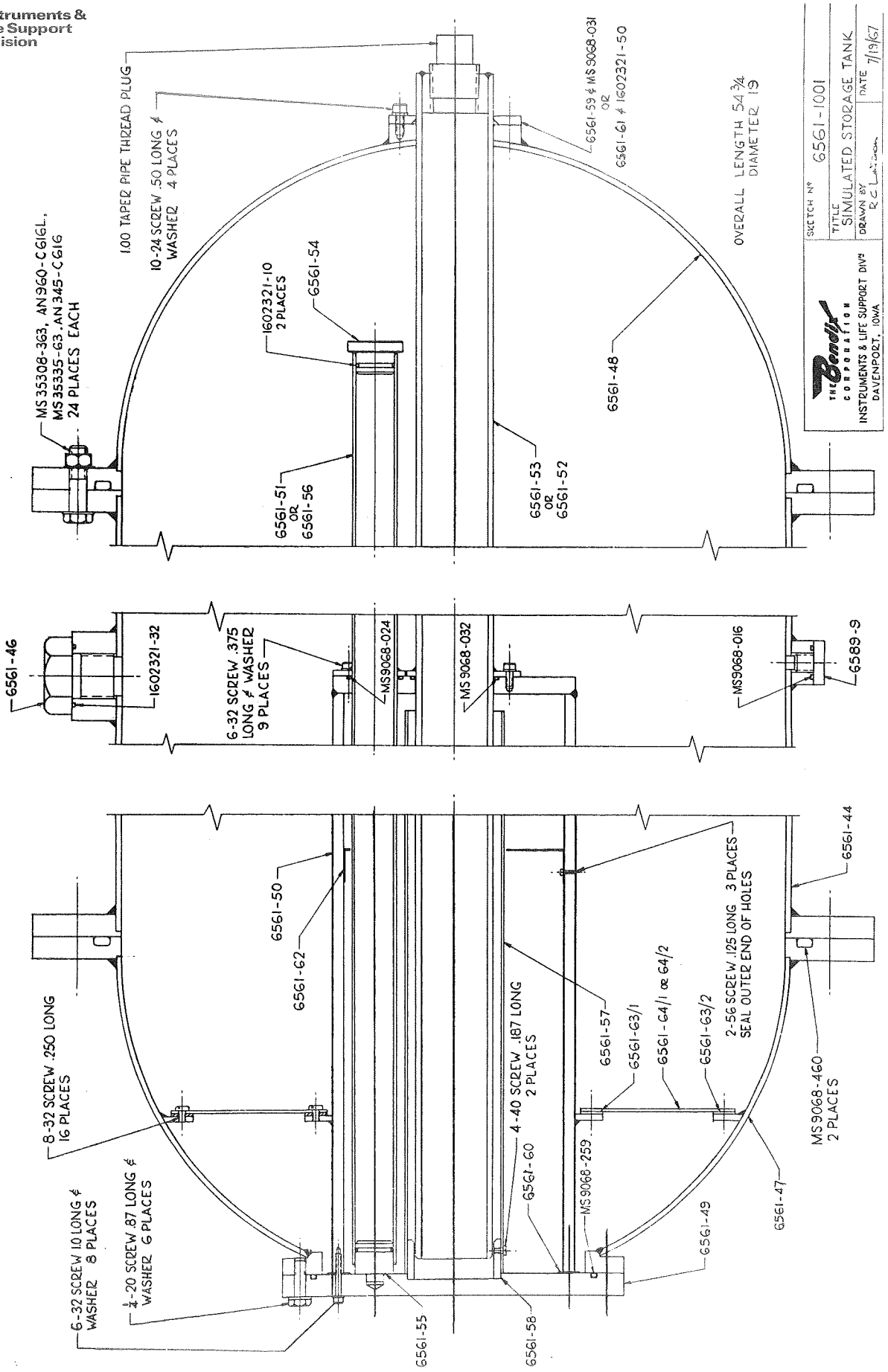
1.00 TAPER PIPE THREAD PLUG
10-24 SCREW .50 LONG ∉ WASHER 4 PLACES
MS 35308-363, AN960-C6I6L, MS 35335-63, AN 345-C6I6 24 PLACES EACH
1602321-10 2 PLACES
6561-54
6561-51 OR 6561-56
6561-53 OR 6561-52
6561-48
6561-59 ∉ MS 9068-031 OR 6561-61 ∉ 1602321-50
OVERALL LENGTH 54 3/4 DIAMETER 19
SKETCH Nº 6561-1001
TITLE SIMULATED STORAGE TANK
DRAWN BY R C Lamson
DATE 7/19/67
THE Bendix CORPORATION
INSTRUMENTS & LIFE SUPPORT DIV. DAVENPORT, IOWA
6561-46
1602321-32
6-32 SCREW .375 LONG ∉ WASHER 9 PLACES
MS9068-024
MS 9068-032
MS9068-016
6589-9
6561-50
6561-62
8-32 SCREW .250 LONG 16 PLACES
6561-44
6561-57
6561-63/1
6561-64/1 OR 64/2
6561-63/2
2-56 SCREW .125 LONG 3 PLACES SEAL OUTER END OF HOLES
4-40 SCREW .187 LONG 2 PLACES
6561-60
MS9068-259
MS9068-460 2 PLACES
6561-47
6561-49
6-32 SCREW .10 LONG ∉ WASHER 8 PLACES
¼-20 SCREW .87 LONG ∉ WASHER 6 PLACES
6561-55
6561-58

FIGURE 3-1

Vibration and acceleration were given as follows:

Vibration	Acceleration
0 - 14 cps @ 1 g	0 - 12 g's in any direction
14 - 40 cps @ 10 g's	
40 - 100 cps @ 20 g's	
100 - 2500 cps @ 40 g's	

The fluid mass influx or outflux conditions in the tank were given as those present for all filling and operating conditions. These were taken as a maximum of 0.5% of full tank mass change in 0.2 second to agree with the accuracy and time response goals.

3.3 PROPELLANT PROPERTIES STUDY

Because the sensitivity of the mass gaging techniques depends on the dielectric constant and loss tangent of the propellants, a knowledge of these propellant properties over the frequency and environmental range of interest was vital to this study. This section details the thorough effort that was made to either locate available information or to measure these dielectric properties.

3.3.1 Literature Search

A search was made of all available technical information concerning the properties of Nitrogen Tetroxide, Aerozine 50 and Monomethyl Hydrazine. The main sources of physical and chemical properties were the reports by the Aerojet Corporation[1] and the Bell Aerospace Report[2] but these did not contain information concerning the electrical properties. In this field, the only published work of value was authored by G. A. Burns and C. J. Meierbachtol[3], who measured the electrical properties of these fluids, at frequencies of approximately 100 MHz and 600 MHz. An extract from their report is shown in Table 3-1. Helix Research, Inc. (Burns and Meierbachtol) were employed as consultants by Bendix, Instruments & Life Support Division to theoretically investigate the equivalent electrical properties of the fluids at frequencies in the range of 500 MHz to 4 GHz. An extract of this information is shown in Table 3-2. These results are for liquids under atmospheric pressure. There is a variation of dielectric constant and loss tangent with pressure as well as temperature, and the results should be plotted as a variation of polarizability.

3.3.2 Electrical Properties as a Function of Frequency and Temperature

In the discussion that follows, equations are presented without proof in the interest of brevity. Debye[8] derived the following equations based on the assumption that dipole equilibrium, when an external field is removed, is attained exponentially with time,

$$\varepsilon' = \varepsilon_o + \frac{\varepsilon_o - \varepsilon_\infty}{1 + (\lambda_m/\lambda_o)^2} \qquad (3.1)$$

$$\varepsilon'' = \frac{(\varepsilon_o - \varepsilon_\infty)\ (\lambda_m/\lambda_o)}{1 + (\lambda_m/\lambda_o)^2} \qquad (3.2)$$

where: ε' and ε'' = respectively the real and imaginary parts of complex relative dielectric constant (i.e., $\varepsilon^* = \varepsilon' - i\varepsilon''$)

ε_o = the static dielectric constant

ε_∞ = the value which is asymptotically approached by ε' at wavelengths sufficiently shorter than λ_m to make ε'' relatively small

λ_m = the wavelength corresponding to the lowest resonance absorption frequency in the material in question

λ_o = the wavelength of the incident radiation.

TABLE 3-I

MEASURED DIELECTRIC PROPERTIES OF PROPELLANTS

MATERIAL	FREQUENCY MH_z	TEMPERATURE ^oF	DIELECTRIC CONSTANT	LOSS TANGENT
Aerozine 50	19.69	30	25.79	0.136
	22.55	90	19.66	0.154
	23.90	150	17.51	0.226
	81.84	30	23.89	0.0393
	87.14	90	21.07	0.0463
	107.68	150	13.80	0.0524
MMH	19.88	-30	25.3	0.0247
	22.17	30	20.34	0.0517
	24.21	90	17.06	0.0817
	27.10	150	13.62	0.1066
	78.18	-30	26.18	0.0349
	85.87	+30	21.70	0.0298
	96.03	90	17.35	0.0328
	106.26	150	14.17	0.0468
N_2O_4	63.76	30	2.46	0.00419
	64.96	60	2.37	0.00297
	256.60	30	2.43	0.00259
	258.20	60	2.40	0.00209

TABLE 3-2

EXTRAPOLATED ELECTRICAL PROPERTIES OF PROPELLANTS FROM 0.5 TO 4 GHz

MATERIAL	FREQUENCY	TEMPERATURE °F	DIELECTRIC CONSTANT	LOSS TANGENT
Aerozine 50	500 MH_z	40	24.36	.0220
	500 MH_z	90	20.36	.0332
	1 GH_z	40	23.96	.0178
	1 GH_z	90	20.30	.0256
	4 GH_z	40	23.72	.0130
	4 GH_z	90	20.26	.0164
MMH	500 MH_z	40	21.00	.0232
	500 MH_z	90	17.48	.0281
	1 GH_z	40	21.24	.0176
	1 GH_z	90	17.78	.0206
	4 GH_z	60	21.76	.0133
	4 GH_z	90	18.08	.0152
N_2O_4	500 MH_z	40	2.428	.00207
	500 MH_z	90	2.368	.00155
	1 GH_z	60	2.434	.00174
	1 GH_z	90	2.384	.00134
	4 GH_z	60	2.442	.00125
	6 GH_z	90	2.618	.00107

The values for ε_o and ε_∞ may be expressed by Debye form of the Clausius-Mossotti equation:

$$\frac{\varepsilon_o - 1}{\varepsilon_o + 2} \frac{M}{\rho} = \frac{4\pi N}{3} \left(\alpha_o + \frac{\mu^2}{3kT}\right) \qquad (3.3)$$

$$\frac{\varepsilon_\infty - 1}{\varepsilon_\infty + 2} \frac{M}{\rho} = \frac{4\,N}{3} \alpha_o \qquad (3.4)$$

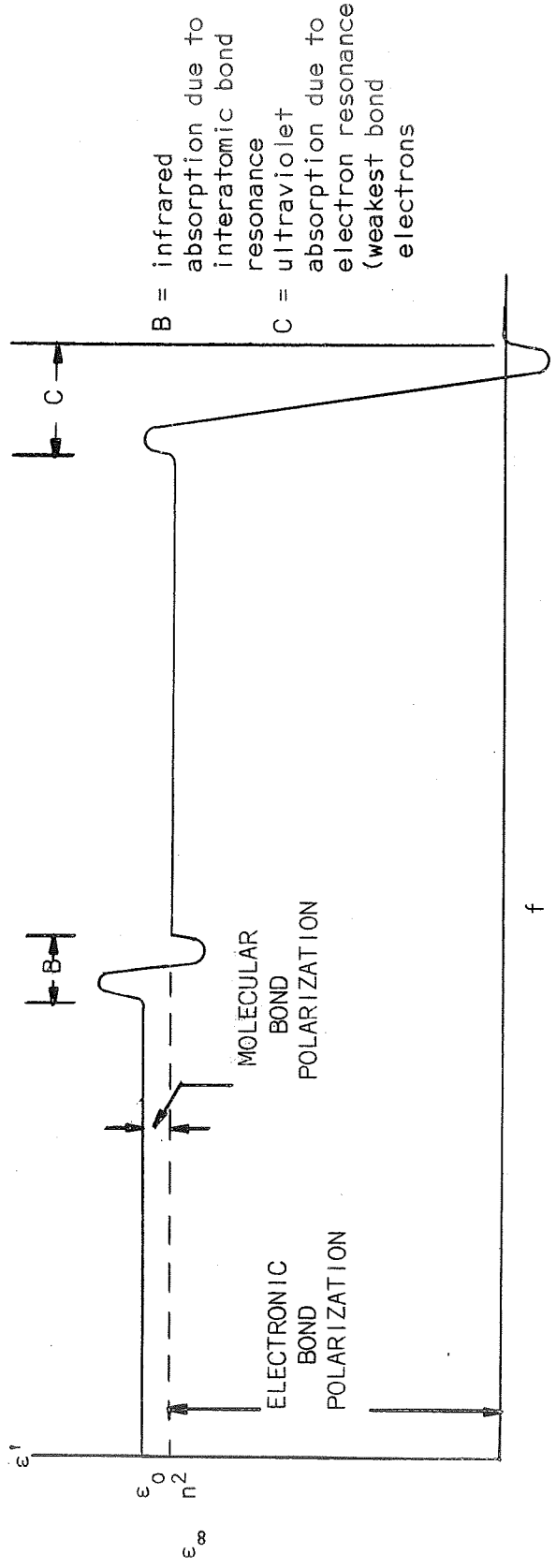

IDEALIZED ε' VERSUS FREQUENCY GRAPH
FOR A NON-POLAR TRANSPARENT MATERIAL

FIGURE 3-2

where: α_o = the polarizability due to bond distortion and $\frac{\mu^2}{3kT}$ is polarizability due to dipole orientation
μ = the permanent dipole moment
N = Avagadro's number
k = Boltzman's constant
T = the temperature in degrees Kelvin
M = molecular weight
ρ = density

Two cases may be considered:

a) Non-Polar Materials (Materials whose molecules do not contain permanent dipoles). In this case $\mu = 0$ and Equations 3.3 and 3.4 result in $\varepsilon_o = \varepsilon_\infty$. Here the lowest resonance absorption frequency falls in the infrared region and is due to molecular bond oscillations as shown in Figure 3-2.

When such is the case, ε_∞ may be set equal to the square of the index of refraction n^2, in Equations 3.1 and 3.2. It may be seen from Equations 3.1 and 3.2 that the variation of ε' and ε'' due to changes in temperature and pressure are due only to the fact that ρ is a function of T and p. Coefficients of thermal expansion and compressibility may be found in the literature.

b) Polar Materials (Materials whose molecules contain permanent dipoles) In this case the lowest absorption frequency falls in the microwave region and is due to dipole orientation in the external field as shown in Figure 3-3. Under this condition Equations 3.3 and 3.4 hold as they are written. A problem arises in evaluating ε_∞, however, since generally α_o is not known. The best solution is to directly measure it at frequencies sufficiently high to insure that the condition in the definition of ε_∞ following Equation 3.2 is met. Other methods might be to measure ε_o in the solid state where the permanent dipoles are effectively "frozen in", and do not contribute to the polarization or, measure ε_o at sufficiently high temperatures to insure cancellation of dipole orientation in the external field by the tendency toward random orientation due to thermal motion.

It may be seen from Equation 3.3 that when a permanent dipole exists, the portion of the polarization due to dipole orientation is an inverse function of the temperature. Solving Equation 3.3 for λ_m^2, we have:

$$\lambda_m^2 = \lambda_o^2 \left(\frac{\varepsilon_o - \varepsilon'}{\varepsilon' - \varepsilon_\infty} \right) \qquad (3.5)$$

Even when ε_o and ε_∞ are known either from Equations 3.3 and 3.4, or from experiment, ε' is still some unknown function of temperature. Therefore, even if ε' were known for the entire radio frequency spectrum at a given temperature, the value of λ_m at some new temperature cannot be predicted without at least one measurement of ε' at the new temperature.

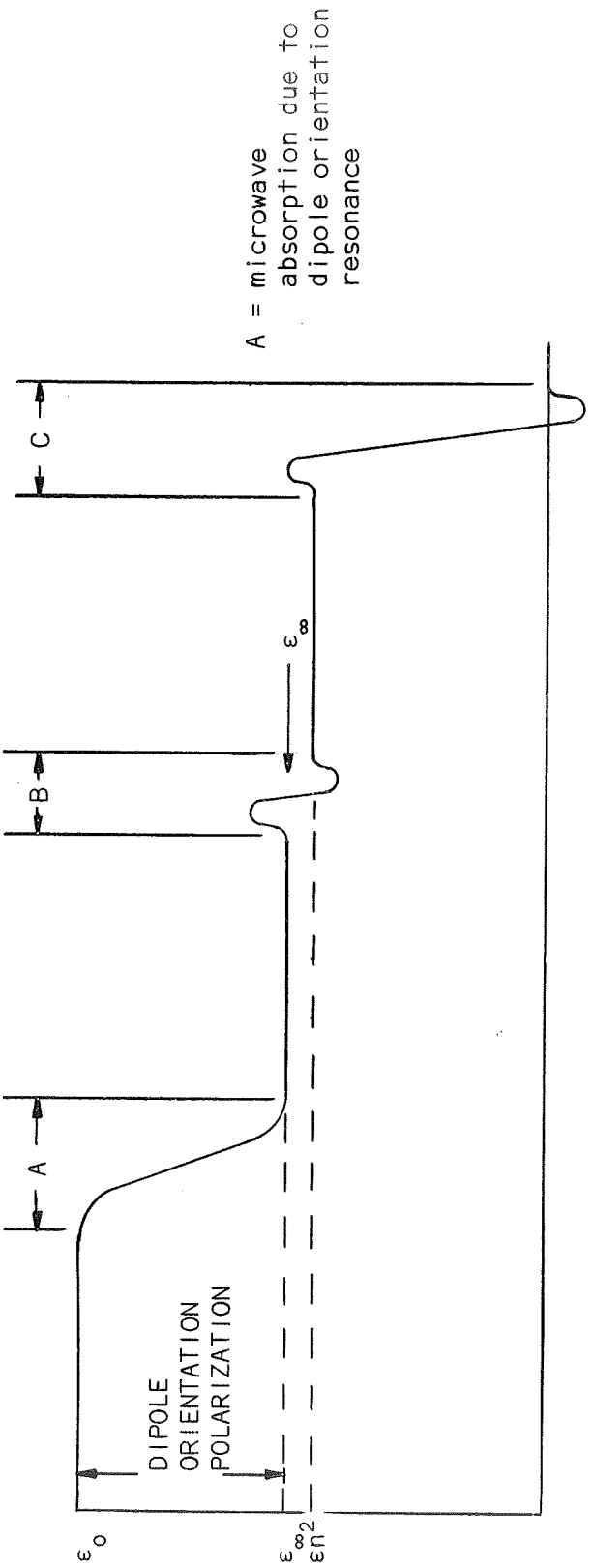

IDEALIZED ε' VERSUS FREQUENCY GRAPH FOR A POLAR TRANSPARENT MATERIAL

FIGURE 3-3

3.3.3 Simulation of Electrical Properties of Propellants

It is desirable to be able to approximate the dielectric constant and loss tangent of certain propellants by room-temperature mixtures that eliminate handling problems. They may be done by mixing a polar liquid (high dielectric constant) with a nonpolar liquid (relatively low dielectric constant). By choosing proper proportions in the mixture, temperature and frequency, almost any desired combination of dielectric constant, ε' and loss tangent may be obtained, provided they fall somewhere between the values of the constituent liquids.

Equations 3.3 and 3.4 may be rewritten for such mixtures as:

$$\frac{\varepsilon_o - 1}{\varepsilon_o + 2} = \frac{4\pi N}{3}\left(C_1\alpha_1 + \frac{C_1\mu_1^2}{3kT} + C_2\alpha_2\right) \qquad (3.6)$$

$$\frac{\varepsilon_\infty - 1}{\varepsilon_\infty + 2} = \frac{4\pi N}{3}\left(C_1\alpha_1 + C_2\alpha_2\right) \qquad (3.7)$$

where C_1 and C_2 are the mole fractions (moles per unit volume) of the polar and nonpolar liquids respectively.

It may be shown that Equations 3.1 and 3.2 may be modified for such a case as:

$$\varepsilon' = \varepsilon_\infty + \frac{4\pi C\, N^2}{27\, kT} \cdot \frac{(\varepsilon_o + 2)(\varepsilon_o + 2)}{1 + \dfrac{\lambda_m^2 (\varepsilon_o + 2)^2}{\lambda_o^2 (\varepsilon_o + 2)^2}} \qquad (3.8)$$

$$\varepsilon'' = \frac{4\pi C\, N^2}{27\, kT} \cdot \frac{(\varepsilon_o + 2)(\varepsilon_\infty + 2)}{1 + \dfrac{\lambda_m^2 (\varepsilon_o + 2)^2}{\lambda_o^2 (\varepsilon_\infty + 2)^2}} \qquad (3.9)$$

where C is the concentration of the polar solute in moles per unit volume.

It must be noted that the above equations were derived without regard to so-called "Solvent Effect". This effect accounts for the measured differences in the values for dipole moments in gases and in solution. The difference is caused by the interaction of the fields of permanent dipoles and by the induction of dipoles in nonpolar molecules due to fields of nearby permanent dipoles.

In Equations 3.3, 3.4, 3.6 and 3.7 values for α and μ should be regarded as average microscopic values at the temperature and concentration in question. Thus, the previous assumption that these values are constant is true only for a given mixture. Because of solvent effect, Equations 3.8 and 3.9 are accurate only for dilute solutions of polar solutes in nonpolar solvents. In more concentrated solutions, the equations can only provide approximate porportions to begin experimental mixing to achieve specific values.

It can be shown that from Equations 3.8 and 3.9, a plot of ε'' against ε' gives a semicircle with ε_o and ε_∞ as opposite ends of a diameter on the ε' axis, when the temperature and pressure are held constant. Since a circle is defined by three points, three measurements of ε' and ε'' at relatively wide frequency spacing should be enough to define the whole variation of ε' and ε'' with frequency. Experimentally, difficulty is found usually because the measurement techniques may have to be different for each of these frequencies.

3.3.4 Methods of Measurement of Dielectric Constant and Loss Tangent

The wide variation of the electrical parameters of materials used in microwave work, together with the wide frequency range of the microwave spectrum, means that there can be no one method of measurement of these parameters. Usually, methods are chosen from a knowledge of the frequency at which the parameters are wanted, and estimated values of the parameters. If the parameters are then different from the estimate, the measurement will not work, but a closer guess can then be made to the values of the parameters, and a better method chosen.

The initial method of measurement decided upon was a transmission-type resonant cavity technique, whereby the resonant frequency and the Q of a given mode are measured when the cavity is empty and when it is filled with the fluid. This method is suitable for low dielectric constant material, and for low loss materials. For high dielectric constants, very little power enters the material because of the large impedance mismatch at the input probe, and for high loss tangents the material absorbs almost all of the power which enters it. Thus, in these cases, the resonance cannot be seen clearly enough without special apparatus. As will be seen from Paragraph 4.2.1, Section IV, when this method was tried with N_2O_4 and MMH, no appreciable power transmission could be obtained with the cavities used, and this indicated either a high dielectric constant or a high loss tangent for the propellants.

A variation on this method is the use, not of the liquids themselves, but of mixtures of the fluid with relatively lossless liquids. From the known volume ratio, the value for an undiluted solution can be found by extrapolation. This method was tried in the laboratories with Methyl Alcohol diluted with Benzene. As can be seen from Paragraph 4.2.2, Section IV, the alcohol was so lossy that only concentrations of a few percent of alcohol could be measured. This would mean that extrapolation to 100% would be very inaccurate. Because of this,

it was decided to abandon this method. Next, the Roberts-Von Hippel method was tried. This has been used successfully in the laboratory to measure Methyl Alcohol, which indicates that it could probably be used to measure Aerozine-50 and MMH, successfully. Another method has been studied which uses small samples of the fluid to perturb the resonant frequency and Q of a cavity. This is a useful method for measuring fluids with large dielectric constant and loss tangents.

The resonant cavity method is one of the most standard methods of measuring the dielectric properties of fluids with reasonable electrical characteristics. Usually, a cylindrical cavity is made from low loss material, and a particular mode, or set of modes is chosen for study. One or two probes are placed in suitable positions in the cavity, and with a swept signal generator and an oscilloscope, the modes are examined. The apparatus may be set up as either Figure 3-4 or 3-5. The method is quite standard, and may be found in most textbooks,[4] for example, "Techniques Of Microwave Measurement" by C. G. Montgomery[4], but a short outline now follows. A resonant cavity is made so that a particular mode has a resonant frequency given by:

$$F \simeq F_o \sqrt{\varepsilon}$$

where F_o is the frequency around which the parameters are to be measured, and ε is a rough guess of the dielectric constant. Two holes are drilled in the cavity to take small probes. The hole positions and probe types are chosen for suitable coupling to the mode. Then, with apparatus such as that shown in Figure 3-4 or 3-5, the mode is examined. The probes are either reduced in size, or, in the case of loop antennas, rotated, until the width of the resonance at the half power points, does not decrease further. The resonant frequency F_1 and the Q of the resonance are then measured. The cavity is then filled with the fluid, and the experiment repeated, giving a resonant frequency F_2 and a Q, Q_2. Then the dielectric constant ε of the liquid is given by:

$$\varepsilon = \left(\frac{F_1}{F_2} \right)^2 \qquad (3.10)$$

The Q's are given by:

$$\frac{1}{Q_1} = \frac{1}{Q_{w(F_1)}}$$

$$\frac{1}{Q_2} = \frac{1}{Q_{w(F_2)}} + \frac{1}{Q_{d(F_2)}}$$

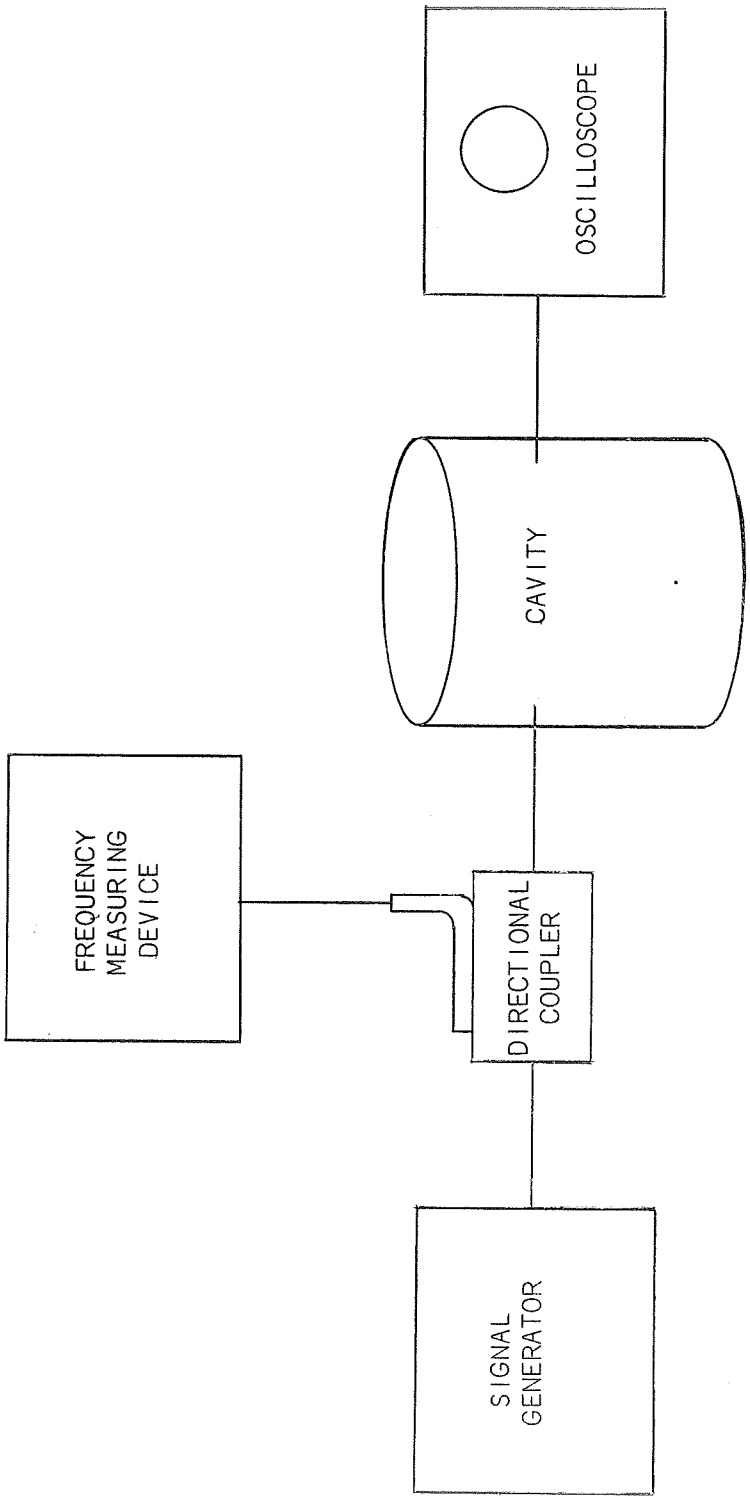

DIELECTRIC MEASUREMENT USING RESONANT CAVITY AND TRANSMITTED POWER TECHNIQUE

FIGURE 3-4

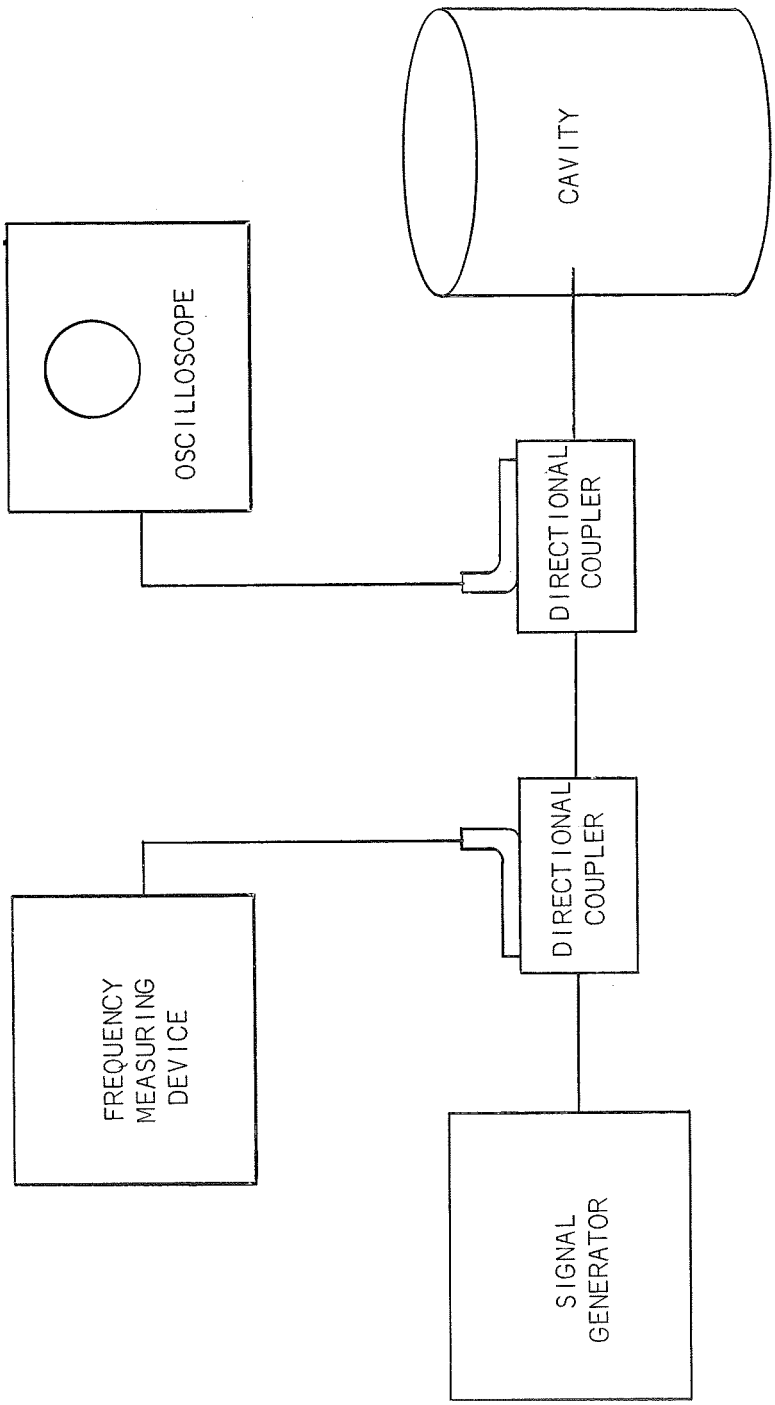

DIELECTRIC MEASUREMENT USING RESONANT CAVITY AND REFLECTED POWER TECHNIQUE

FIGURE 3-5

where: $Q_{w(F_1)}$ = the Q of the walls of the cavity at frequency F_1

$Q_{w(F_2)}$ = the Q of the walls of the cavity at frequency F_2

$Q_{d(F_2)}$ = the Q of the dielectric at frequency F_2

Now:

$$Q_{w(F)} \propto \sqrt{\left(\frac{\sigma}{F}\right)}$$

where σ = the electrical conductivity of the metal walls

Then:

$$Q_{w(F)} \propto \sqrt{\frac{1}{F}}$$

Thus:

$$Q_{w(F_1)} \propto (\sqrt{F_1})^{-1}$$

and:

$$Q_{w(F_2)} \propto (\sqrt{F_2})^{-1}$$

Therefore:

$$Q_w^{-1}(F_2) = Q_w^{-1}(F_1)\sqrt{F_2F_1^{-1}}$$

$$= Q_1^{-1}\sqrt{F_2F_1^{-1}}$$

$$= \varepsilon^{-1/4} Q_1^{-1}$$

Therefore:

$$Q_2^{-1} = \varepsilon^{-1/4} Q_1^{-1} + Q_d^{-1}(F_2)$$

Q_d of the dielectric is related to the loss tangent by:

$$Q_d^{-1} \equiv \tan \delta$$

Therefore:

$$Q_2^{-1} = \varepsilon^{-1/4} Q_1^{-1} + \tan \delta$$

Thus:

$$\tan \delta = Q_2^{-1} - \varepsilon^{-1/4} Q_1^{-1} \qquad (3.11)$$

Thus, Equations 3.10 and 3.11 give the dielectric constant and the loss tangent of the dielectric material.

For greater accuracy, the Q of the probe, or probes, may be taken into account by using slotted line techniques. The slotted line is inserted before the input probe, and the impedance of the probe is measured versus frequency as the resonance is passed through. This impedance is plotted on a Smith Chart, and from this, the Q of the probe may be separated from the Q of the cavity. For the two probe method, the second probe is terminated in a matched load while the measurement is made, and then the process is repeated with the other probe as an input probe, while the first is terminated in a matched load. By this method, the Q of the probe or probes, may be found. These Q's are measured, both when the cavity is full, and when it is empty, and they are subtracted from the measured Q's, Q_2 and Q_1, to give more accurate values of Q_2 and Q_1. Three small cylindrical cavities were made, of different dimensions, to cover the frequency range from 2 to 8 GHz. A computer program was run to find the resonant frequencies of all of the lower order modes of the cavities. It was intended to consider the effect of the fluids on a selected few of these modes. The modes and their respective frequencies are given on Table 3-3.

For lossy liquids, measurements may be made by mixing the liquids with a less lossy liquid, and measuring the final result. By repeating the measurements with various concentrations, the actual value of the parameters may be obtained by extrapolation.

A second method that of Von Hippel is probably the most versatile method of dielectric measurement. Based on a paper by Roberts and Von Hippel[5], the method utilized the measurement of impedance at the surface of the liquid when placed at the end of a short-circuited waveguide. The apparatus is shown in Figure 3-6. By measuring the voltage standing wave ratio (VSWR), and position of the minimum of the standing wave pattern, the surface impedance may be calculated. From this, and the known thickness of liquid, the dielectric constant and loss tangent of the liquid may be calculated as follows:

Suppose the liquid thickness is d cm, and the characteristic impedance of the waveguide is Z_o. Then the impedance at the surface of the liquid is given by:

$$Z_s = Z_o' \tanh \delta d$$

where: Z_o' = the characteristic impedance of the waveguide filled with liquid
δ = the propagation constant in the liquid

Now by definition:

$$Z_o = \frac{j\omega\mu_o}{\delta_o}$$

$$= \frac{j\omega\mu_o}{j\,\beta_o}$$

$$= \frac{\omega\mu_o}{\beta_o}$$

TABLE 3-3

COMPUTED RESONANT FREQUENCIES OF THREE TEST CAVITIES

CAVITY	MODE TYPE	RESONANT FREQUENCY (GHz) EMPTY
5.906" high by 2.954" diameter	TE_{111}	2.551
	TM_{010}	3.065
	TE_{112}	3.084
	TM_{011}	3.224
	TM_{012}	3.661
	TE_{113}	3.811
	TE_{211}	4.019
	TM_{013}	4.291
	TE_{212}	4.377
	TE_{114}	4.640
3.704" high by 2.954" diameter	TM_{010}	3.065
	TE_{111}	3.084
	TM_{011}	3.661
	TE_{211}	4.377
	TE_{112}	4.640
	TM_{110}	4.883
	TM_{012}	5.042
	TM_{111}	5.278
	TE_{011}	5.278
	TE_{212}	5.584
1.476" high by 1.476" diameter	TM_{010}	6.130
	TE_{111}	6.168
	TM_{011}	7.321
	TE_{211}	8.753
	TE_{112}	9.321
	TM_{110}	9.767
	TM_{012}	10.081
	TE_{011}	10.555
	TM_{111}	10.555
	TE_{212}	11.306

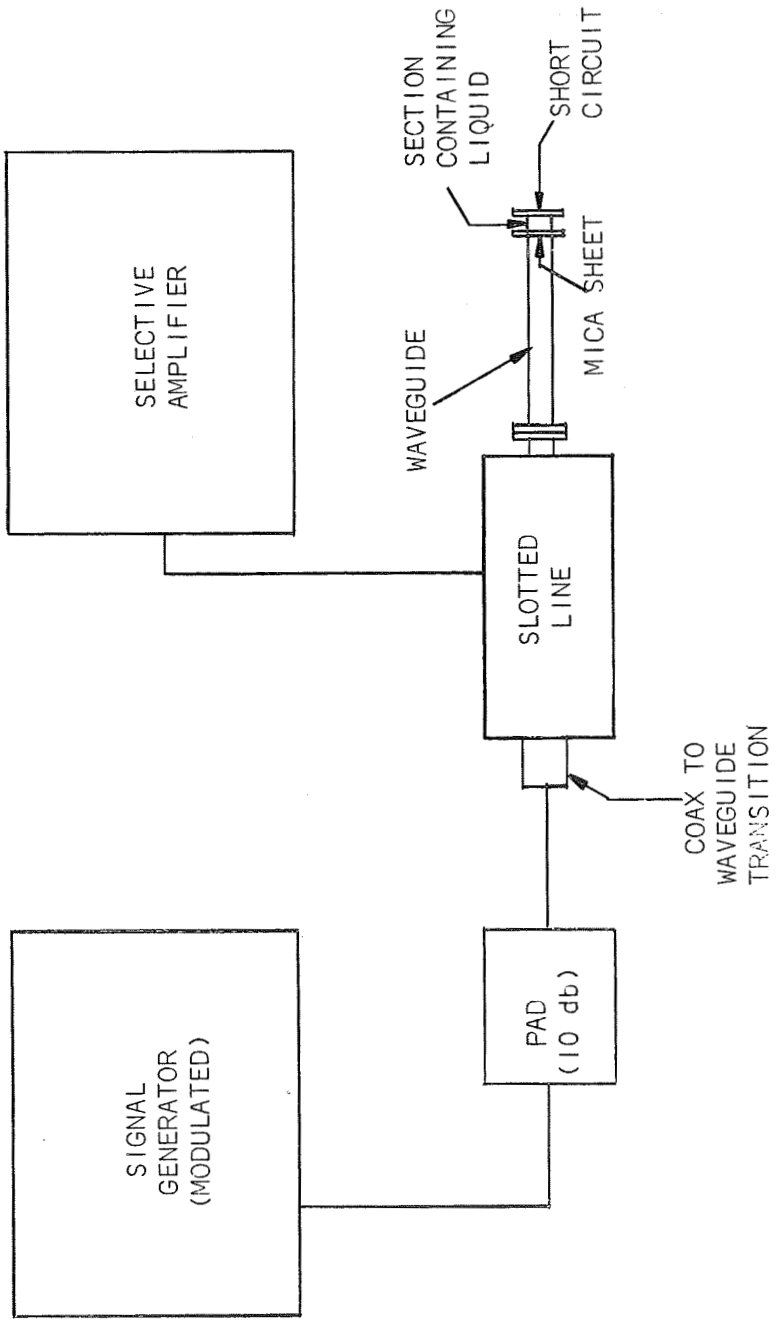

APPARATUS FOR ROBERTS-VON HIPPEL METHOD

FIGURE 3-6

where: ω = the radian frequency
δ_o = the propagation constant in air
= $j\beta_o$ for no loss, where β_o is the phase change per cm in air
μ_o = the permeability of free space.

Also:

$$Z_o' = \frac{j\omega\mu}{\delta}$$

$$= \frac{j\omega\mu_o}{\delta}$$

for non-magnetic liquids.

Therefore:

$$Z_o' Z_o^{-1} = j\beta_o\delta^{-1}$$

Therefore:

$$Z_s = Z_o' \tanh \delta d$$

$$= Z_o \frac{j\beta_o}{\delta} \tanh \delta d$$

This is the impedance at the surface of the liquid. The impedance at the minimum position is given by:

$$S^{-1} = (Z_s Z_o^{-1} + j \tan \beta_o X_o)(1 + jZ_s Z_o^{-1} \tan \beta_o X_o)^{-1}$$

Where S is the VSWR, and X_o is the distance from liquid surface to the minimum position.

This last equation may be written:

$$Z_s Z_o^{-1} = (S^{-1} - j \tan \beta_o X_o)(1 - j S^{-1} \tan \beta_o X_o)^{-1}$$

Substituting for $Z_s Z_o^{-1}$ gives:

$$j\beta_o\delta^{-1} \tanh \delta d = (S^{-1} - j \tan \beta_o X_o)(1 - j S^{-1} \tan \beta_o X_o)$$

or:

$$(\delta d)^{-1} \tanh \delta d = (j\beta_o d)^{-1} (S^{-1} - j \tan \beta_o X_o)(1 - j S^{-1} \tan \beta_o X_o)$$

or putting $\beta_o = 2\pi\lambda g^{-1}$ where λ_g = guide wavelength.

$$(\delta d)^{-1} \tanh \delta d = -j\lambda_g (2\pi d)^{-1} (S^{-1} - j \tan 2\pi X_o \lambda_g^{-1}) \ldots$$

$$(1 - jS^{-1} \tan 2\pi X_o \lambda_g^{-1}) \qquad (3.12)$$

Given the minimum position X_o, and VSWR(S) means that the right-hand side of the equation can be computed. It is a complex number, and solutions to the resulting complex equation may be found from graphs in Von Hippel's book.[6] Thus, δd is known, and since d is known, so is δ. This is resolved into its real and imaginary parts, α and β. Then the dielectric constant and loss tangent are found from the wave guide equations.

$$\varepsilon\,\varepsilon = [(2\,\pi_c^{-1})^2 + \beta^2 - \alpha^2]\,(2\pi\lambda_c^{-1})^{-2} \qquad (3.13)$$

$$\tan\delta = 2\alpha\beta[(2\pi\lambda_c^{-1})^2 + \beta^2 - \alpha^2]^{-1} \qquad (3.14)$$

where: λ_c is the cutoff wavelength of the wave guide.

These are the general equations to find the dielectric constant, and loss tangent. For relatively low loss material, Equation 3.12 can be simplified by assuming S tends to infinity, i.e., 1/S is very small. Then:

$$\frac{\tanh\ \delta d}{\delta d} = -j\,\frac{\lambda_g}{2\pi d}\left(\frac{1}{S} - j\tan\frac{2\pi X_o}{\lambda_g}\right)\left(1 + j\left(\frac{1}{S}\right)\tan\frac{2\pi X_o}{\lambda_g}\right)$$

$$= -j\,\frac{\lambda_g}{2\pi d}\left(\frac{1}{S} - j\tan\frac{2\pi X_o}{\lambda_g} + \frac{1}{S}\tan^2\frac{2\pi X_o}{\lambda_g}\right)$$

where terms of the order of $(1/S)^2$ and above have been ignored.

Expanding tanh δd into real and imaginary parts gives:

$$\frac{\tanh\ \delta d}{\delta d} = \frac{\tan\alpha d + j\tan\ \beta d}{1 + j\tanh\alpha d\tan\beta d}\cdot\frac{1}{d\,(\alpha + j\beta)}$$

Taking δ small gives:

$$\frac{\tanh\ \delta d}{\delta d} = (\alpha d + j\tan\beta d)\,(1 - j\,\alpha d\tan\beta d)\left(\frac{\alpha - j\beta}{\beta^2 d}\right)$$

Substituting in the previous equation gives:

$$\frac{(\alpha - j\beta)\,(\alpha d + j\tan\beta d)\,(1 - j\alpha\, d\tan\beta d)}{\beta^2 d}$$

$$= -\,j\,\frac{\lambda_g}{2\pi d}\left(\frac{1}{S}\sec^2\frac{2\pi X_o}{\lambda_g} - j\tan\frac{2\pi X_o}{\lambda_g}\right)$$

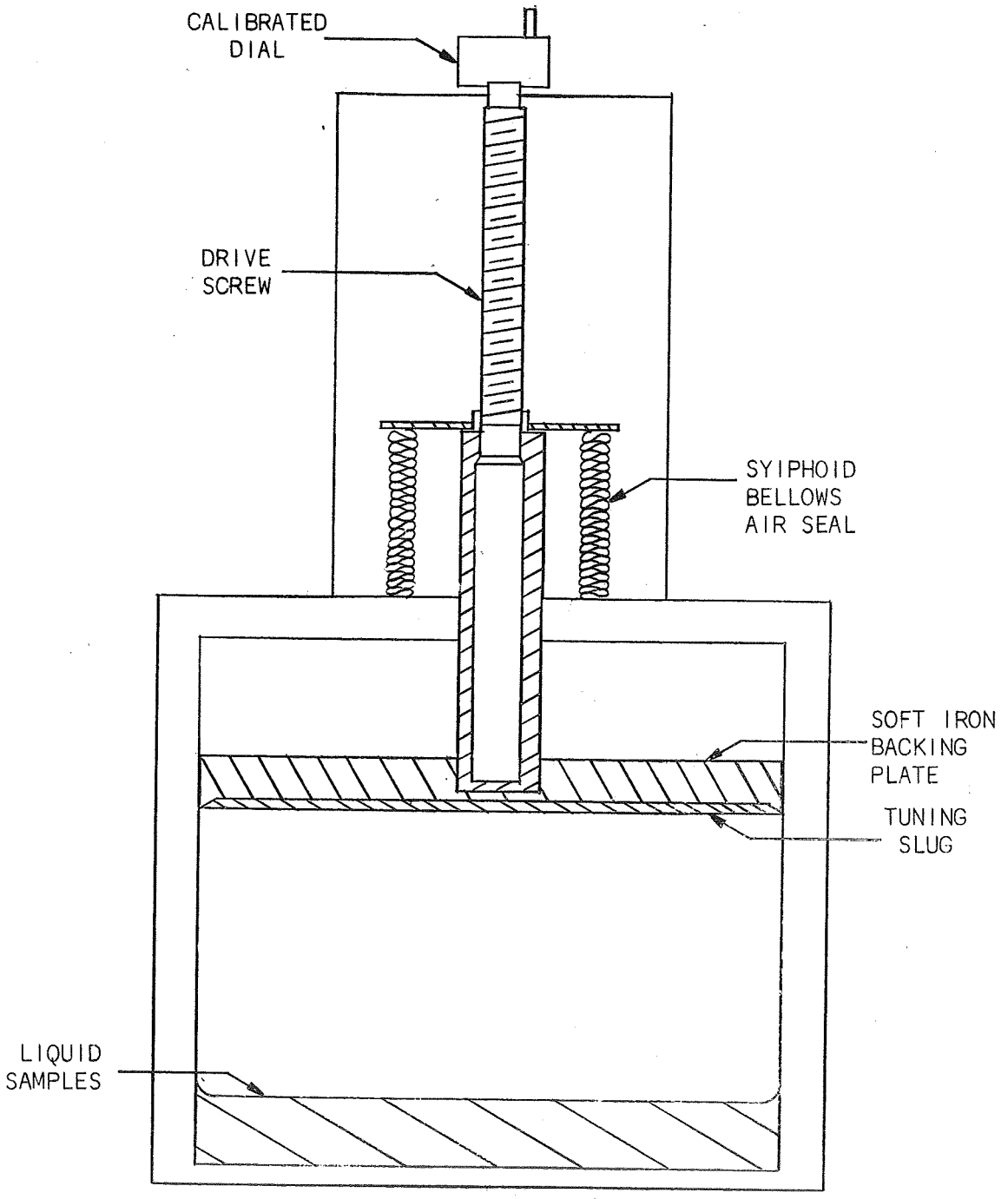

TE_{011} MODE RESONANT STRUCTURE
FOR DIELECTRIC MEASUREMENT

FIGURE 3-7

Equating real parts gives:

$$\frac{\tan \beta d}{\beta d} = - \frac{\lambda_g}{2\pi d} \tan \frac{2\pi X_o}{\lambda_g} \qquad (3.15)$$

Equating imaginary parts gives:

$$\alpha \frac{(\tan \beta d - \beta d \sec^2 \beta d)}{\beta^2 d} = - \frac{\lambda_g}{2\pi d} \frac{1}{S} \sec^2 \frac{2\pi X_o}{\lambda_g} \qquad (3.16)$$

Equations 3.15 and 3.16 give α and β, without the use of tables, for use with Equations 3.13 and 3.14.

A third technique of measuring dielectric properties of fluids is the resonant-cavity perturbation method. It has been well established by a number of authors that the resonant frequency of a cavity mode depends in a simple way upon the real part of the complex dielectric constant of the material within the cavity and the Q of the resonant cavity is simply related to the imaginary part of the complex dielectric constant. Generally, the mode selected for performing these measurements is the dominant mode in the particular structure. In this case, the task is to determine the complex dielectric constants of several liquids over a frequency range covering 100 MHz to 10 GHz. Clearly, a single resonant structure will not be able to tune to resonance over the entire frequency band of interest, so it will be necessary to construct several structures to perform the necessary measurements. To minimize the number of structures required, it is desired to make each structure tune over the widest possible frequency band. This is one fundamental consideration in the specification of the structure to be used in performing the measurements. A second basic factor to consider is the ease of tuning the resonator structure. Tuning should be accomplished with little expenditure of time, good precision, and repeatability. A third factor to be considered is the amount of effort required to prepare and mount the sample in the structure to facilitate the measurements.

At the lower end of the frequency range of interest, frequencies below 2 GHz, coaxial resonators can be used. At such frequencies rectangular or cylindrical cavity resonators become too large to be practical. The emphasis in this discussion will be on specification of the resonant structures which can be used to measure the complex dielectric constants of liquids at frequencies above 2 GHz.

After careful consideration, it becomes apparent that a circular cylindrical resonator operating in the TE_{011} mode will satisfy most of the restrictions placed upon the resonator in preceding paragraphs. A structure supporting this mode is tunable because the fields are characterized by a half-sine-wave spatial variation along the axis of revolution. Tuning can be easily and quickly accomplished by screwing a metal slug, which serves as one end wall of the resonant structure, into and out of the resonator. The liquid sample could be placed over the fixed end wall to some depth. A sketch of this structure is shown in Figure 3-7, and the fields in Figure 3-8.

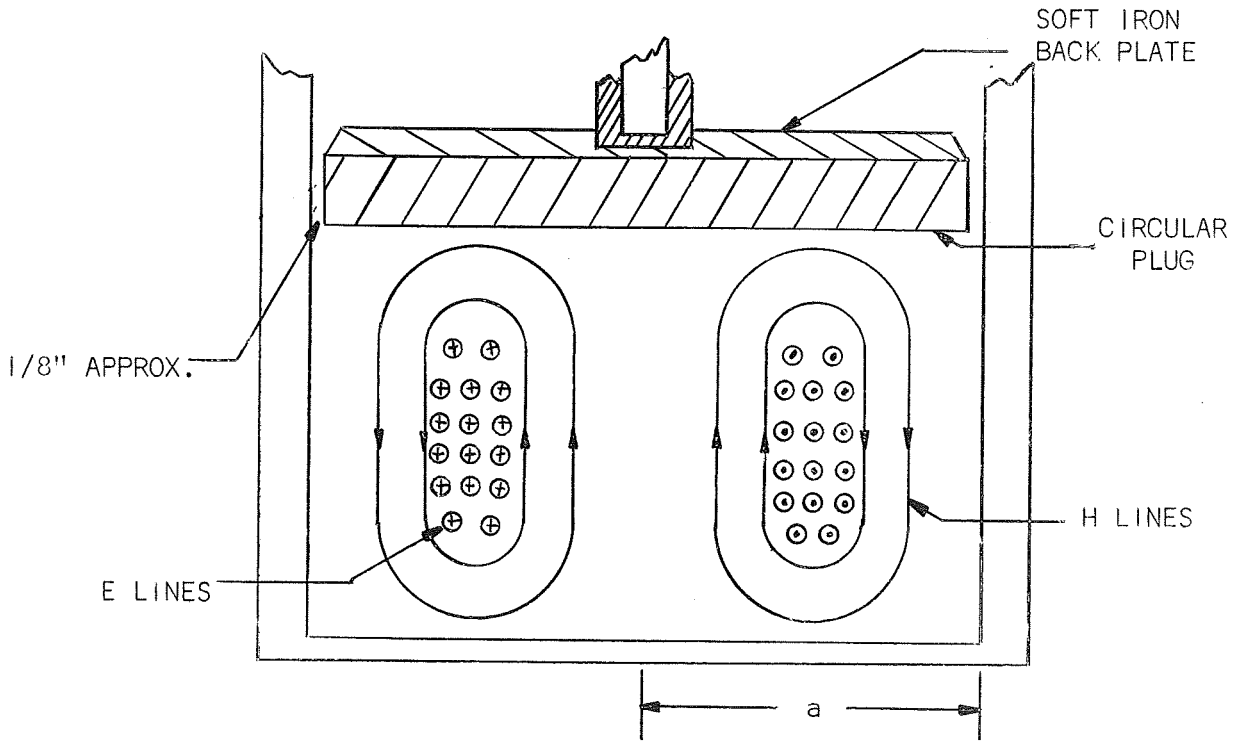

FIELDS OF TE_{011} MODE IN
RIGHT CIRCULAR CYLINDER

FIGURE 3-8

The soft iron backing plate is used to dissipate any unwanted modes in the resonator. The gap between the tuning slug and the side walls of the resonator prevents conduction currents from flowing up the side walls and across the end walls. This serves to suppress all modes except TE^{o}_{onp} resonances.

Consider the basic cylindrical resonator configuration shown in Figure 3-9. For modes TM^{z}, the mode equations and the wave function are:

$$\psi^{TM^z}_{npq} = J_n \left(\frac{X_{np}\rho}{a} \right) \left\{ \begin{matrix} \sin n\phi \\ \cos n\phi \end{matrix} \right\} \cos \left(\frac{q\pi z}{d} \right)$$

$$E_\rho = \frac{1}{\hat{y}} \frac{\partial^2 \psi}{\partial \rho \partial z} \qquad H_\rho = \frac{1}{\rho} \frac{\partial \psi}{\partial \phi}$$

$$E\phi = \frac{1}{\hat{y}} \frac{\partial^2 \psi}{\partial \phi \partial z} \qquad H_\phi = - \frac{\partial \psi}{\partial \phi}$$

$$E_Z = \frac{1}{\hat{y}} \left(\frac{\partial^2}{\partial z^2} + k^2 \right) \psi \qquad H_Z = 0$$

where: X_{np} = the pth root of $J_n(X) = 0$

$\hat{y}$ = $j\omega\varepsilon$

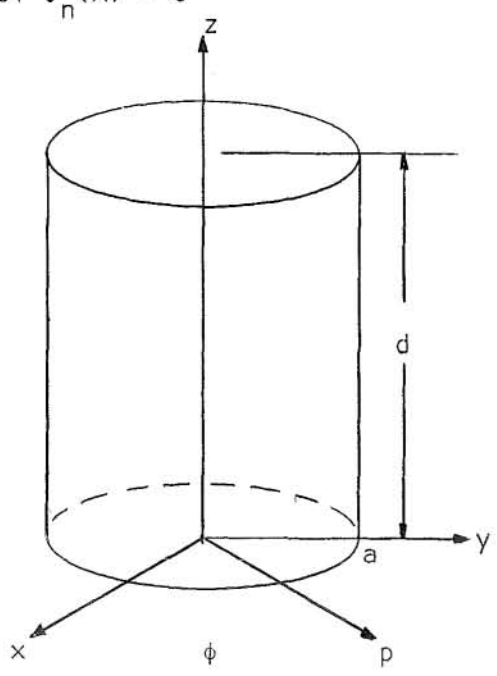

CYLINDRICAL RESONATOR COORDINATES

FIGURE 3-9

For modes TE^z, the mode equations and the wave dunction are:

$$\psi_{npq}^{TE^z} = J_n\left(\frac{x'_{np}\rho}{a}\right)\left\{\begin{matrix}\sin n\phi \\ \cos n\phi\end{matrix}\right\}\sin\left(\frac{q\pi z}{d}\right)$$

$$E_\rho = -\frac{1}{\rho}\frac{\partial\psi}{\partial\phi} \qquad H_\rho = \frac{1}{\hat{z}}\frac{\partial^2\psi}{\partial\rho\partial z}$$

$$E_\phi = \frac{\partial\psi}{\partial\rho} \qquad H_\phi = \frac{1}{\hat{z}\rho}\frac{\partial^2\psi}{\partial\phi\partial z}$$

$$E_z = 0 \qquad H_Z = \frac{1}{\hat{z}}\left(\frac{\partial^2}{\partial z} + k^2\right)\psi$$

where: x'_{np} = the pth root of $\dfrac{\partial j_n(x)}{\partial x} = 0$

$\hat{z} = j\omega\mu$

If one takes into account the gap between the tuning slug, and the side wall which prevents longitudinal currents from flowing, thus suppressing H_ϕ in both cases, the result is:

$$TM^z \text{ modes: } \partial\phi/\partial\rho = 0.$$

This means that $E_\rho = 0$, and since E_ϕ and E_z must be zero at $\rho = a$, and also have no variation with ρ, they must be identically zero. Therefore, these modes cannot exist in the structure.

$$TE^z \text{ modes: } \frac{\partial^2\psi}{\partial\phi\partial z} = 0$$

$\partial\phi/\partial z$ cannot be zero for TE^z modes, since such modes must have zero electric field at $z = 0$ and $z = d$. Thus, $\partial\psi/\partial\phi$ must be zero, this makes $E_\rho = 0$. The final field equations are:

$$\psi = J_o\left(\frac{x'_{op}\rho}{a}\right)\sin\left(\frac{q\pi z}{d}\right)$$

$$E_\phi = \frac{\partial\psi}{\partial\rho}$$

$$H_\rho = \frac{1}{\hat{z}}\frac{\partial^2\psi}{\partial\rho\partial z}$$

$$H_z = \frac{1}{\hat{z}}\left(\frac{\partial^2}{\partial z} + k^2\right)\psi$$

Now one can determine the resonant frequency of a partially filled resonator as shown in Figure 3-10.

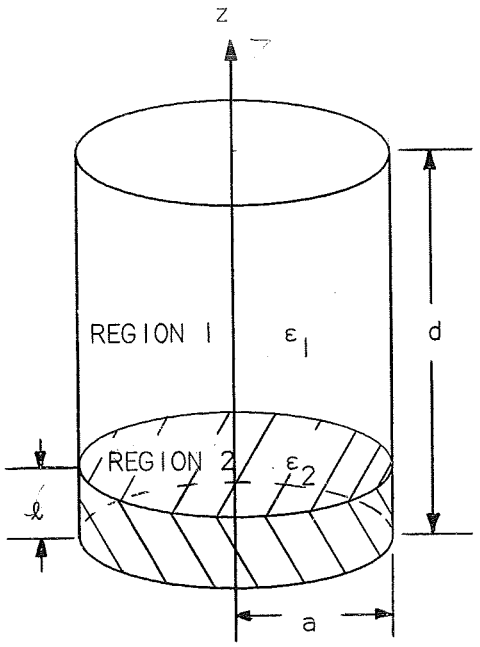

PARTIALLY FILLED CYLINDER

FIGURE 3-10

The wave functions are:

Region 1:

$$\psi_1 = J_o \left(\frac{X'_{01}\,\rho}{a} \right) \sin k_{z_1} (d - Z)$$

Region 2:

$$\psi_2 = J_o \left(\frac{X'_{01}\,\rho}{a} \right) \sin k_{z_2} Z$$

The separation equations are:

$$k_{z_1}^2 + \left(\frac{X'_{01}}{a} \right)^2 = \omega^2 \mu_o \varepsilon_1$$

$$k_{z_2}^2 + \left(\frac{X'_{01}}{a} \right)^2 = \omega^2 \mu_o \varepsilon_2$$

The z directed wave impedance Z is defined as:

$$Z_z = -\frac{E_\phi}{H_\rho} = -\hat{z}\,\frac{\partial\psi/\partial\rho}{\partial^2\psi/\partial\rho\partial z}$$

$$Z_z^1 = \frac{-j\omega\mu_o}{-k_{z_1}}\;\frac{\sin k_{z_1}(d-z)}{\cos k_{z_1}(d-z)}$$

$$Z_z^2 = \frac{j\omega\mu_o}{k_{z_1}}\;\frac{\sin k_{z_1} z}{\cos k_{z_1} z}$$

Equating the wave impedances at $z = \ell$ results in the characteristic equation:

$$-\frac{1}{k_{z_1}}\tan k_{z_1}(d-\ell) = \frac{1}{k_{z_2}}\tan k_{z_2}\ell$$

One would have to solve the set of equations:

$$-k_{z_2}\tan k_{z_2}(d-\ell) = k_{z_1}\tan k_{z_2}\ell$$

$$k_{z_2}^2 + \left(\frac{X'_{01}}{a}\right)^2 = \omega^2\mu_o\varepsilon_2$$

$$k_{z_1}^2 + \left(\frac{X'_{01}}{a}\right)^2 = \omega^2\mu_o\varepsilon_1$$

A plot of resonant frequency versus dielectric constant ε' with fill level as a parameter should be made to facilitate the interpretation of the measurements. Determination of the loss term ε'' would require measurement of the unloaded Q of the resonator.

$$Q = \frac{2\pi f\,[\text{Maximum Energy Stored/Cycle}]}{[\text{Power Dissipated in the Structure}]}$$

Now:

$$[\text{Max Energy Stored/Cycle}] = \iiint \varepsilon |E|^2 \, d_\tau$$

$$= \int_o^a \int_o^{2\pi} \int_o^{\ell} \varepsilon_o \varepsilon' \, |E_\phi^{(2)}|^2 \, \partial d\partial d\phi dZ + \int_o^a \int_o^{2\pi} \int_o^{\ell} \varepsilon_o |E_\phi^{(1)}|^2 \, \rho d\rho d\phi dz$$

Here $\varepsilon_2 = \varepsilon_o \varepsilon'$ and $\varepsilon_1 = \varepsilon_o$

The power dissipated in the structure =

$$\int_o^a \int_o^{2\pi} \int_o^{\ell} \varepsilon_o \varepsilon' \tan\delta |E_\phi^{(2)}|^2 \, \rho d\rho d\phi \, dz + \iint |H_\tau|^2 \, R_s \, ds$$

These calculations could be made once k_{z_1}, k_{z_2} and ω were determined and thus ε'' would be determined.

A perturbational analysis of this resonator leads to some useful results. From the field equations:

$$E_\phi = \frac{X'_{01}}{a} J_o \left(\frac{X'_{01}\rho}{a} \right) \sin \frac{\pi z}{d}$$

is the unperturbed electric field.

Using the perturbation formula:

$$\frac{\omega - \omega_o}{\omega_o} \approx - \frac{\iiint (\Delta\varepsilon |E_o|^2 + \Delta\mu |H_o|^2) d_\tau}{\iiint (\varepsilon |E_o|^2 + \mu |H_o|^2) \, d_\tau}$$

One can show that:

$$\frac{\omega - \omega_o}{\omega_o} \approx - \frac{(\varepsilon - 1)}{d} \int_o^{\ell} \sin^2 \frac{\pi z}{d} \, dz$$

$$\frac{\omega - \omega_o}{\omega_o} \approx - \left(\frac{\varepsilon - 1}{d}\right) \left(\frac{\ell}{2} - \frac{d}{4\pi} \sin \frac{2\pi\ell}{d} \right)$$

for small ℓ/d.

$$\frac{\omega - \omega_o}{\omega_o} \approx - \frac{(\varepsilon - 1)}{d} \left(\frac{d}{4\pi} \left(\frac{2\pi \ell}{d} \right)^3 \frac{1}{3!} \right)$$

$$\frac{\omega - \omega_o}{\omega_o} \approx - \frac{(\varepsilon - 1)\pi^2}{3} \left(\frac{\ell}{d} \right)^3$$

Set: $\varepsilon = \varepsilon' (1 - j \tan \delta)$

and use: $\omega \approx \omega_r \left(1 + \frac{j}{2Q}\right)$

then:

$$\omega_r - \omega_o + j \frac{\omega_r}{2Q} \approx - \omega_o [(\varepsilon' - 1) - j \varepsilon' \tan\delta] \frac{\pi^2}{3} \left(\frac{\ell}{d} \right)^3$$

or: $$\omega_r - \omega_o \approx \omega_o [(\varepsilon' - 1)] \frac{\pi^2}{3} \left(\frac{\ell}{d} \right)^3$$

$$\frac{1}{2Q} \approx \varepsilon' \tan \delta \left(\frac{\pi^2 \ell}{3} \right) \left(\frac{\ell}{d} \right)^3$$

try a 20% fill $\varepsilon' = 20, \tan \delta = \frac{1}{20}$

$$\frac{1}{2Q} \approx 1 \left(\frac{10}{3}\right) \left(\frac{8}{1000}\right)$$

$$Q \approx \frac{300}{16} - 20$$

This is too low.

Use 10% fill,

$$\frac{1}{2Q} \approx 1 \left(\frac{10}{3}\right)\left(\frac{1}{1000}\right) \approx \frac{1}{300}$$

$$Q \approx 150$$

$$\frac{\omega_r - \omega_o}{\omega_o} \approx -(19)\frac{1}{300} \approx \frac{1}{15}$$

A determination of cavity dimensions may be made as follows.

For a TE_{011} mode use:

$$f_r = \frac{1}{2\pi a \sqrt{\mu\varepsilon}} \left[(3.83)^2 + \left(\frac{\pi a}{a}\right)^2\right]^{1/2}$$

$$f_{r_1} = \frac{1}{2\pi a \sqrt{\mu\varepsilon}} \left[(3.83)^2 + \left(\frac{\pi a}{d_1}\right)^2\right]^{1/2}$$

$$f_{r_2} = \frac{1}{2\pi a \sqrt{\mu\varepsilon}} \left[(3.83)^2 + \left(\frac{\pi a}{d_2}\right)^2\right]^{1/2}$$

Now chosing $f_{r_2} = 2f_r$, the equations reduce to:

$$3\left(\frac{3.83}{\pi}\right)^2 = \frac{a^2}{d_2^2} - \frac{4a^2}{d_1^2}$$

For different values of a/d_1, a/d_2 is given in Table 3-4.

TABLE 3-4

RESONANT CAVITY PARAMETERS

a/d_1	$4(a/d_1)^2$	$3\left(\frac{3.83}{\pi}\right)^2 - 4\,(a/d_1)^2$	a/d_2
.25	.25	4.72	2.17
.5	1.0	5.47	2.34
1.0	4.0	8.47	2.91
2.0	16.0	20.47	4.52

Choosing $f_r = 2 \times 10^9 = \frac{.477 \times 10^{10}}{a} [14.7 + 9.85 (a/d_1)^2]^{1/2}$

we get the following Table 3-5 for the parameters of the cavity.

TABLE 3-5

CAVITY DIMENSIONS FOR 2 GHz OPERATION

a/d_1	a/d_2	$a^{(cm_1)}$	$d_1^{(cm_1)}$	$d_2^{(cm_1)}$
0.25	2.17	9.32	37.20	4.28
0.50	2.34	9.91	19.80	4.23
1.00	2.91	11.82	11.82	4.06
2.00	4.52	17.60	8.80	3.90

These parameters can be used in determining the dimensions of the cavities.

3.4 TECHNIQUE A THEORY

The basis of a mass gaging system that is to be independent of propellant location within a spacecraft tank is that the propellant measurement must be independent of any geometric property of the propellant. The ideal propellant mass gaging system for any gravity environment should have the following characteristics:

a) Each molecule of propellant should have a uniform influence on the measurement irrespective of location or grouping.

b) The time rate of change of the molecular distribution of the propellant mass must not influence the measurement.

c) The measurement must be insensitive to all tank parameter variations and the effect of secondary propellant parameter variations.

In the development of a measurement system for gaging propellants under zero gravity conditions, the dominant criteria of the system must be the uniform illumination of the propellant tank with some form of energy. The measurement of the energy stored in the propellant tank provides the most promising system. The energy storage systems measure the propellant mass by determining the amount of energy stored, the frequency or frequencies at which it is stored, or the frequency shift caused by using the tanks as an energy storage element. The principal advantage of energy storage systems is that a relatively uniform illumination of the propellant tank is possible in many cases. The type of energy used in these systems varies across the entire frequency spectrum. The radio frequency band of the electromagnetic spectrum was chosen as being the most physically realizable portion for obtaining uniform illumination of a propellant tank.

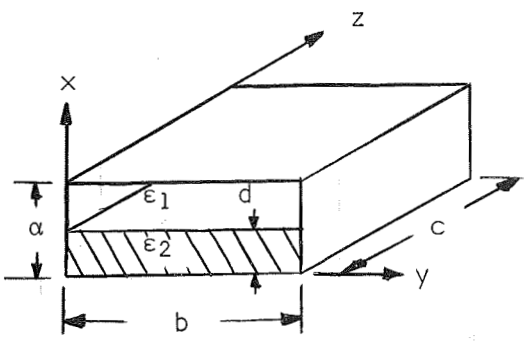

PARTIALLY FILLED RECTANGULAR CAVITY

FIGURE 3-11

Here we have a rectangular cavity (Figure 3-11) for which an analysis of the loading behavior of a cavity may be made for different orientations of the interface:

$$\pm k_{x_1}^2 + \left(\frac{n\pi}{b}\right)^2 + \left(\frac{n\pi}{c}\right)^2 = \varepsilon_r \left(\frac{\omega}{c}\right)^2 \qquad (3.17)$$

$$k_{x_2}^2 + \left(\frac{n\pi}{b}\right)^2 + \left(\frac{p\pi}{c}\right)^2 = -\left(\frac{\omega}{c}\right)^2 \qquad (3.18)$$

$$TM_x \text{ modes} \quad -x_1 \tan k_{x_1} d = \varepsilon_r k_{x_2} \tan k_{x_2} (a - d) \qquad (3.19)$$

$$TE_x \text{ modes} \quad -x_1 \cot k_{x_1} d = k_{x_2} \cot k_{x_2} (a - d) \qquad (3.20)$$

where: n = half wavelength variations along the y axis

p = half wavelength variations along the z axis

x_1 = wave number in medium 2

k_{x_2} = wave number in medium 2

c = speed of light

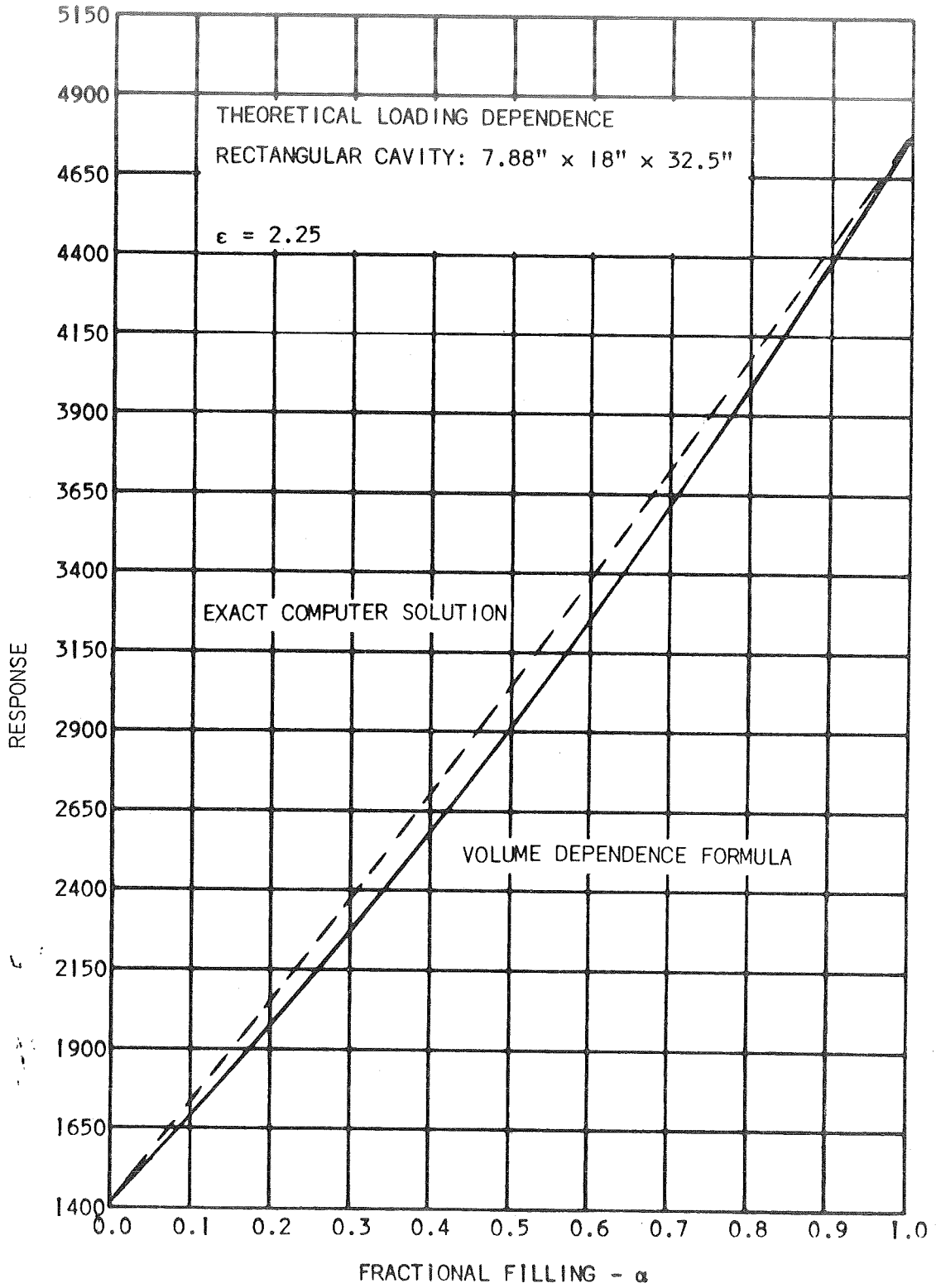

NP 3745-67-209

FIGURE 3-12

ε_r = relative dielectric constant

\+ = standing waves in both media

\- = standing waves in media 2 only

A computer program based on these equations was developed and the number of modes determined for the interface normal to each of the cartesian axis over the empty to full loading range. The results are shown in Figure 3-12 and are given in Table 3-6.

It is interesting to note that the response deviation from one orientation to another is small although the dimensions along which loadings are taken vary considerably. Computations of this type were made for another cavity having two equal sides and the results gave a similar small deviation from one orientation to another at a given loading.

An additional insight into the behavior of a partially filled cavity can be gained by looking at the form of the response curve (loading). The response curve looking at Figure 3-12 is linear. This says that the effect on the response of an incremental change in the tank content is dependent only on this change and not on the dielectric content. This fact, together with the fact that the curve remains essentially invariant with three mutually orthogonal directions of loading, means that the loading can be split up into smaller units and randomly distributed throughout the tank. That is, if a loading is split up into M parts, each part will contribute 1/M the effect of the whole regardless of the position of these parts. We can then say, that on this basis the analysis of the tanks for regular loading along the edges can be extended to cover irregular mass distributions in the tank.

TABLE 3-6

LOADING DEPENDENCY-RECTANGULAR CAVITY

Fractional Filling	System Response			
	⊥to 7.88 in	⊥to 18 in	⊥to 35.2 in	Volume Dependency
Empty	1419	1419	1419	1423
0.01	1421	1426	1431	1431
0.10	1707	1733	1745	1700
0.20	2042	2039	2080	1995
0.30	2392	2388	2417	2300
0.40	2738	2745	2745	2605
0.50	3076	3078	3091	2890
0.60	3400	3412	3428	3290
0.70	3750	3759	3767	3680
0.80	4087	4093	4095	4020
0.90	4446	4424	4438	4420
1.00	4764	4764	4764	4781

The fact that the dielectric can be arbitrarily subdivided and not affect the overall system response has been evidenced by experiments using paraffin blobs. A fill test was made for a cigar-shaped tank shown in Figure 3-13, and the tests are shown in Figure 3-14.

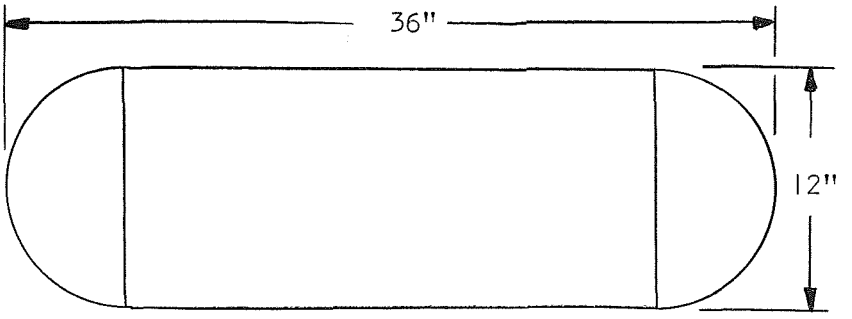

CIGAR-SHAPED TANK
FIGURE 3-13

The test material here was paraffin which has a dielectric constant ε_1 similar to N_2O_4. The paraffin was made up into arbitrarily shaped pieces varying from a fraction of a cubic inch to 10 cubic inches in volume. As the tank was loaded, it was subjected to tilting to three mutually perpendicular orientations. Response deviations at any loading were equivalent to less than ± 2% of the full scale tank content. It can be seen that the loading curve for this test was both linear and independent of dielectric content location and size distribution. Further tests conducted with paraffin on another tank with one end inverted as in Figure 3-15 gave a similarly straight loading curve and an independence of position of ± .25% of full scale as shown in Figure 3-16.

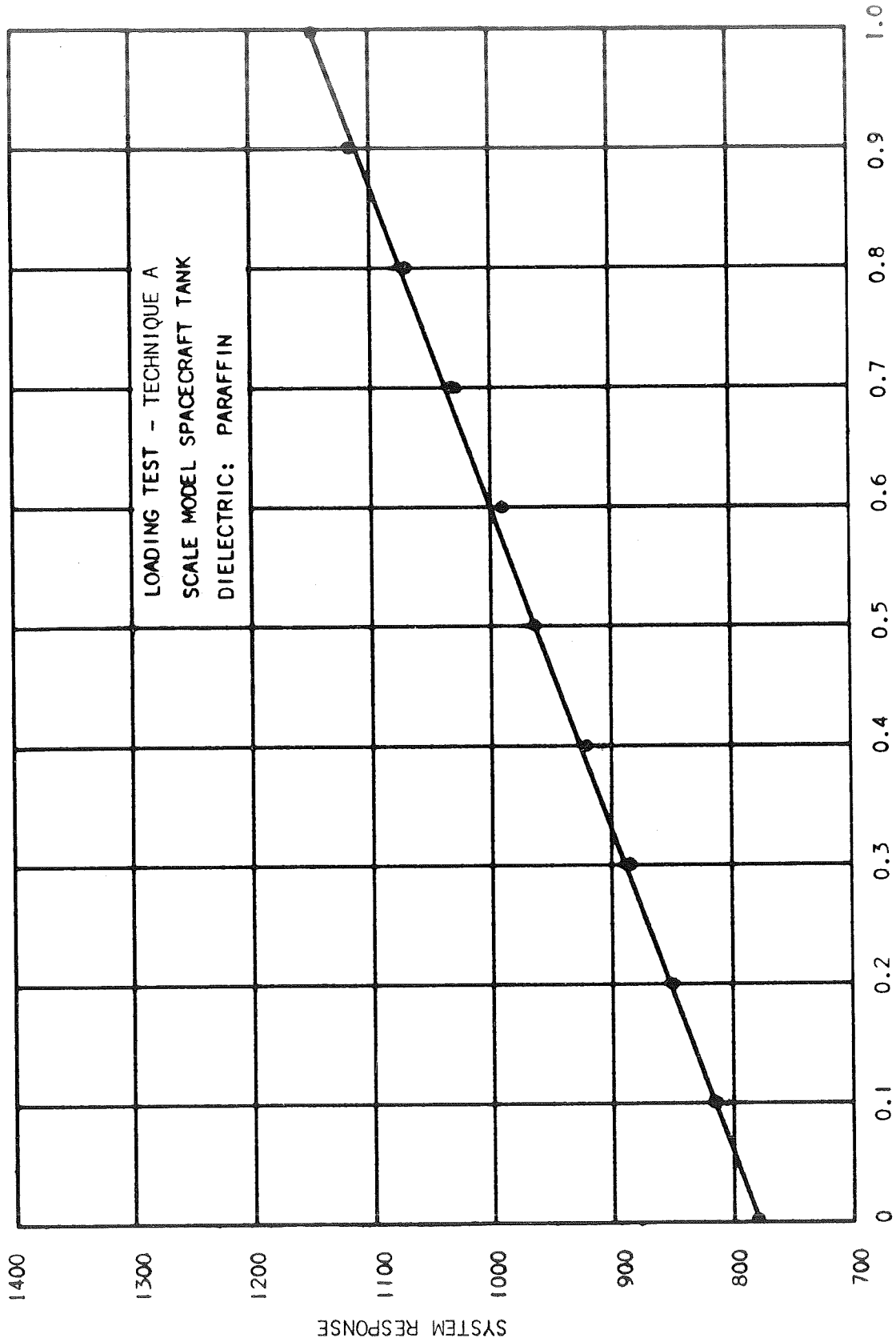
LOADING TEST - TECHNIQUE A
SCALE MODEL SPACECRAFT TANK
DIELECTRIC: PARAFFIN
SYSTEM RESPONSE
1400
1300
1200
1100
1000
900
800
700
0
0.1
0.2
0.3
0.4
0.5
0.6
0.7
0.8
0.9
1.0
FRACTIONAL FILLING-α
NP A3914-68-245

FIGURE 3-14

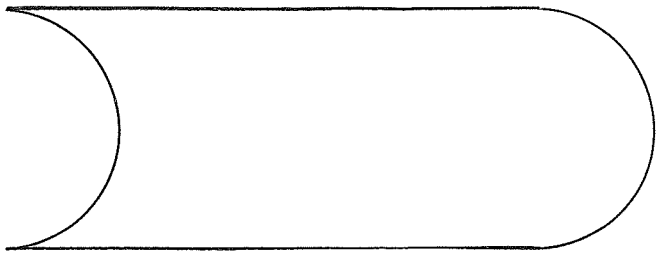

RE-ENTRANT TANK
FIGURE 3-15

This discussion of the expected loading dependence and relative independence of propellant relocation or distribution tends to show that a uniform illumination of the tank interior can be achieved using proper RF excitation. A non-uniformity of the tank illumination would show up as a non-linearity of the loading curve or shift in this curve with propellant movement from region to region in the tank.

Now the results discussed this far are based on a response prediction made using the exact electromagnetic field equations. Previous work in the prediction of the response had been based on the use of a variational theory.

The results agree with that derived on an exact basis at empty and full as $\alpha = 0.1$. It gives, however, a non-linear prediction for the loading dependence as shown in Figure 3-12 and 3-17, Table 3-6. While the non-linearity is not serious for this example it would be greater for the higher dielectric constant fluids such as Aerozine 50 or MMH. Thus an exact formula should be used for system response prediction.

For N_2O_4, Aerozine 50 and MMH a predicted response curve is shown in Figure 3-18 for cigar-shaped cavity similar in shape to the SPS tank without internal hardware.

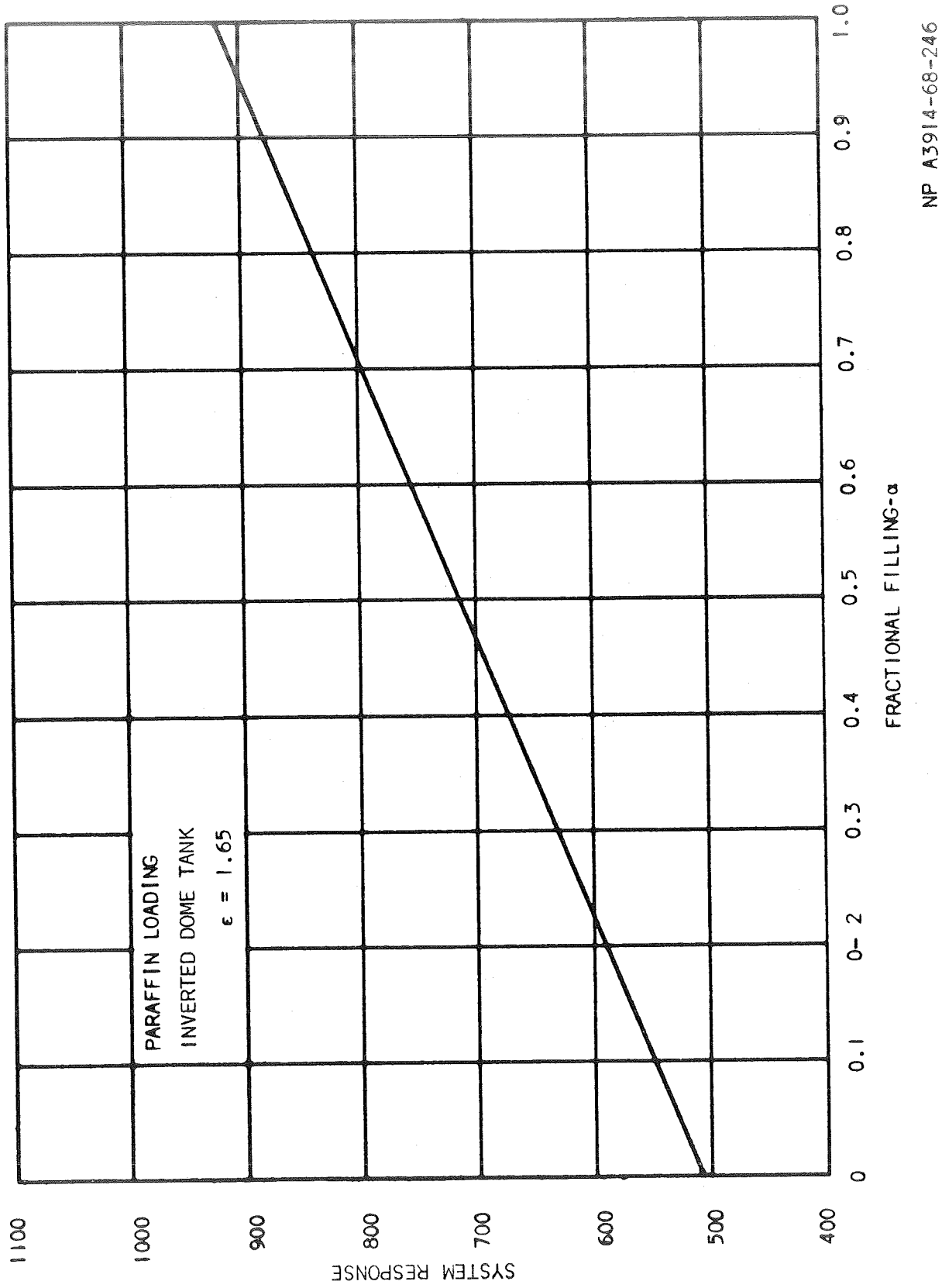
PARAFFIN LOADING
INVERTED DOME TANK
ε = 1.65
SYSTEM RESPONSE
1100
1000
900
800
700
600
500
400
0
0.1
0.2
0.3
0.4
0.5
0.6
0.7
0.8
0.9
1.0
FRACTIONAL FILLING-α
NP A3914-68-246

FIGURE 3-16

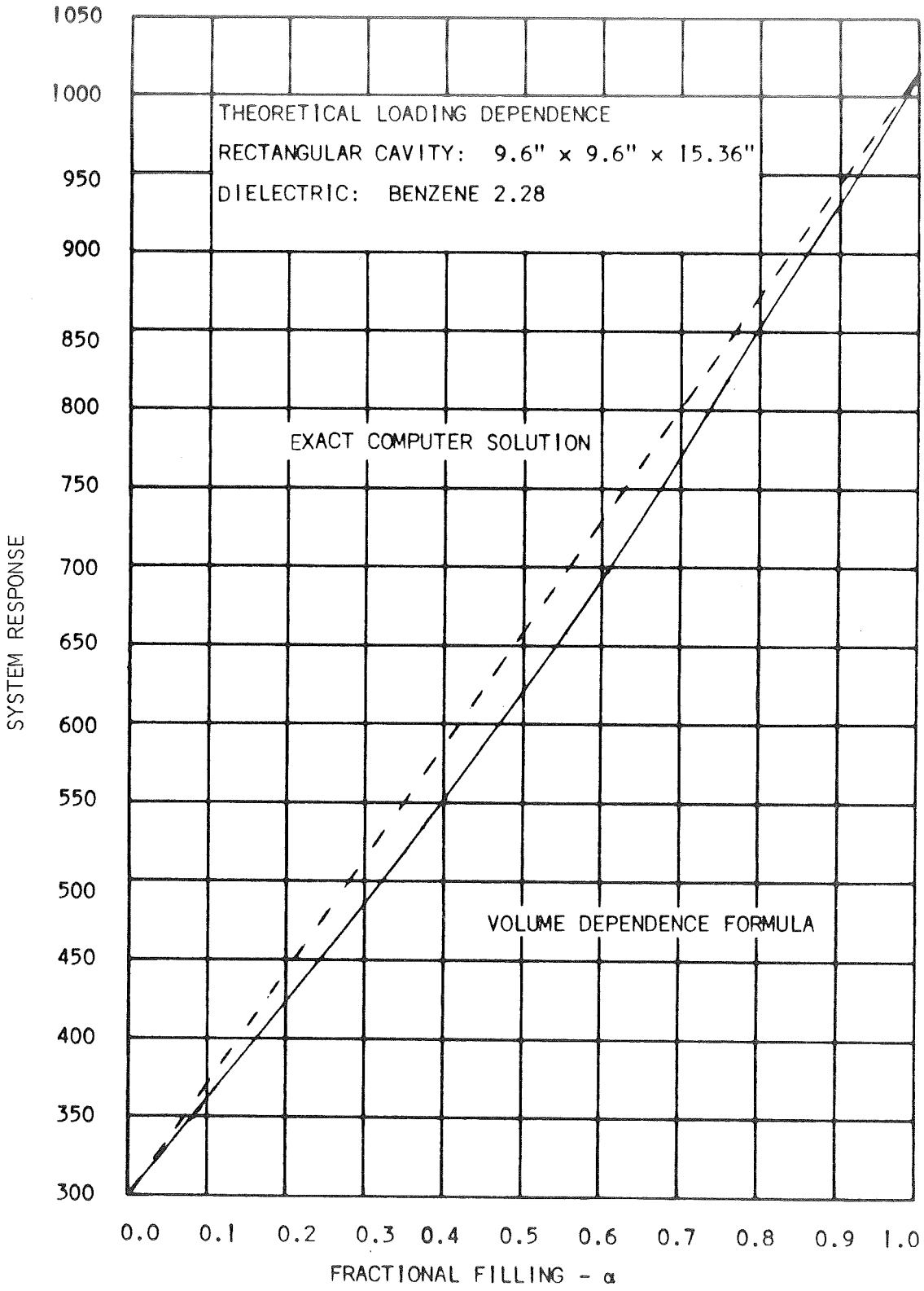

NP 3745-67-244

FIGURE 3-17

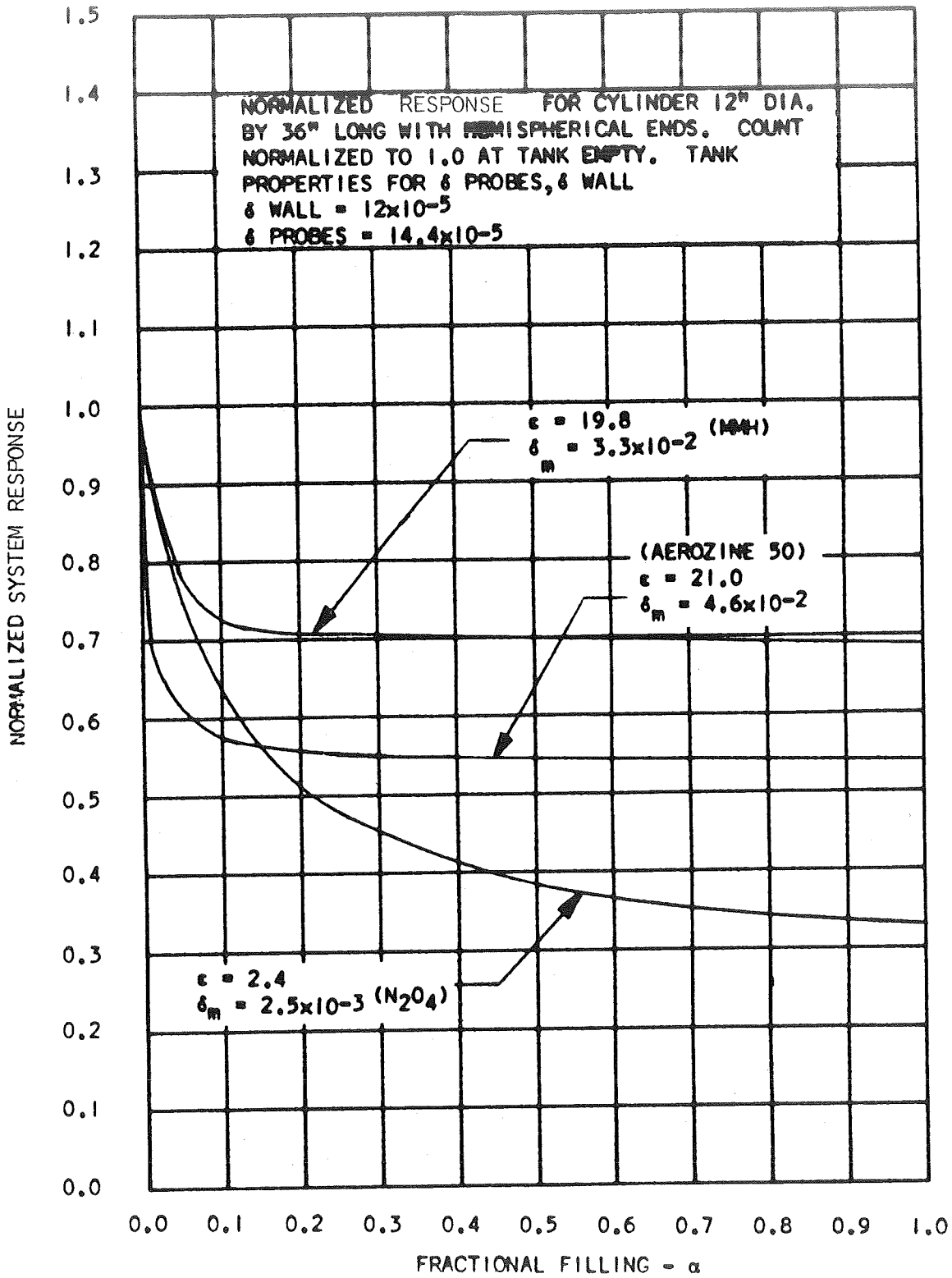

NP A3914-68-269

FIGURE 3-18

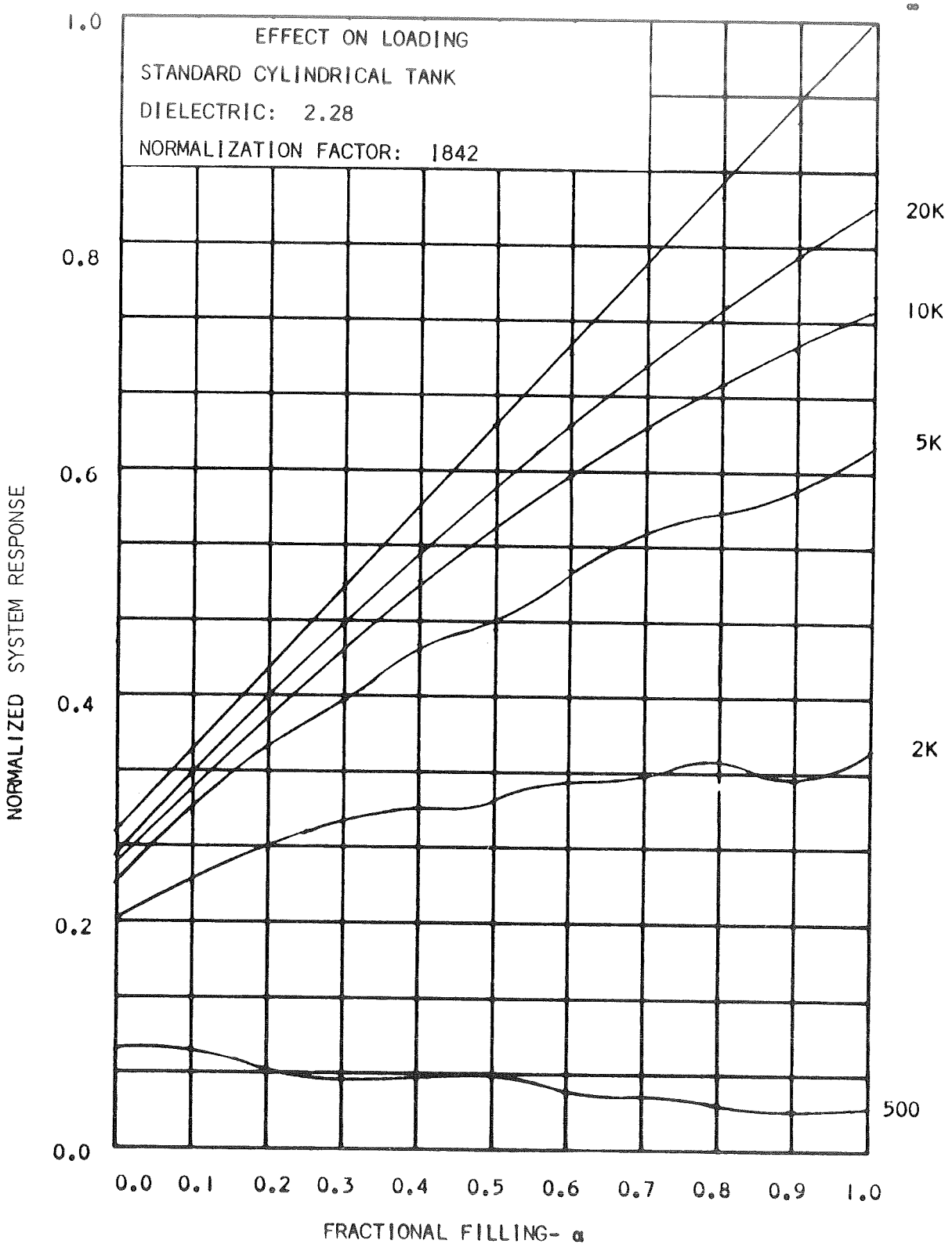
EFFECT ON LOADING
STANDARD CYLINDRICAL TANK
DIELECTRIC: 2.28
NORMALIZATION FACTOR: 1842
∞
20K
10K
5K
2K
500
1.0
0.8
0.6
0.4
0.2
0.0
NORMALIZED SYSTEM RESPONSE
0.0 0.1 0.2 0.3 0.4 0.5 0.6 0.7 0.8 0.9 1.0
FRACTIONAL FILLING- α
NP 3745-67-219

FIGURE 3-19

The curve for MMH and Aerozine 50 should be ignored past $\alpha = .05$. An examination of the higher loading region for MMH and Aerozine 50 should be done using a more exact analysis of the effect of tank loss on system response. An idea of the results of this type of program is shown in Figure 3-19. At best though, the system response to loading with Aerozine 50 or MMH for the presumed values of ε_r will degrade at higher loadings.

In the following theory sections several other techniques are examined for sensitivity to provide an answer to the question of whether another technique could be used to achieve a better loading response.

3.5 TECHNIQUE B THEORY

The system response of Technique B is shown as a function of fractional filling of the cavity with MMH, Aerozine 50 and N_2O_4 in Figures 3-20, 3-21 and 3-22.

The present analysis should show the trend of the experimental results to be expected and assist in determining whether the technique shows a promising response.

3.6 TECHNIQUE C THEORY

Advantage may be taken of the uniform illumination of the cavity by the RF energy which makes the resultant Technique C response of the cavity independent of propellant location.

3.6.1 Predicted System Response

An evaluation was made of the predictions of theory for the system response. The curves of Figures 3-23 through 3-26 and Tables 3-7 through 3-10 indicate the trend the measured variable could follow with tank loading and they are not exact. In some cases such as for N_2O_4, they are more non-linear than the actual experimental data. Because of this, it is felt that the actual response of the C technique will always be better than these curves. Thus, they constitute a lower bond to the expected sensitivity. All curves are normalized to their full tank response to give an idea of the variability in sensitivity that might occur with loading. The non-linearity is inherent and would have to be taken care of with a non-linear function generator if a linear response were desired.

Again, as in Technique A, the lower values of dielectric constant could make the response of Aerozine 50 and MMH more linear.

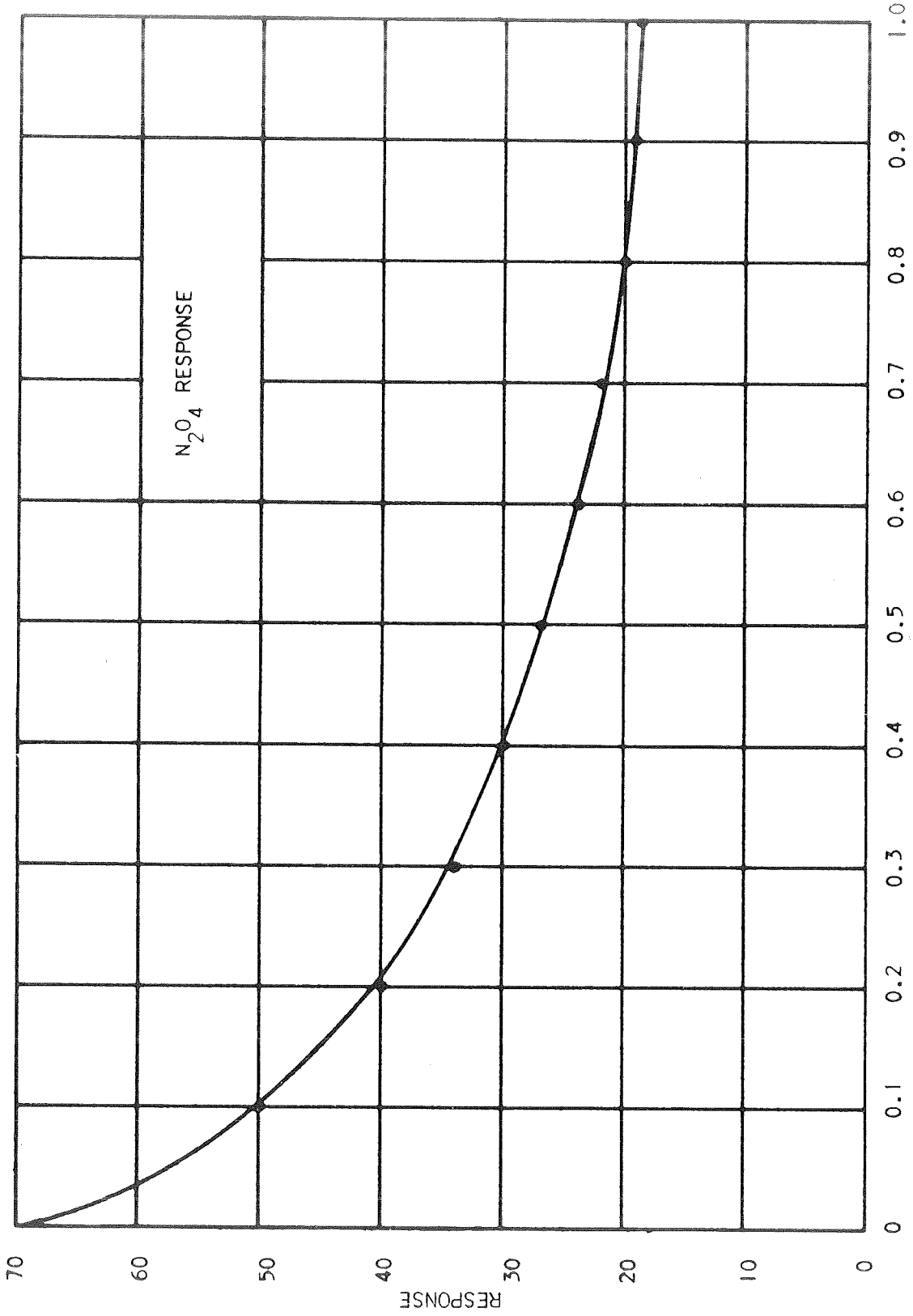
N_2O_4 RESPONSE
RESPONSE
70
60
50
40
30
20
10
0
0
0.1
0.2
0.3
0.4
0.5
0.6
0.7
0.8
0.9
1.0
FRACTIONAL FILLING-α
NP A3914-68-248

FIGURE 3-20

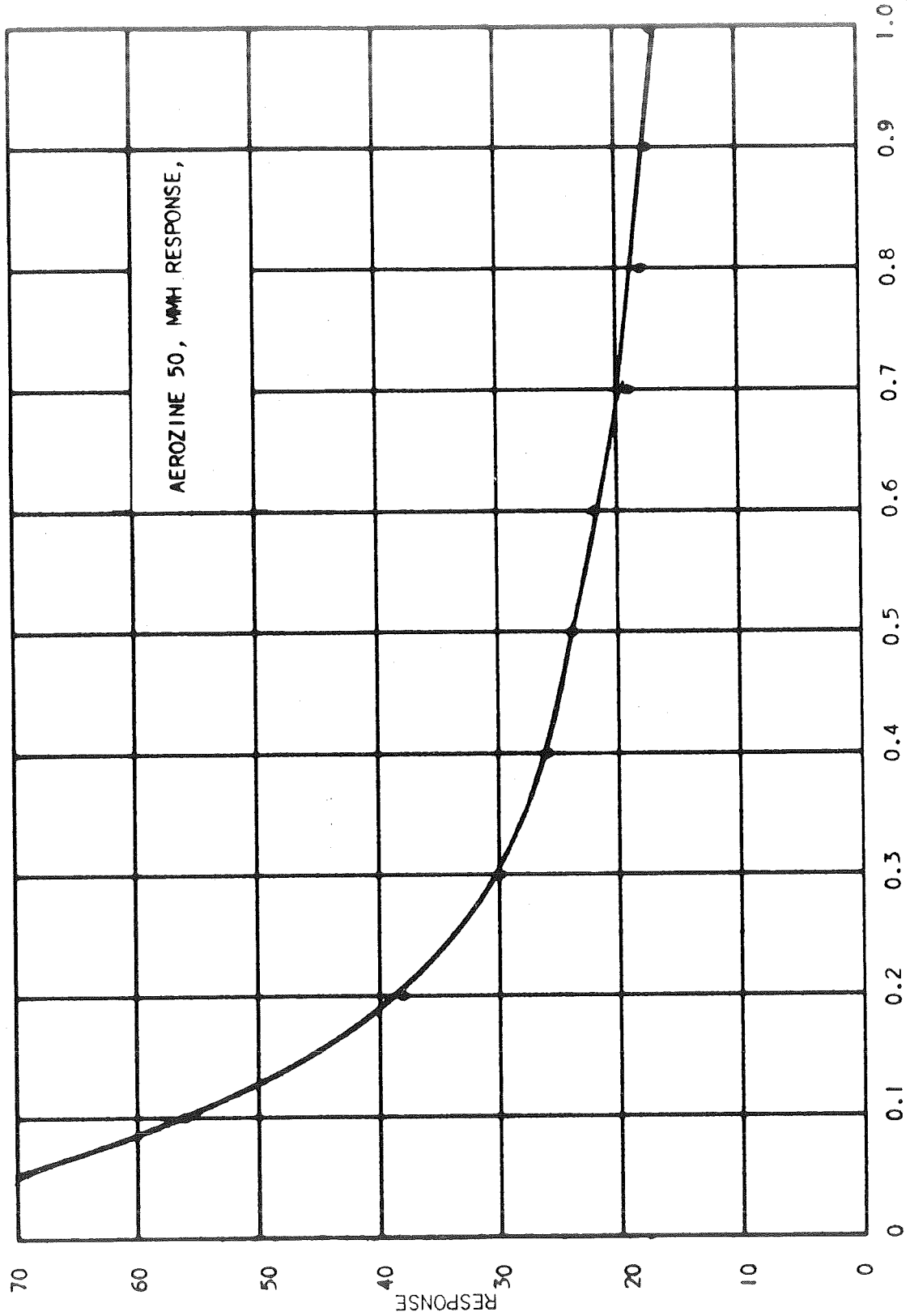

NP A3914-68-249

FIGURE 3-21

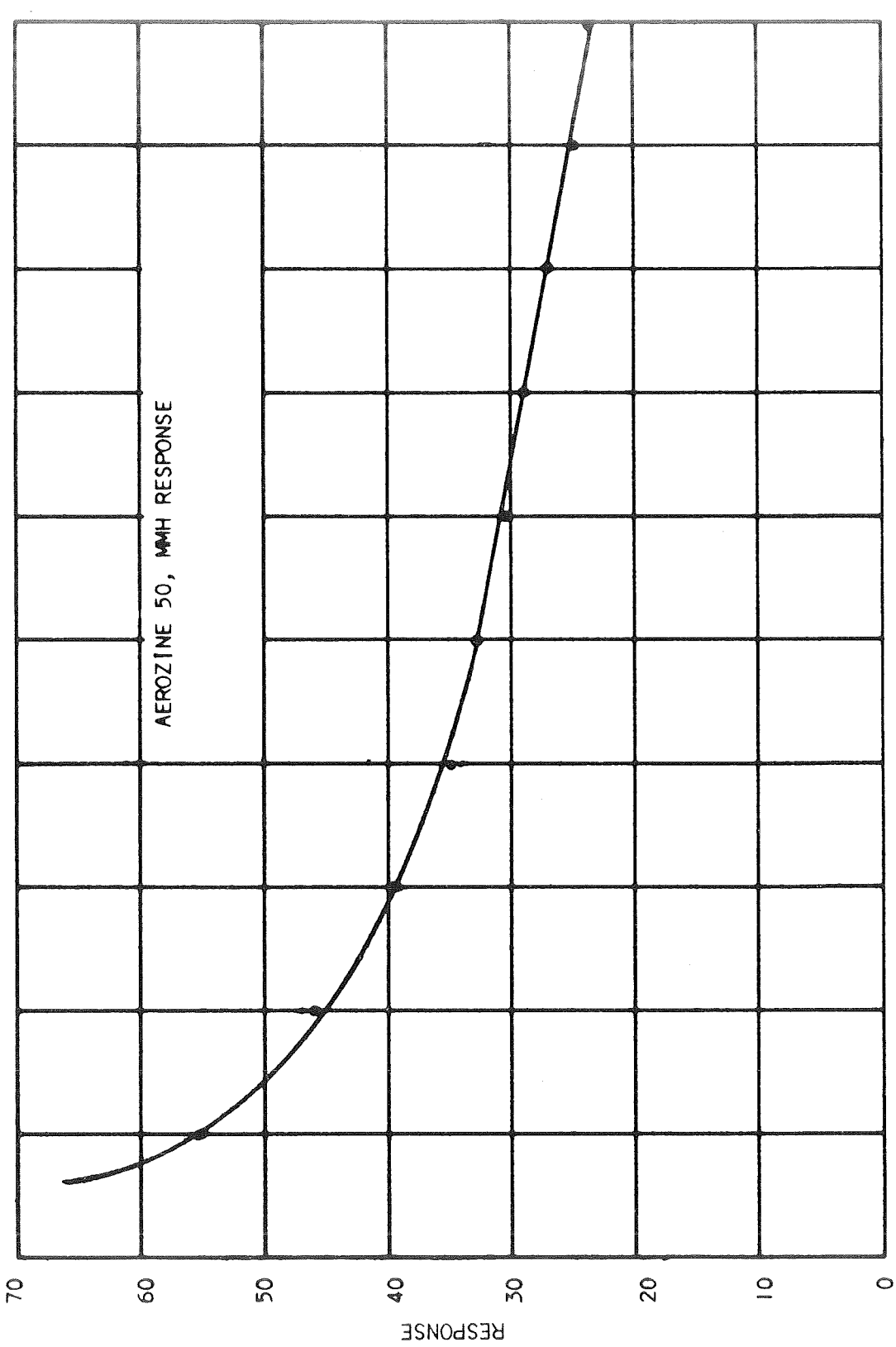

NP A3914-68-250

FIGURE 3-22

TABLE 3-7

RESPONSE OF N_2O_4

FRACTIONAL FILLING	NORMALIZED RESPONSE
0.0	0.000
0.1	0.190
0.2	0.377
0.3	0.523
0.4	0.643
0.5	0.736
0.6	0.814
0.7	0.868
0.8	0.922
0.9	0.960
1.0	1.000

TABLE 3-8

AEROZINE 50, MMH RESPONSE

FRACTIONAL FILLING	NORMALIZED RESPONSE
0.000	0.000
0.025	0.227
0.050	0.413
0.075	0.534
0.100	0.620
0.200	0.792
0.300	0.863
0.400	0.915
0.500	0.942
0.600	0.958
0.700	0.970
0.800	0.977
0.900	0.992
1.000	1.000

TABLE 3-9

AEROZINE 50, MMH RESPONSE

FRACTIONAL FILLING	NORMALIZED RESPONSE
0.000	0.000
0.050	0.311
0.100	0.489
0.200	0.722
0.300	0.818
0.400	0.877
0.500	0.913
0.600	0.943
0.700	0.967
0.800	0.977
0.900	0.988
1.000	1.000

TABLE 3-10

AEROZINE 50, MMH RESPONSE

FRACTIONAL FILLING	NORMALIZED RESPONSE
0.00	0.000
0.05	0.237
0.10	0.422
0.20	0.623
0.30	0.743
0.40	0.828
0.50	0.868
0.60	0.925
0.70	0.938
0.80	0.963
0.90	0.986
1.00	1.000

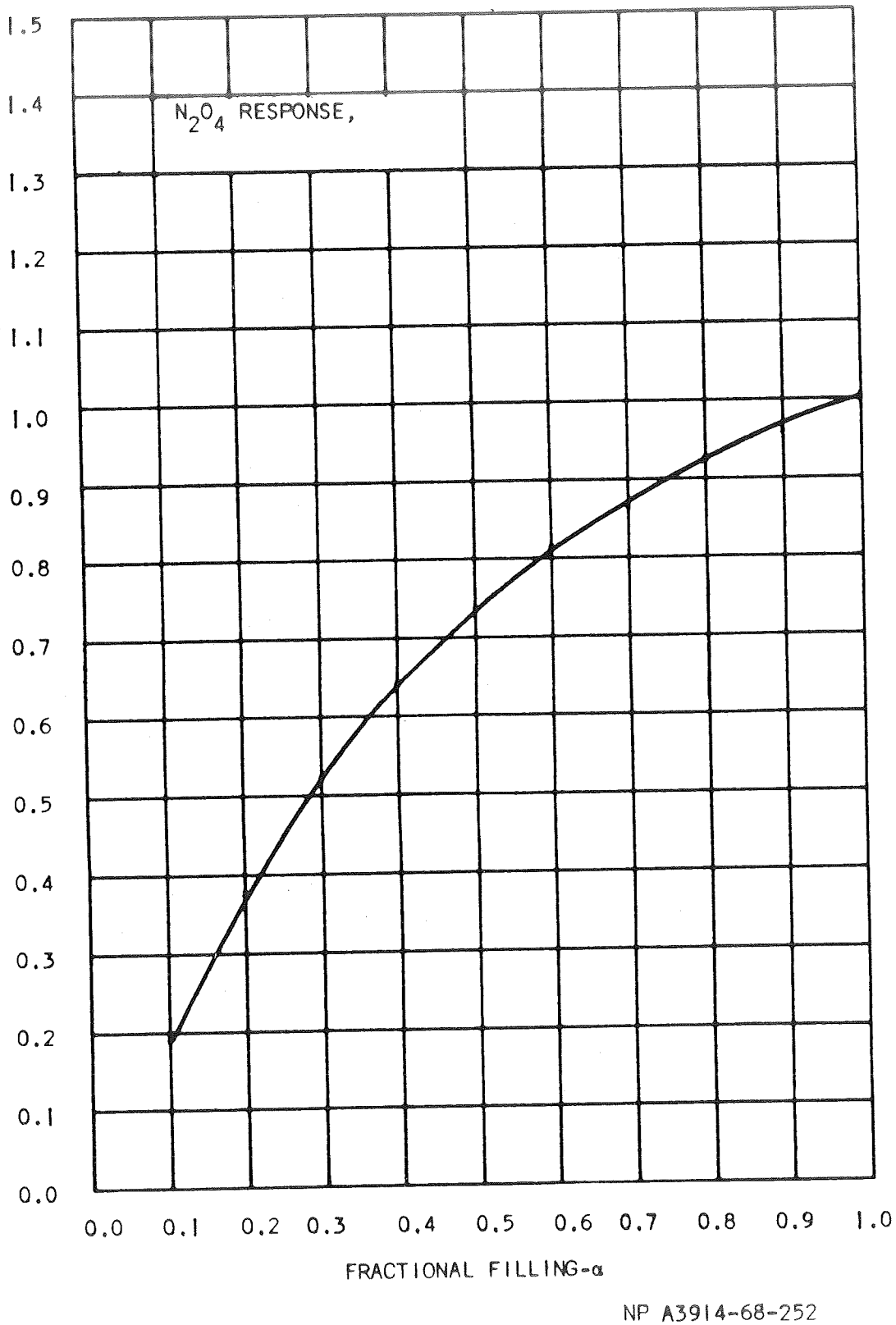
N_2O_4 RESPONSE,
NORMALIZED RESPONSE
1.5
1.4
1.3
1.2
1.1
1.0
0.9
0.8
0.7
0.6
0.5
0.4
0.3
0.2
0.1
0.0
0.0 0.1 0.2 0.3 0.4 0.5 0.6 0.7 0.8 0.9 1.0
FRACTIONAL FILLING-α
NP A3914-68-252

FIGURE 3-23

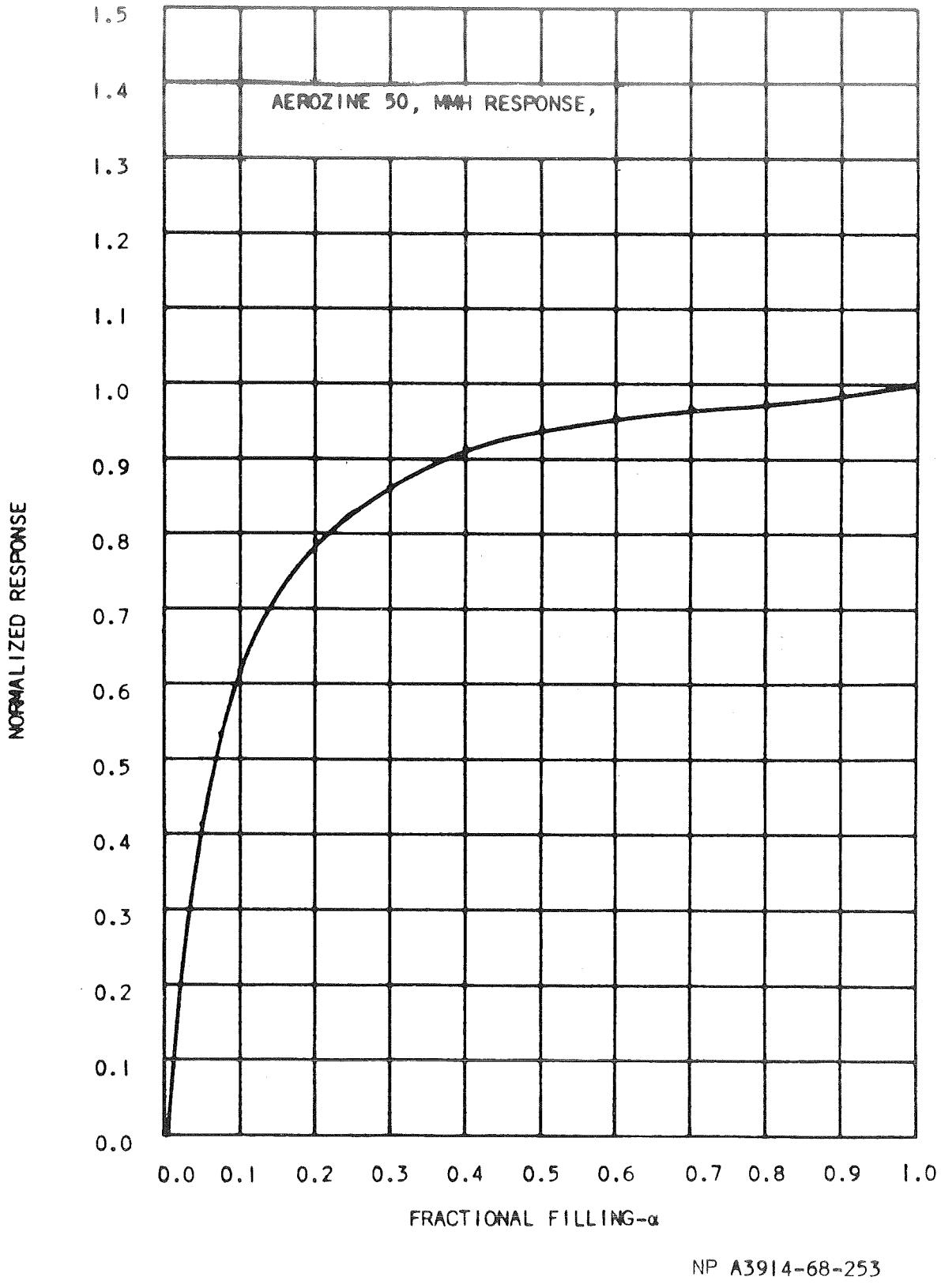
AEROZINE 50, MMH RESPONSE,
NORMALIZED RESPONSE
1.5
1.4
1.3
1.2
1.1
1.0
0.9
0.8
0.7
0.6
0.5
0.4
0.3
0.2
0.1
0.0
0.0 0.1 0.2 0.3 0.4 0.5 0.6 0.7 0.8 0.9 1.0
FRACTIONAL FILLING-α
NP A3914-68-253

FIGURE 3-24

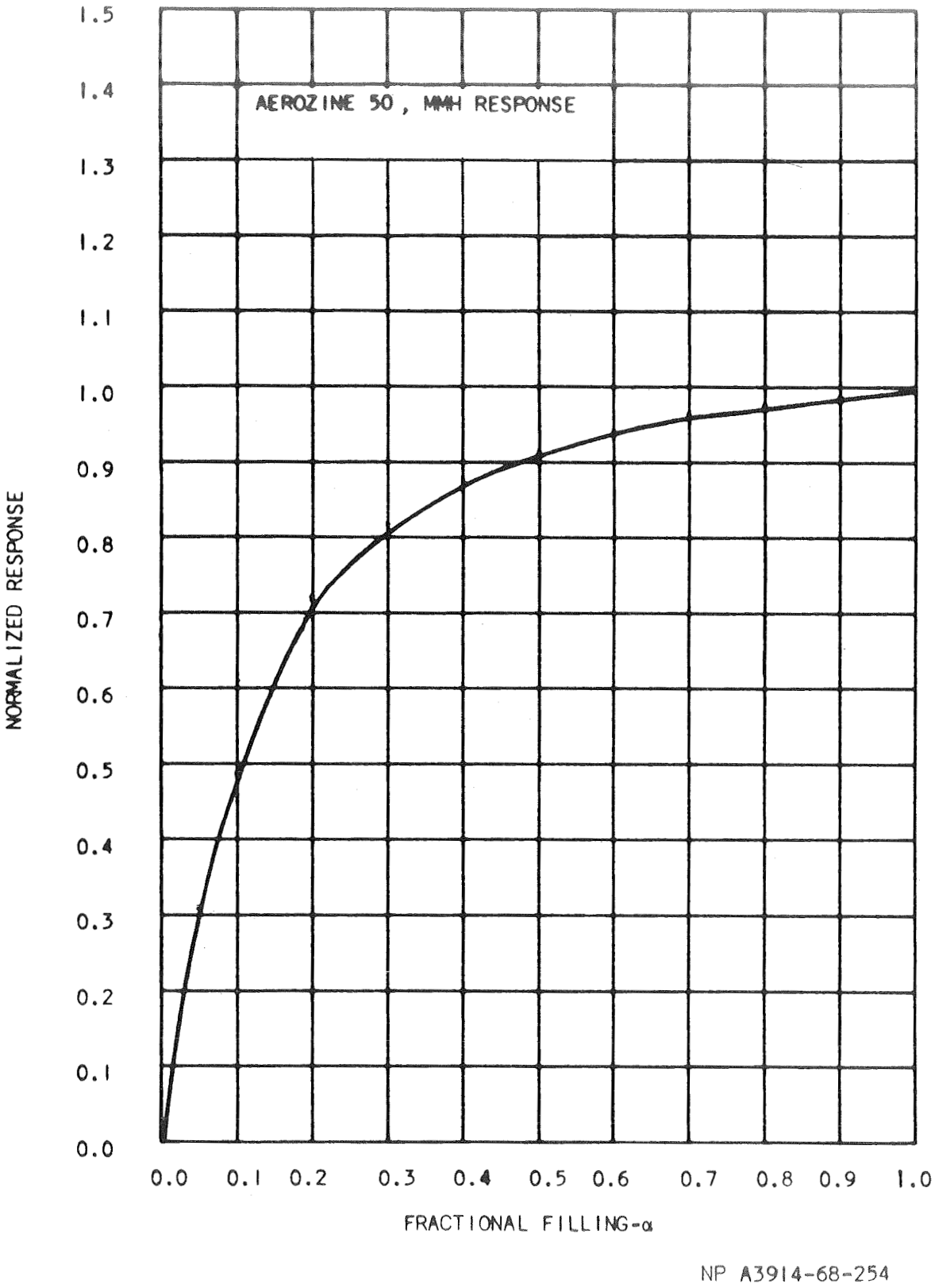
AEROZINE 50, MMH RESPONSE
NORMALIZED RESPONSE
1.5
1.4
1.3
1.2
1.1
1.0
0.9
0.8
0.7
0.6
0.5
0.4
0.3
0.2
0.1
0.0
0.0 0.1 0.2 0.3 0.4 0.5 0.6 0.7 0.8 0.9 1.0
FRACTIONAL FILLING-α
NP A3914-68-254

FIGURE 3-25

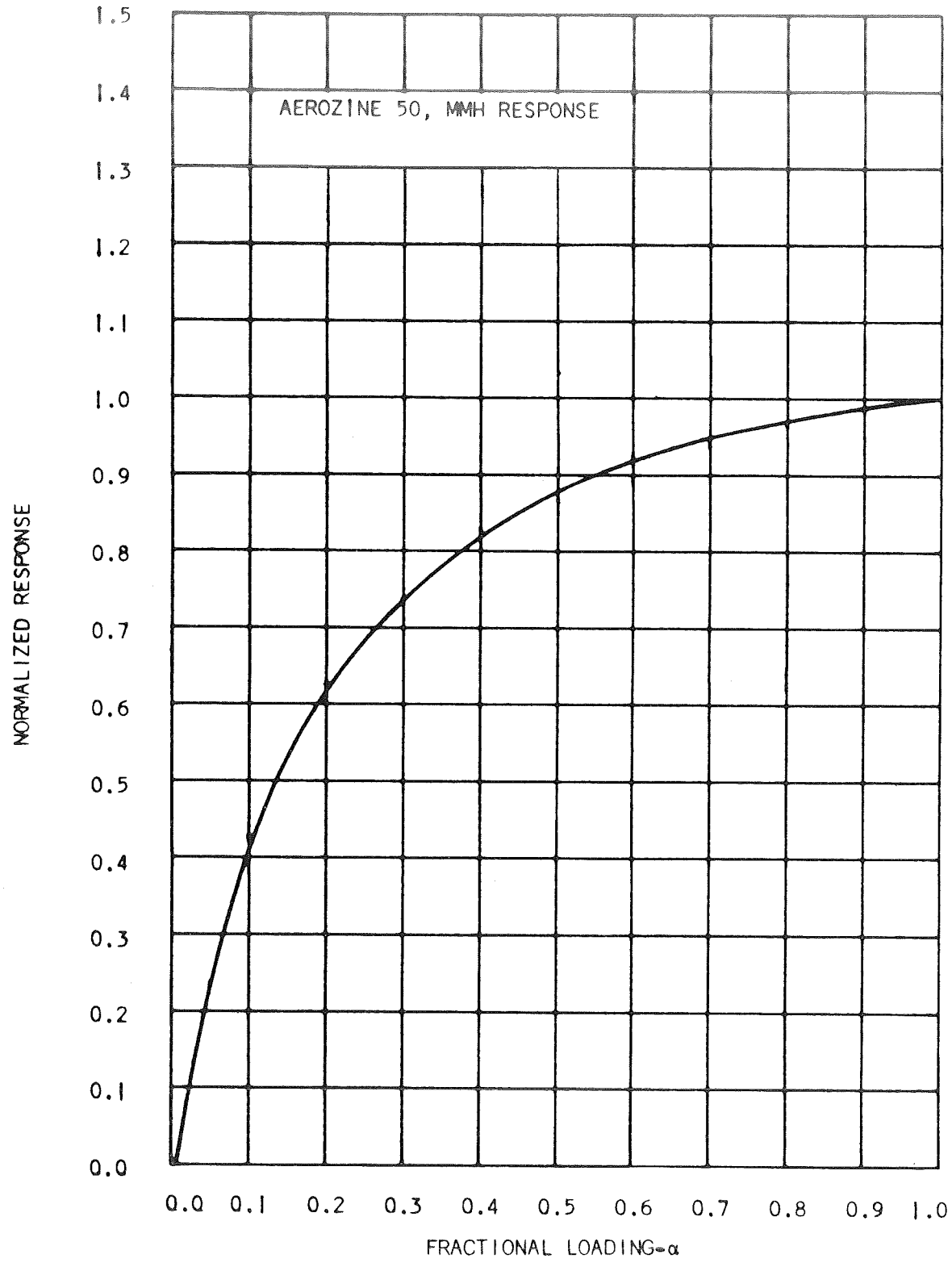
AEROZINE 50, MMH RESPONSE
NORMALIZED RESPONSE
1.5
1.4
1.3
1.2
1.1
1.0
0.9
0.8
0.7
0.6
0.5
0.4
0.3
0.2
0.1
0.0
0.0 0.1 0.2 0.3 0.4 0.5 0.6 0.7 0.8 0.9 1.0
FRACTIONAL LOADING=α
NP A3914-68-251

FIGURE 3-26

SECTION IV

EXPERIMENTAL STUDIES

4.1 INTRODUCTION

This section is an experimental evaluation of the theory outlined in Section III which included 1) A discussion of the techniques needed to perform dielectric properties measurement, and 2) An analysis of three techniques of mass gaging for comparison purposes.

This section contains an analysis of the dielectric measurement tests that were made, followed by the results obtained for loading responses using the above techniques. The most satisfactory technique was pursued in greater depth, to determine its response under reorientation.

4.2 DIELECTRIC PROPERTIES OF PROPELLANTS

The experimental results and a discussion of these results concerning the dielectrical properties of MMH, Aerozine 50 and N_2O_4 are presented in this section. Several different measurement techniques were evaluated with simulant liquids to ascertain their suitability for the actual liquids of interest. One of the techniques in Roberts-Von Hippel technique outlined in Paragraph 3.3.4, Section III, was additionally evaluated with actual fluids.

Tests were also performed to determine the power transmission coefficient for a bladder material sample provided by NASA-MSC. The power transmission coefficients were measured for the case of normally-incident plane waves. The tests were performed in the frequency ranges from 2 to 4 GHz and 8 to 12 GHz. The sample was also tested using a time domain reflectometer in an attempt to measure the voltage reflection coefficient.

4.2.1 Resonant Cavity Method - Pure Fluids

The resonant cavity technique was based on measuring the Q and resonant frequency of a given mode when the cavity is empty and filled with the fluid. A detailed analysis is presented in Paragraph 3.3.4, Section III.

These closed cylinders were made out of aluminum for use with the resonant-cavity method. The dimensions of the cylinders are as follows:

1) 5.906" high and 2.954" diameter

2) 3.704" high and 2.954" diameter

3) 1.476" high and 1.476" diameter

These dimensions were inserted in a computer program, which yielded the resonant frequencies of the first few modes.

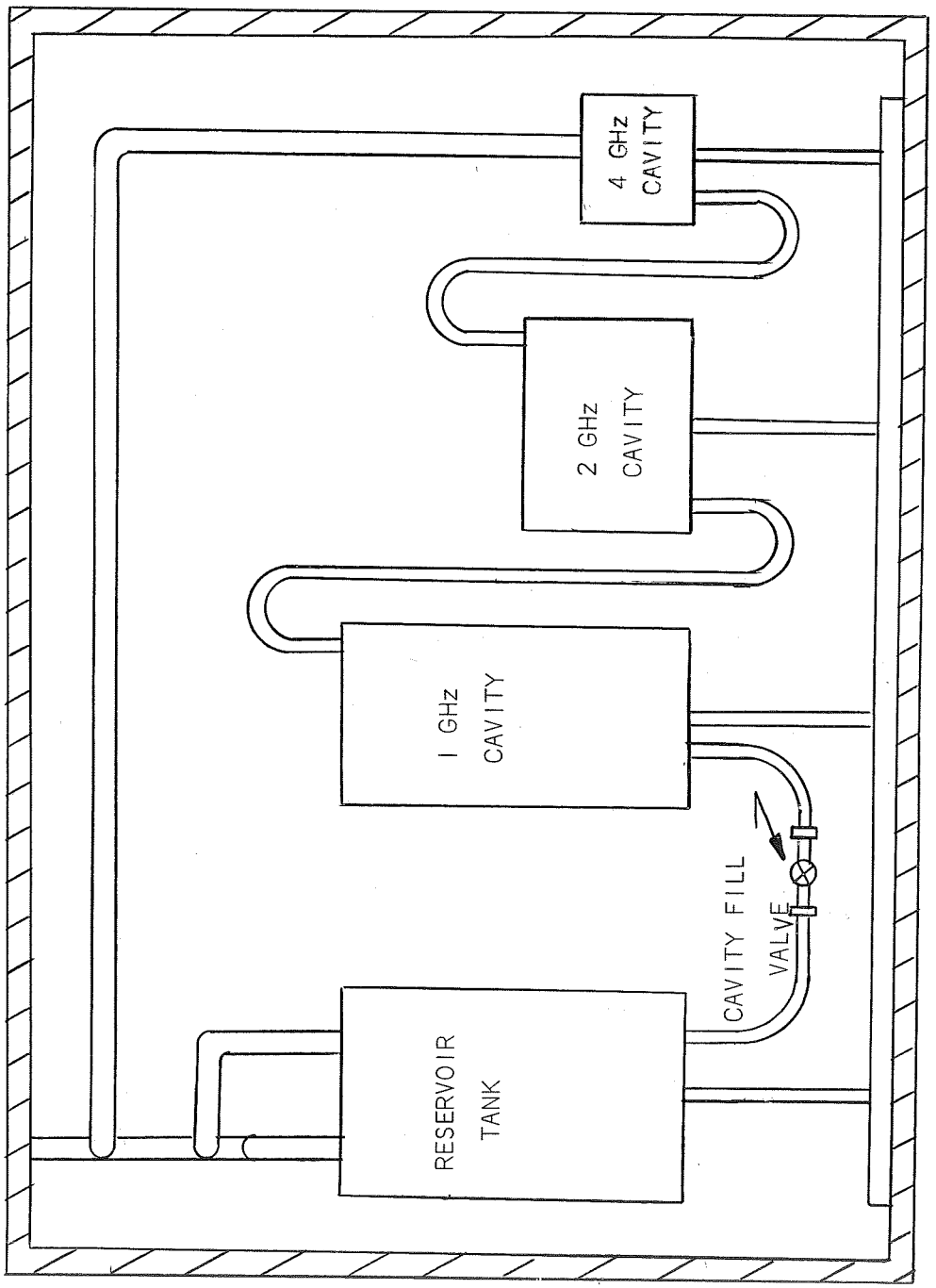

EXPERIMENTAL SETUP FOR RESONANT CAVITY METHOD

FIGURE 4-1

The cavities cover a range from 2.5 GHz to 12 GHz, when excited in the lower order modes. The cavities, together with a reservoir cavity used for keeping the cavities full of fluid were tested in a suitable protected enclosure. See Figure 4-1. The experimental setup is shown in Figure 4-2. It was found that not enough power could be transmitted through the cavities when N_2O_4 or MMH was put into them. When the probe lengths were increased, some power could be transmitted, but the mode pattern was distorted greatly by the resulting overcoupling to the field in the cavity. Because of this, it was decided to abandon this method of measurement.

4.2.2 Resonant Cavity Method - Diluted Fluids

The next method tried was a dilution method outlined in Paragraph 3.3.4, Section III. It is possible for the propellant to be diluted with Freon, which is relatively lossless. To simulate this in the laboratory, experiments were performed with mixtures of Methyl Alcohol and Benzene using the experimental setup shown in Figure 4-2. Mixtures were made of 0.1% alcohol in Benzene. It was found that the 10% solution was too lossy to measure using the resonant cavity technique. On the lower concentration, use of a slotted line with one of the cavities gave the dielectric constant of a sample of industrial Benzene as 2.22 with a loss tangent of 1.54×10^{-4}. Since no more than a few percent concentration of alcohol could be measured, it was decided that extrapolation up to 100% from the measured results would be too inaccurate, and the method was abondoned.

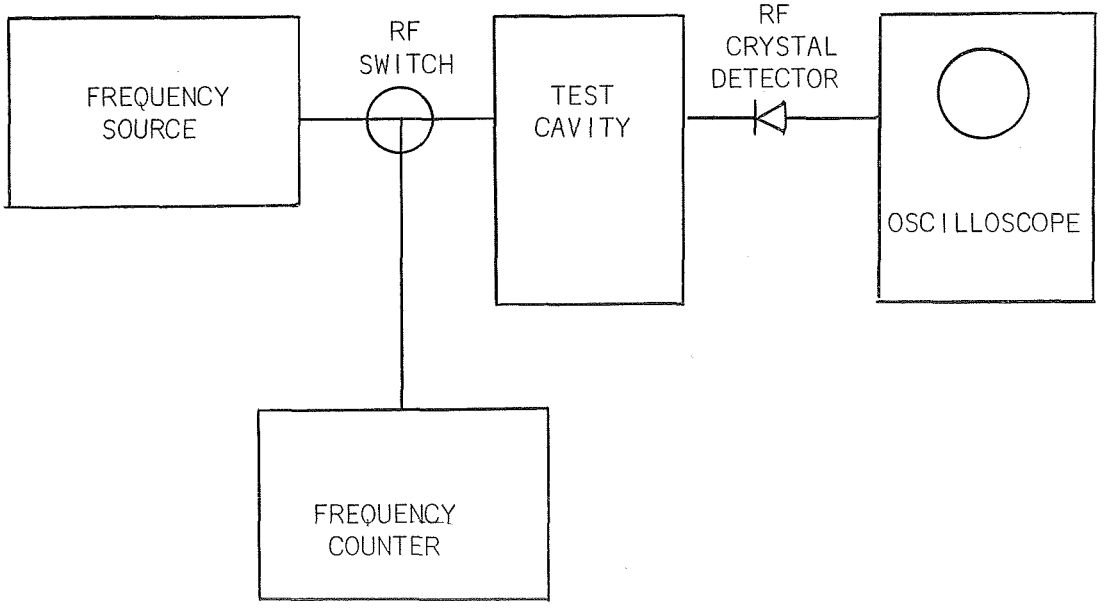

EXPERIMENTAL SETUP FOR DIELECTRIC PROPERTIES MEASUREMENT

FIGURE 4-2

4.2.3 Von Hippel Method

The third method tried was the Roberts-Von Hippel method outlined in Paragraph 3.3.4, Section III. Three X-band waveguide sections were made up in brass. They were 1/2", 3/8" and 1/10" in length, and had normal waveguide flanges. The sections were each in turn connected to the end of a slotted line, and a short circuit plate was connected to the other end of the small section (Figure 3-6, Section III). The VSWR was then measured using the twice-minimum method used by Von Hippel, and the position of the minimum was then noted. The section was then filled with the test liquid, and a thin mica sheet was used to seal the section. The new VSWR and minimum positions were noted. From these measurements, the dielectric constant and loss tangent were calculated. The dielectric constant of Benzene was measured to within ± 10% of the value obtained from the suppliers. For a given sample of Transformer Oil, both the 1/2" and 3/8" sections gave the dielectric constant as 1.96 ± 0.01 with a loss tangent of 0.002 at 6.7 GHz.

Experimental data was taken for other liquids such as Methyl Alcohol (dielectric constant ~ 20) and Ethylene Glycol (dielectric constant ~ 12). These liquids were chosen because their electrical properties are similar to the propellants in question.

These liquids were chosen because their electrical properties are similar to the propellants in question. The relevant data for 3/8" sample of Methyl Alcohol, measured in the 2 GHz to 4 GHz region is shown in Table 4-1 and the calculated dielectric constant and loss tangent is shown in Figures 4-3a and 4-3b. The measured variation in dielectric constant follows quite closely that of Figure 3-3, Section III. This preliminary experimentation, coupled with the fact that much experimentation with materials having dielectric constants and loss tangents over the range of interest has been performed by Von Hippel, shows that the technique is useable. Some experimental procedures and the data processing need to be refined, but no major obstacles to the use of the technique are foreseen.

4.2.4 Dielectric Properties of Bladder Material

The power transmission coefficients of the bladder material supplied by the NASA-MSC were measured for the case of normally incident plane waves. This bladder material was measured to determine if its presence would have any effect on the distribution of electromagnetic energy in the propellant tanks.

For the tests in the 2 to 4 GHz frequency range, the sample was mounted in a coaxial holder as shown in Figure 4-4. A block diagram is shown in Figure 4-5.

TABLE 4-I

STANDING WAVE RATIO DATA FOR 3/8" SPACER
FOR METHYL ALCOHOL, IN THE 2-4 GHz REGION

FREQUENCY	3 dB ABOVE MINIMUM HIGHER READING	3 dB ABOVE MINIMUM LOWER READING	3 dB ABOVE MINIMUM HIGHER READING	3 dB ABOVE MINIMUM LOWER READING
2.40	16.42	15.92	16.60	16.51
2.45	17.74	17.20	18.05	17.97
2.50	19.13	18.49	19.51	19.30
2.55	20.42	19.61	20.84	20.58
2.60	21.53	20.90	22.00	21.73
2.65	22.65	22.00	23.02	22.83
2.70	23.60	22.99	23.99	23.86
2.75	24.52	23.97	24.83	24.73
2.80	25.37	24.86	25.78	25.62
2.85	26.20	25.69	26.50	26.39
2.90	27.00	26.47	27.27	27.19
2.95	27.76	27.21	28.01	27.95
3.00	28.41	27.93	28.73	28.68
3.05	29.12	28.59	29.44	29.38
3.10	29.77	29.28	30.13	30.08
3.15	30.40	29.91	30.81	30.74
3.20	31.00	30.49	31.46	31.40
3.25	31.61	31.10	32.12	32.02
3.30	32.22	31.69	32.73	32.67
3.35	28.33	27.88	33.33	33.28
3.40	29.01	28.38	33.95	33.85
3.45	25.33	24.63	34.51	34.45
3.50	26.05	25.30	35.04	34.99
3.55	26.78	25.93	35.58	35.52
3.60	27.47	26.57	36.08	36.01
3.65	28.17	27.13	36.55	36.49
3.70	28.53	27.95	36.98	36.93
3.75	29.06	28.56	37.42	37.38
3.80	29.38	28.88	37.83	37.79
3.85	30.10	29.60	38.25	38.20
3.90	30.55	30.12	38.64	38.60
3.95	31.03	30.50	39.88	39.83

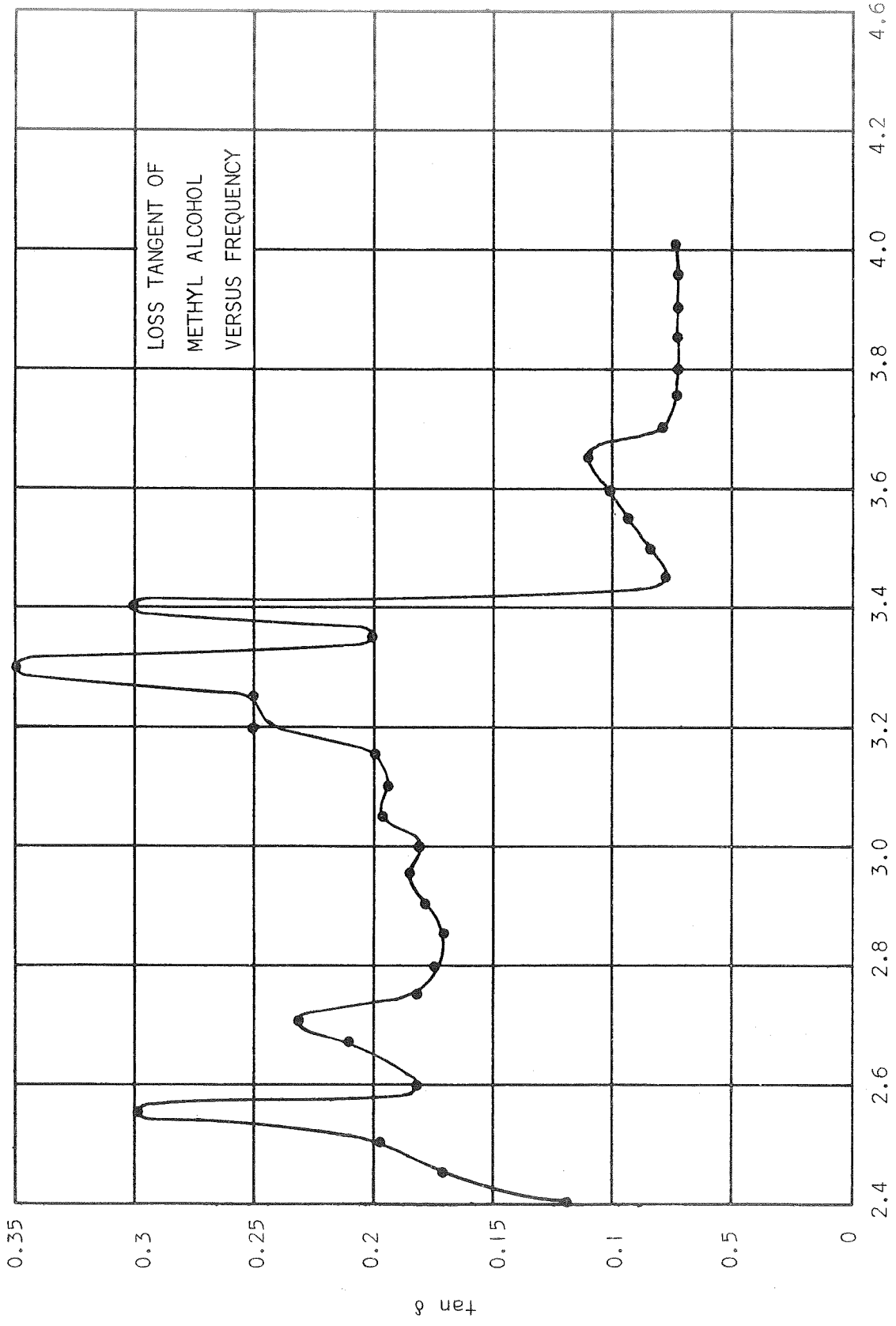
LOSS TANGENT OF
METHYL ALCOHOL
VERSUS FREQUENCY
tan δ
0.35
0.3
0.25
0.2
0.15
0.1
0.5
0
2.4
2.6
2.8
3.0
3.2
3.4
3.6
3.8
4.0
4.2
4.6
FREQUENCY (GHz)
A3914-68-225-1

FIGURE 4-3a

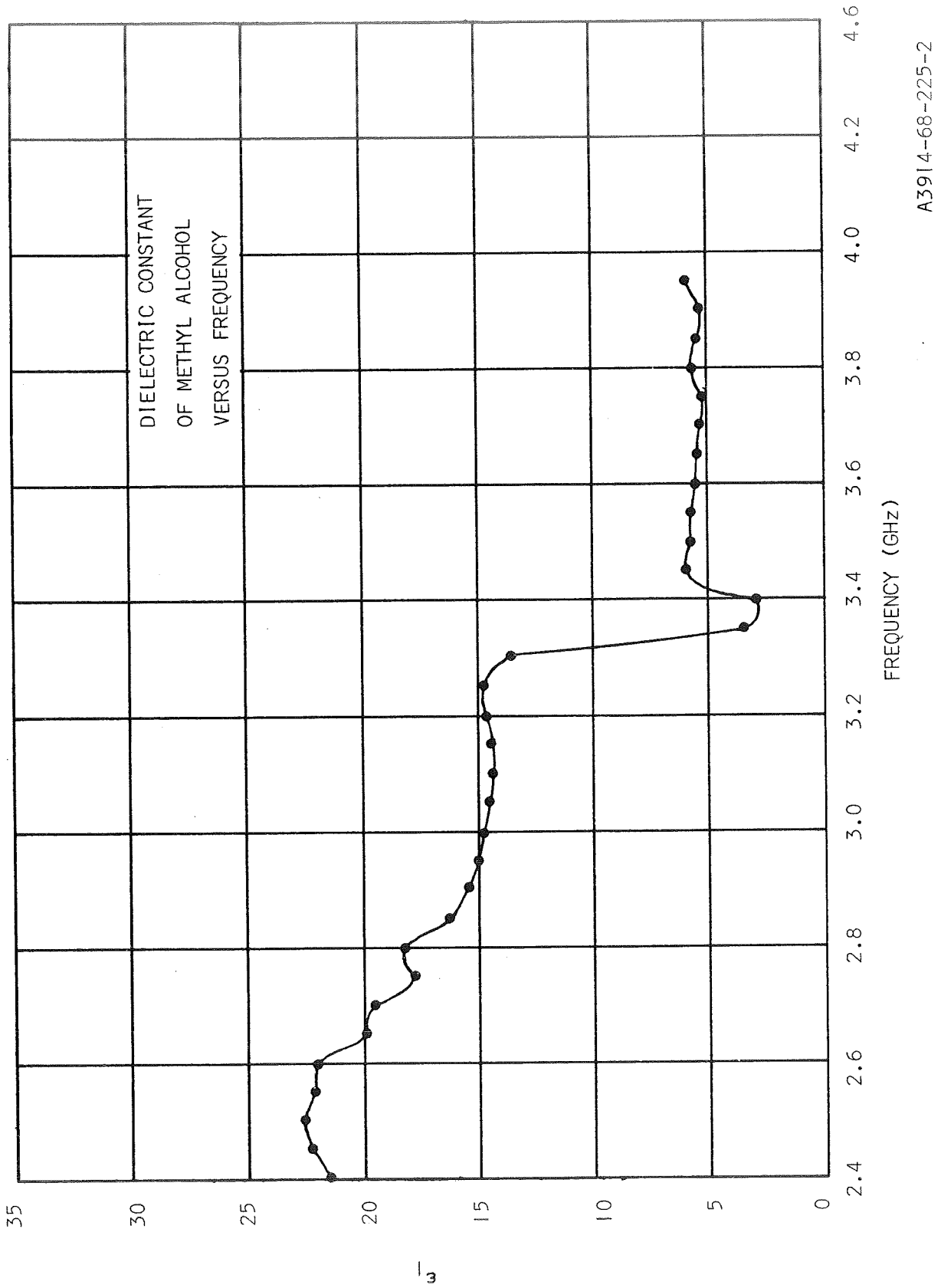
DIELECTRIC CONSTANT
OF METHYL ALCOHOL
VERSUS FREQUENCY
35
30
25
20
15
10
5
0
2.4
2.6
2.8
3.0
3.2
3.4
3.6
3.8
4.0
4.2
4.6
FREQUENCY (GHz)
A3914-68-225-2

FIGURE 4-3b

The measurements were performed by a substitution method wherein the power level was set by inserting a sample-free holder in the circuit, then the sample was placed in the system and the transmitted power measured. It was estimated that this technique would measure a loss of less than 0.1 dB quite accurately. The experimental results are presented in Table 4-2.

TABLE 4-2

TRANSMITTED POWER FOR A FREQUENCY RANGE OF 2 TO 4 GHz

FREQUENCY GHz	POWER LEVEL dBm	TRANSMITTED POWER dBm	LOSS dB
2.0	+5.0	+5.0	<0.1 dB
2.2	+5.0	+5.0	<0.1 dB
2.4	+5.0	+5.0	<0.1 dB
2.6	+5.0	+5.0	<0.1 dB
2.8	+5.0	+5.0	<0.1 dB
3.0	+5.0	+5.0	<0.1 dB
3.2	+5.0	+5.0	<0.1 dB
3.4	+5.0	+5.0	<0.1 dB
3.6	+5.0	+5.0	<0.1 dB
3.8	+5.0	+5.0	<0.1 dB
4.0	+5.0	+5.0	<0.1 dB

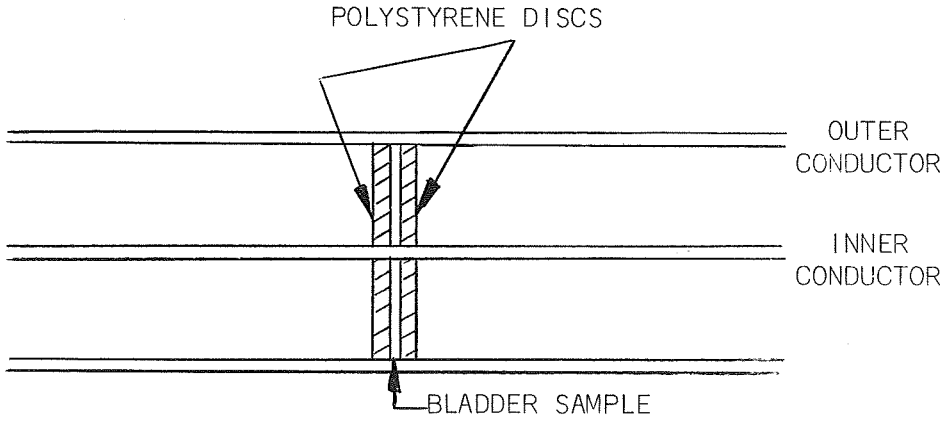

COAXIAL HOLDER FOR BLADDER SAMPLE - 2 TO 4 GHz FREQUENCY RANGE

FIGURE 4-4

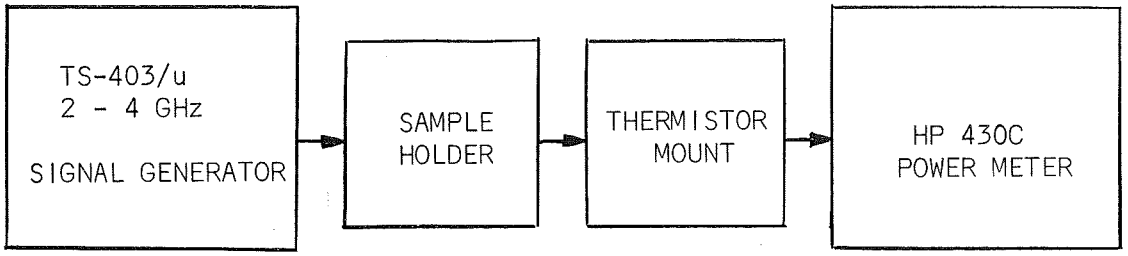

BLOCK DIAGRAM FOR EXPERIMENTAL SETUP - 2 TO 4 GHz FREQUENCY RANGE

FIGURE 4-5

For the tests in the 8-12 GHz frequency range, the sample was mounted in a holder fashioned from X-band waveguide. The sample was held in place between two X-band waveguide cover flanges as shown in Figure 4-6. The experimental setup used is shown in Figure 4-7.

Again, the basic process by which the power transmission coefficient was to be measured was to substitute a sample bearing holder into the circuit after a measurement using a sample-free holder has been accomplished. As before, a loss of less than 0.1 dB should be measurable. The experimental results are presented in Table 4-3.

TABLE 4-3

ATTENUATION CHARACTERISTICS OF BLADDER SAMPLE

FREQUENCY GHz	NO SAMPLE		WITH SAMPLE		LOSS dB
	P_1 dBm	P_2 dBm	P_1 dBm	P_2 dBm	
8.194	7.63	6.33	7.60	6.30	---
9.000	8.40	7.70	8.40	7.70	---
10.000	9.60	7.70	9.59	7.68	0.01
11.003	9.32	9.08	9.32	9.08	---
12.002	8.95	8.05	8.95	8.05	---

The coaxial sample holder was used in an effort to determine the voltage reflection coefficient by means of the time domain reflectometer. The results of the test indicated that the voltage reflection coefficient of the bladder material is virtually immeasurable. It was concluded that from the results of the power transmission tests and the voltage reflection test that the bladder material was transparent to microwave energy in the 2 to 8 GHz frequency region.

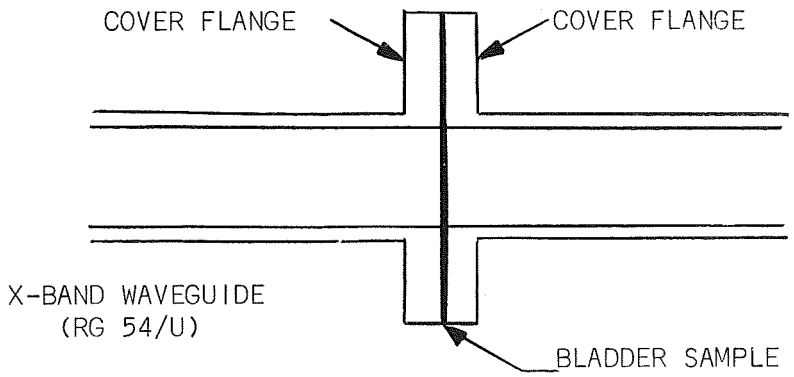

HOLDER FOR BLADDER - 8 TO 12 GHz FREQUENCY RANGE

FIGURE 4-6

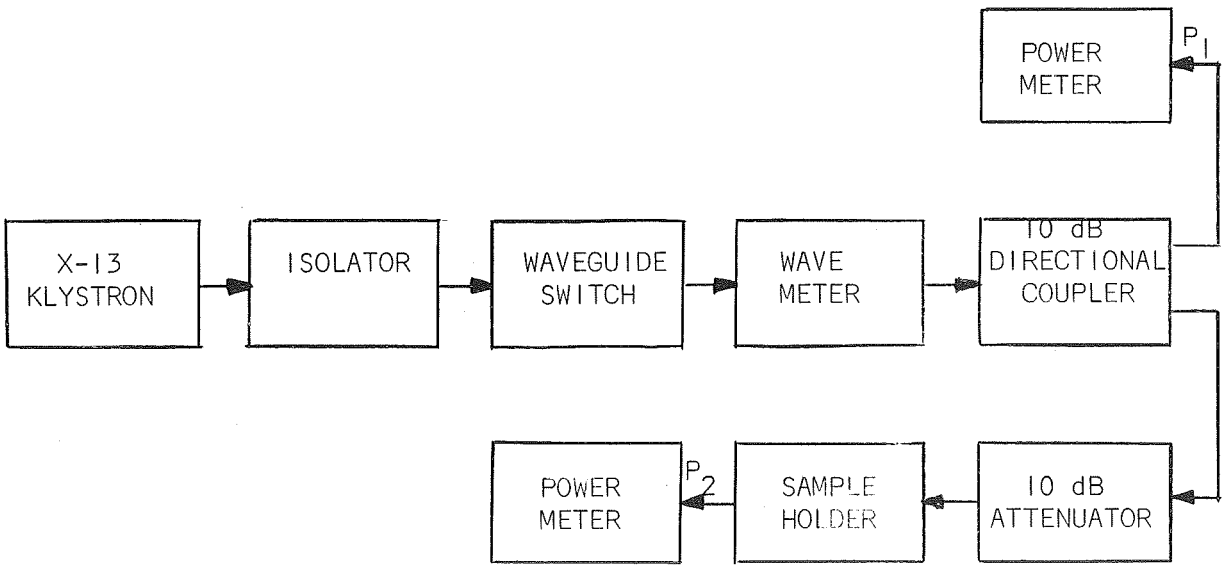

BLOCK DIAGRAM OF EXPERIMENTAL SETUP - 8 TO 12 GHz FREQUENCY RANGE

FIGURE 4-7

4.3 TECHNIQUE A EXPERIMENTATION

Experimentation on the technique A outlined in Paragraph 3.4.1, Section III, was directed toward verifying predicted system response to fluid mass.

4.3.1 Tests Conducted

Preliminary system tests were initiated to obtain uniform illumination of the cavity interior. The experimental setup is shown in Figure 4-8. The probe type antenna was then chosen for further tests. A propellant simulant, Transformer Oil Type 10C, was then used in the cavity in order to optimize the system response range. The properties of Transformer Oil (Type 10C) are in correspondence with those of N_2O_4.

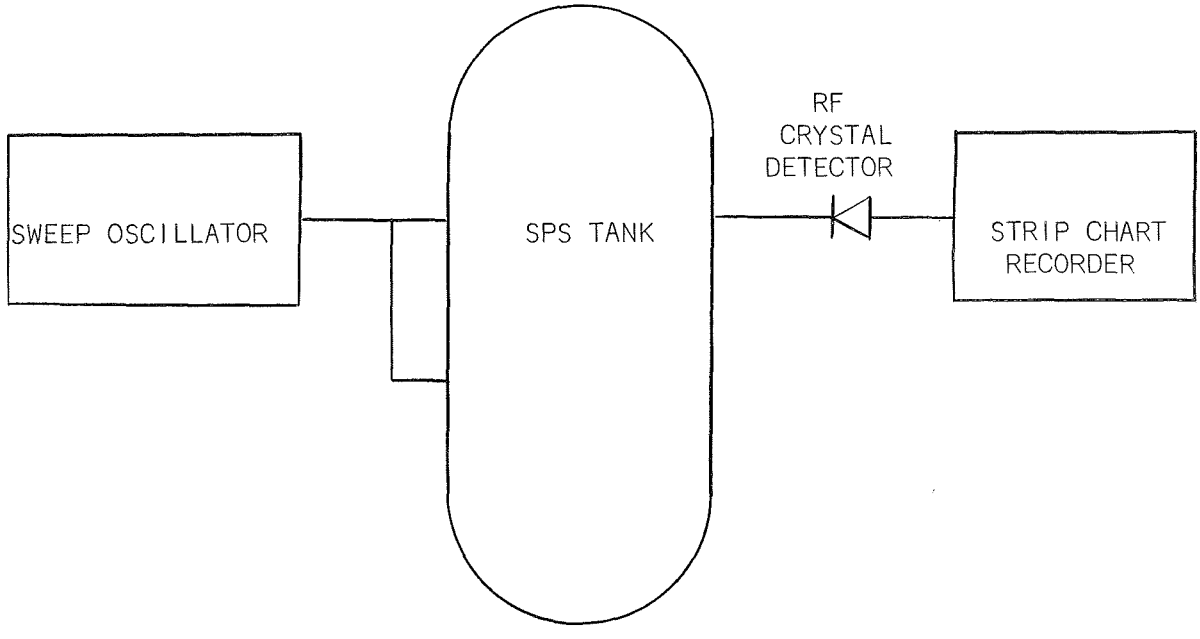

EXPERIMENTAL SETUP FOR PRELIMINARY
SYSTEM TESTS ON THE MODE COUNT TECHNIQUE

FIGURE 4-8

A series of tests were run with the scale model SPS tank with the internal hardware. The results of the partial loadings are shown in Figure 4-10 which correlates with the theoretical curve of Figure 3-27, Section III of this report.

A loading test was conducted for 10% incremental loading of Transformer Oii. The desired response was obtained for the tank in the vertical horizontal and inverted positions. Figure 4-9 shows the experimental setup used. The data obtained is shown in Table 4-4 and the average value of the response is plotted in Figure 4-10. Table 4-5 shows the response various angular positions for a 50% filling.

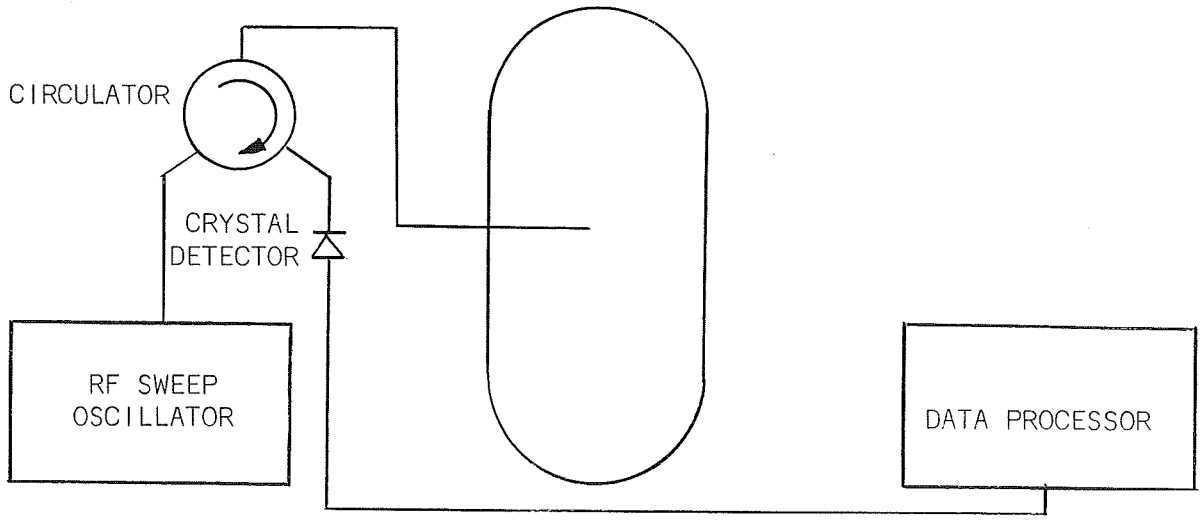

SINGLE ANTENNA EXPERIMENTAL SYSTEM

FIGURE 4-9

TABLE 4-4

LOADING DEPENDENCE - SPS TANK EXCLUSIVE OF INTERNAL HARDWARE

FRACTIONAL FILLING	RESPONSE		
	VERTICAL	HORIZONTAL	INVERTED
0.0	265	265	265
0.1	173	159	162
0.2	152	132	133
0.3	123	114	112
0.4	111	100	98
0.5	104	96	93
0.6	102	83	90
0.7	91	90	86
0.8	90	82	75
0.9	99	84	80
1.0	78	78	78

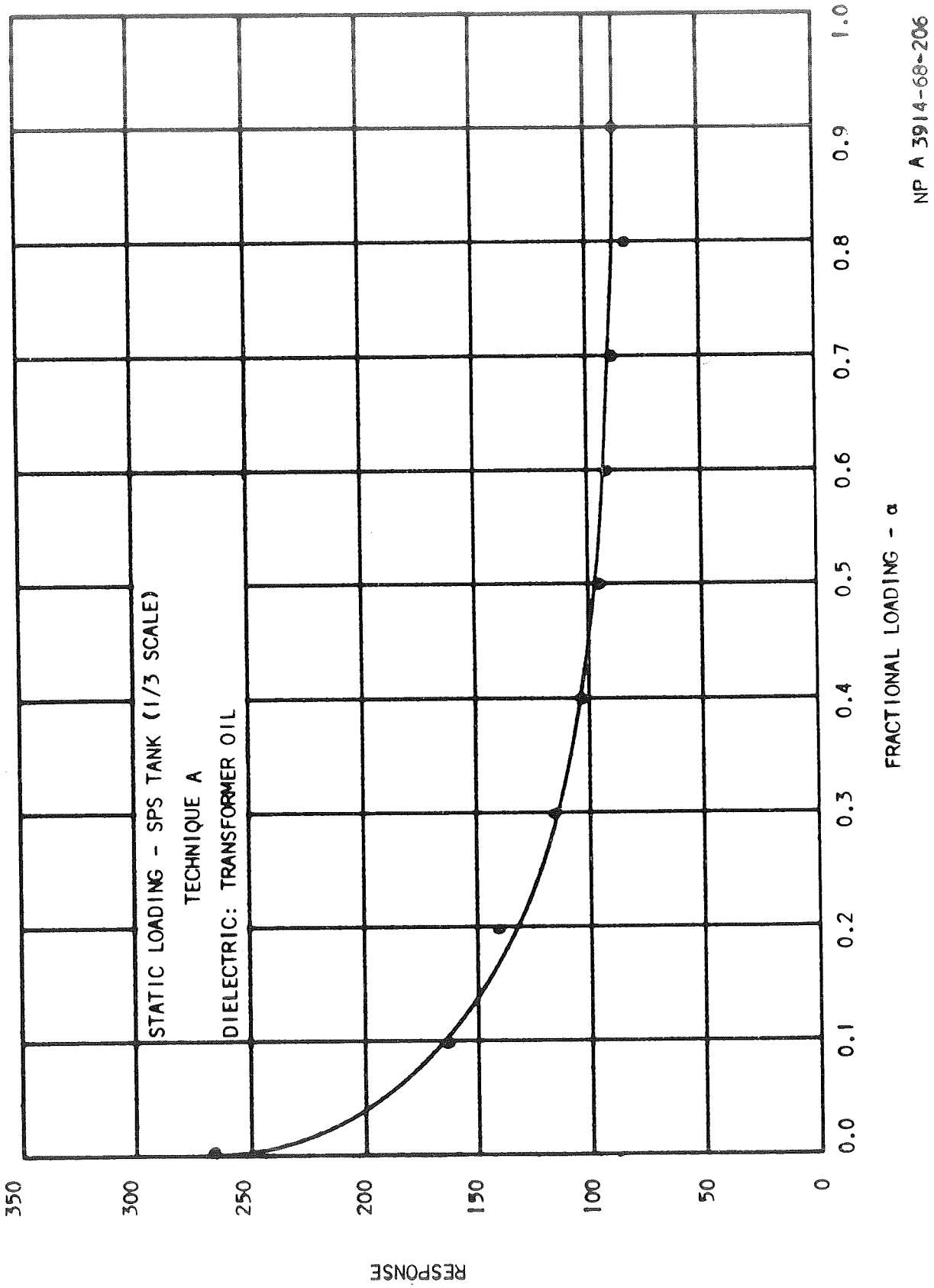
STATIC LOADING - SPS TANK (1/3 SCALE)
TECHNIQUE A
DIELECTRIC: TRANSFORMER OIL
RESPONSE
350
300
250
200
150
100
50
0
0.0
0.1
0.2
0.3
0.4
0.5
0.6
0.7
0.8
0.9
1.0
FRACTIONAL LOADING - α
NP A 3914-68-206

FIGURE 4-10

TABLE 4-5

RESPONSE FOR A 50% LOADING TANK AT VARIOUS ANGULAR POSITIONS TO VERTICAL

ANGULAR POSITION (DEGREES)	RESPONSE
10	107
30	116
45	113
60	104
75	105

The tank was then assembled with all its internal perturbations to study the effect of the perturbations on the response. The tank was set up such that uniform tank illumination was obtained. Table 4-6 shows the response obtained.

TABLE 4-6

LOADING DEPENDENCE - SPS TANK INCLUSIVE OF ALL INTERNAL HARDWARE

FRACTIONAL FILLING	RESPONSE HORIZONTAL	VERTICAL	INVERTED
0.0	235	235	235
0.1	187	169	181
0.2	142	131	127
0.3	116	115	99
0.4	112	104	97
0.5	100	99	94
0.6	92	88	78
0.7	80	70	70
0.8	77	67	76
0.9	73	62	77
1.0	72	70	72

4.3.2 Discussion

In comparison with the response of the matched tank without internal perturbations, the above table was in close agreement, even though the volume was reduced by approximately 15% due to the internal perturtations.

The response of the empty tank yielded response indicative of the new volume. However, the response shown in Figure 4-12 was comparable to the expected response with a loss sensitivity beyond the 40% fill point.

4.4 TECHNIQUE B

On the basis of the analysis outlined in Paragraph 3.4.3, Section III, experiments were conducted to study the response obtained from Technique B. Testing was performed on a limited basis with Transformer Oil as a simulant for N_2O_4 to verify the theoretical predictions outlined in Section III.

4.4.1 Tests Conducted

Preliminary tests were conducted to confirm the optimum response. These tests were conducted with the experimental setup in Figure 4-11, over various frequency bands and the results are shown in Figures 4-13 through 4-16. The general trend of the curves shows a high sensitivity for small partial fillings but no sensitivity at higher fillings. The discontinuities present in the response are attributed to the fact that the illumination was not yet uniform.

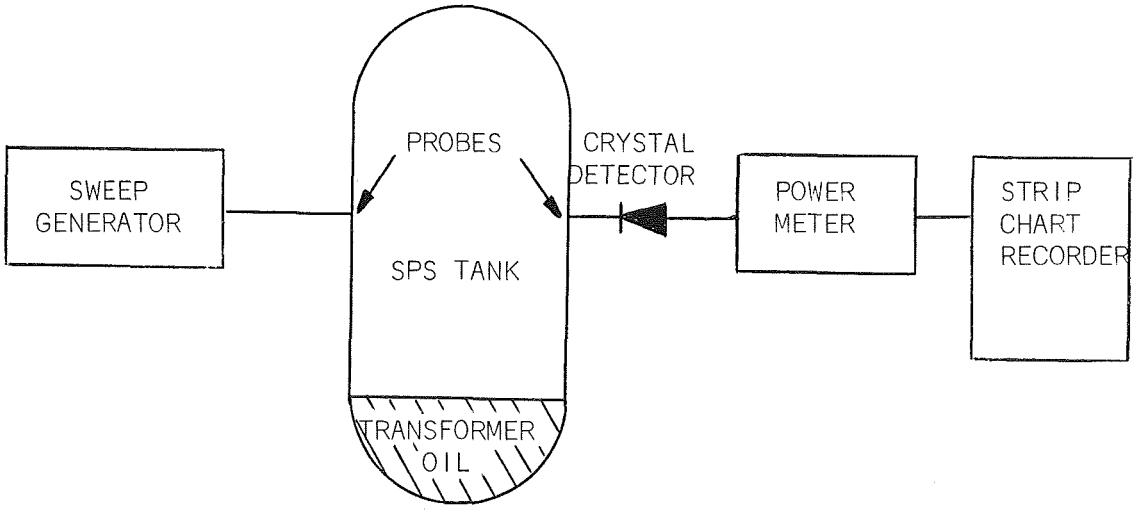

EXPERIMENTAL SETUP FOR POWER ABSORPTION MEASUREMENTS ON SPS TANK

FIGURE 4-11

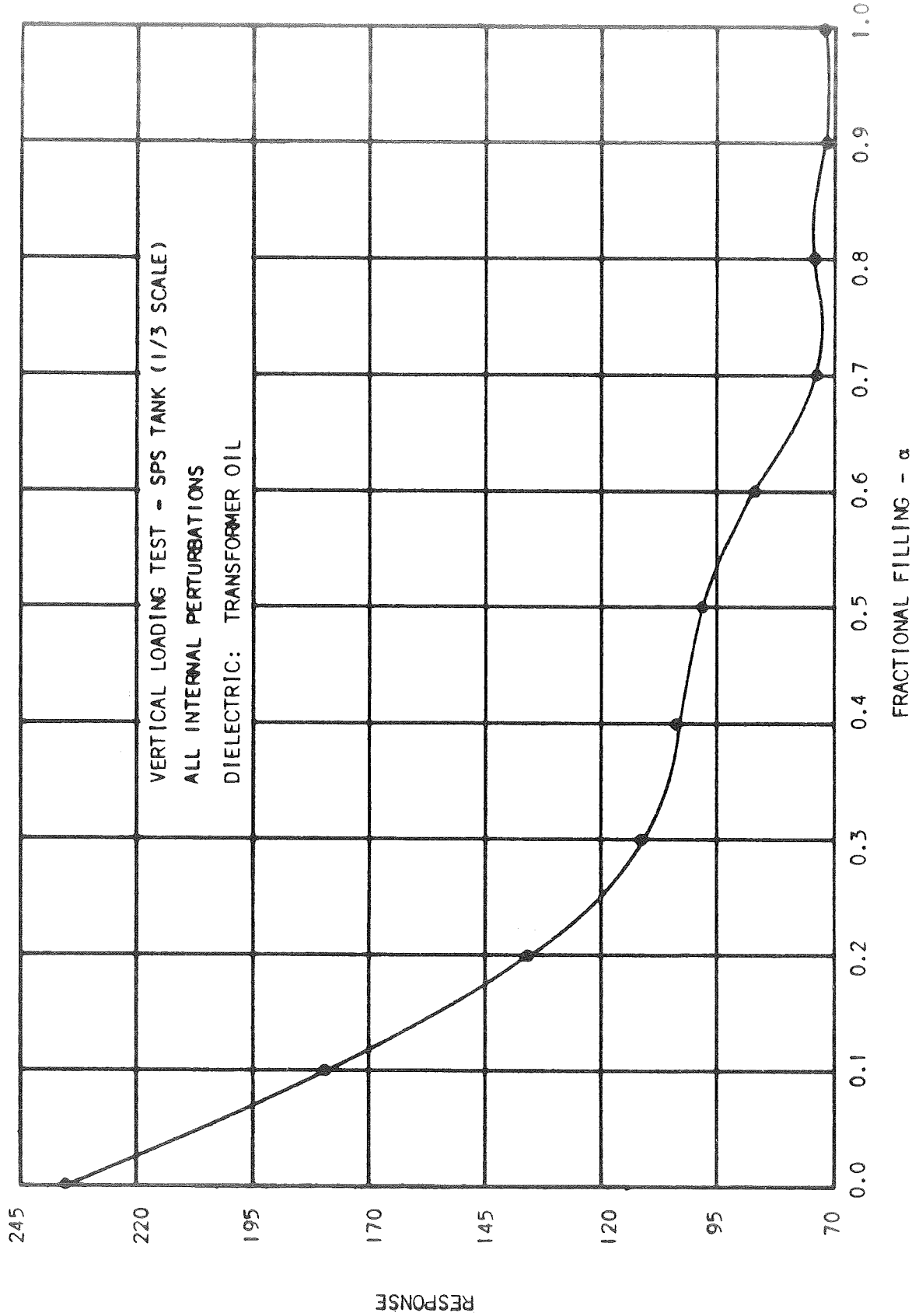
VERTICAL LOADING TEST - SPS TANK (1/3 SCALE)
ALL INTERNAL PERTURBATIONS
DIELECTRIC: TRANSFORMER OIL
RESPONSE
245
220
195
170
145
120
95
70
0.0
0.1
0.2
0.3
0.4
0.5
0.6
0.7
0.8
0.9
1.0
FRACTIONAL FILLING - α

FIGURE 4-12

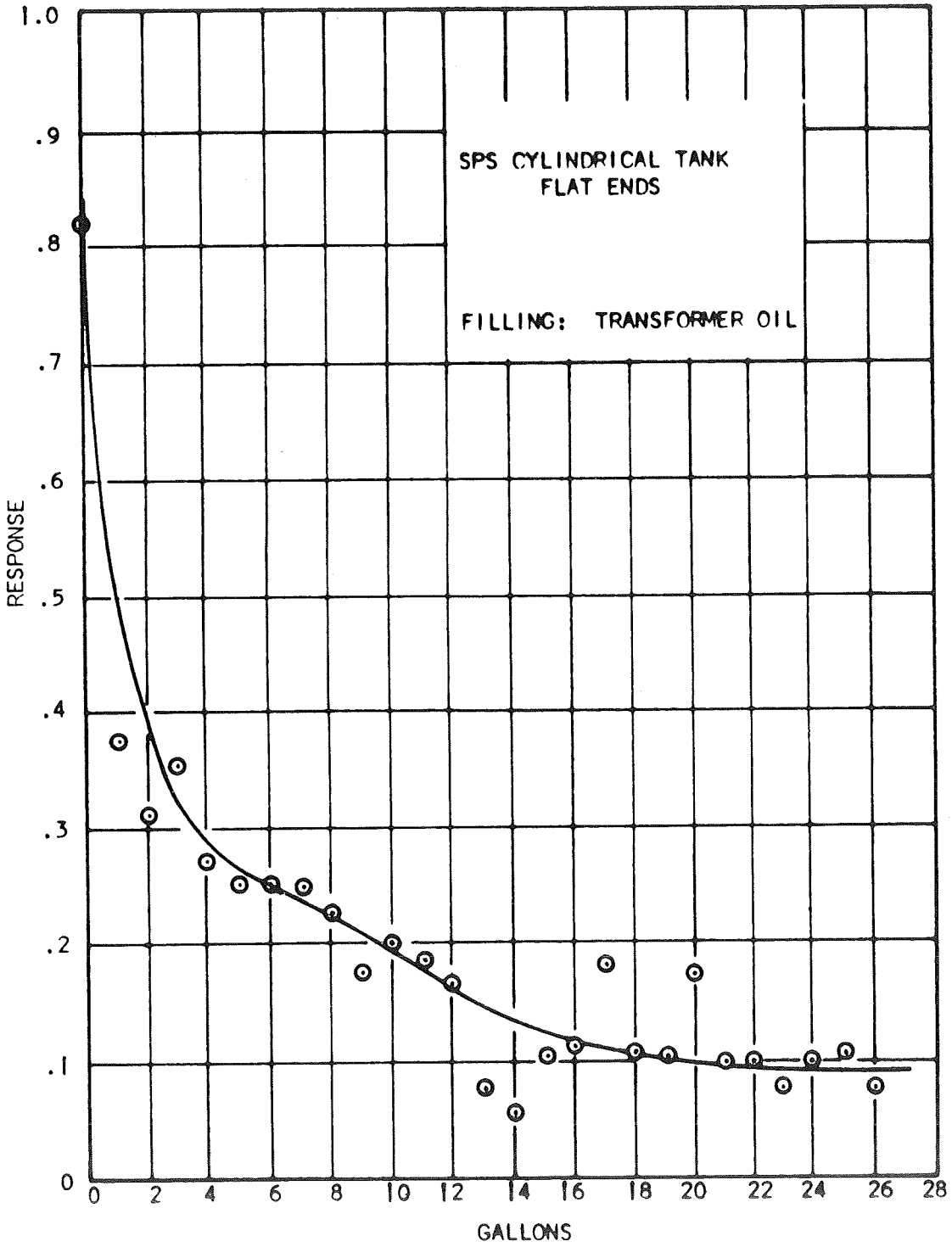

NP A-3914-68-261

FIGURE 4-13

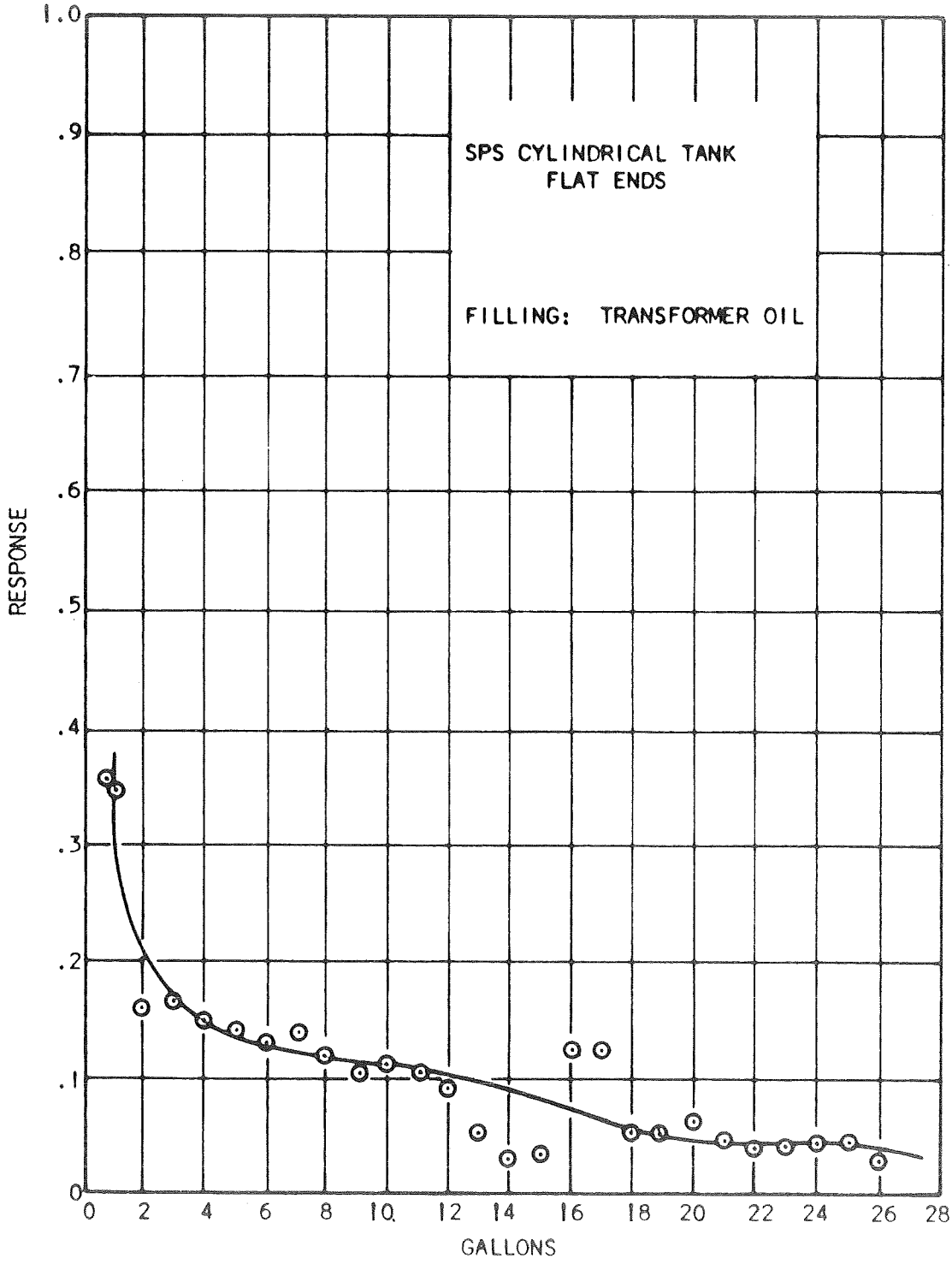

FIGURE 4-14

NP A-3194-68-262

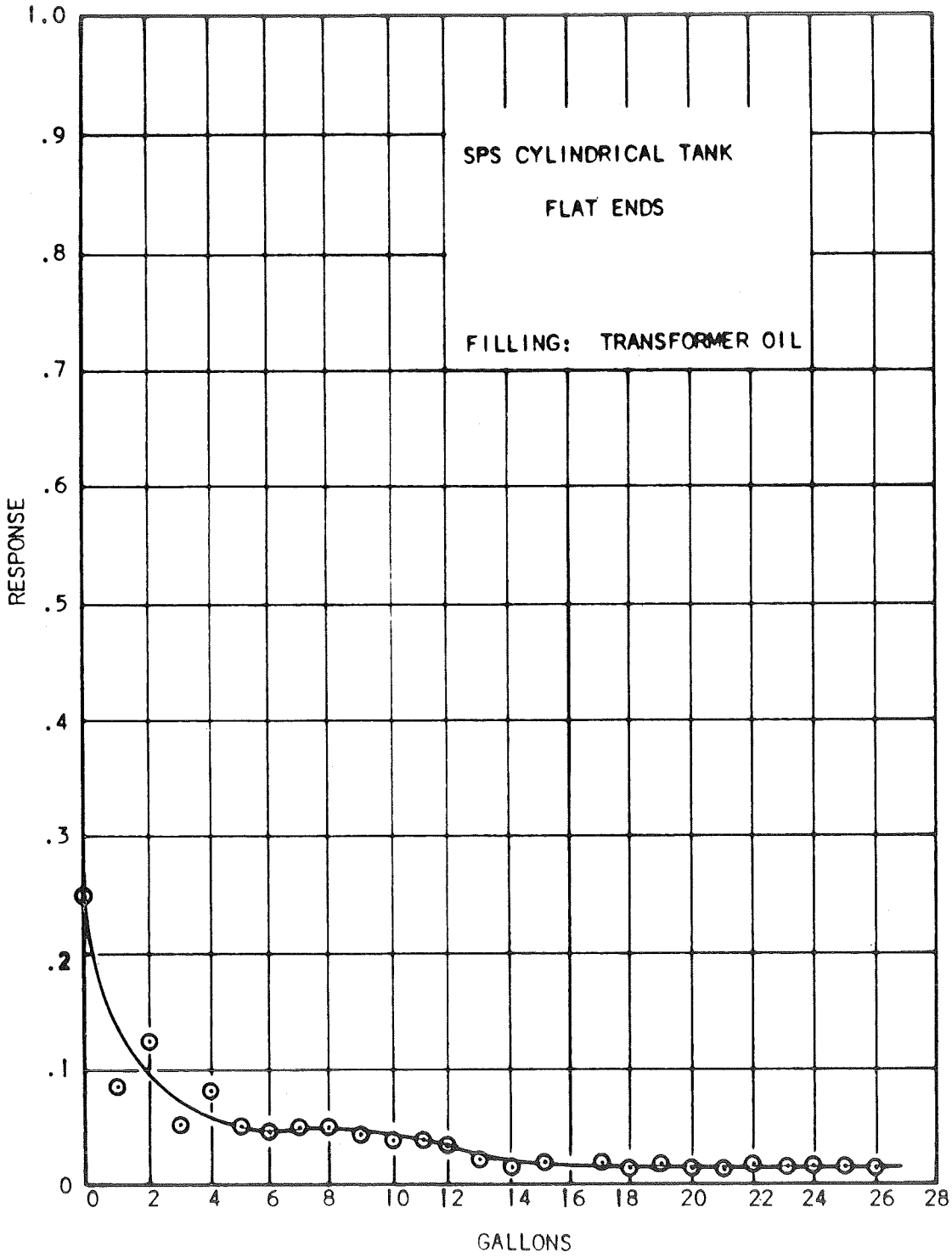

NP A-3914-68-263

FIGURE 4-15

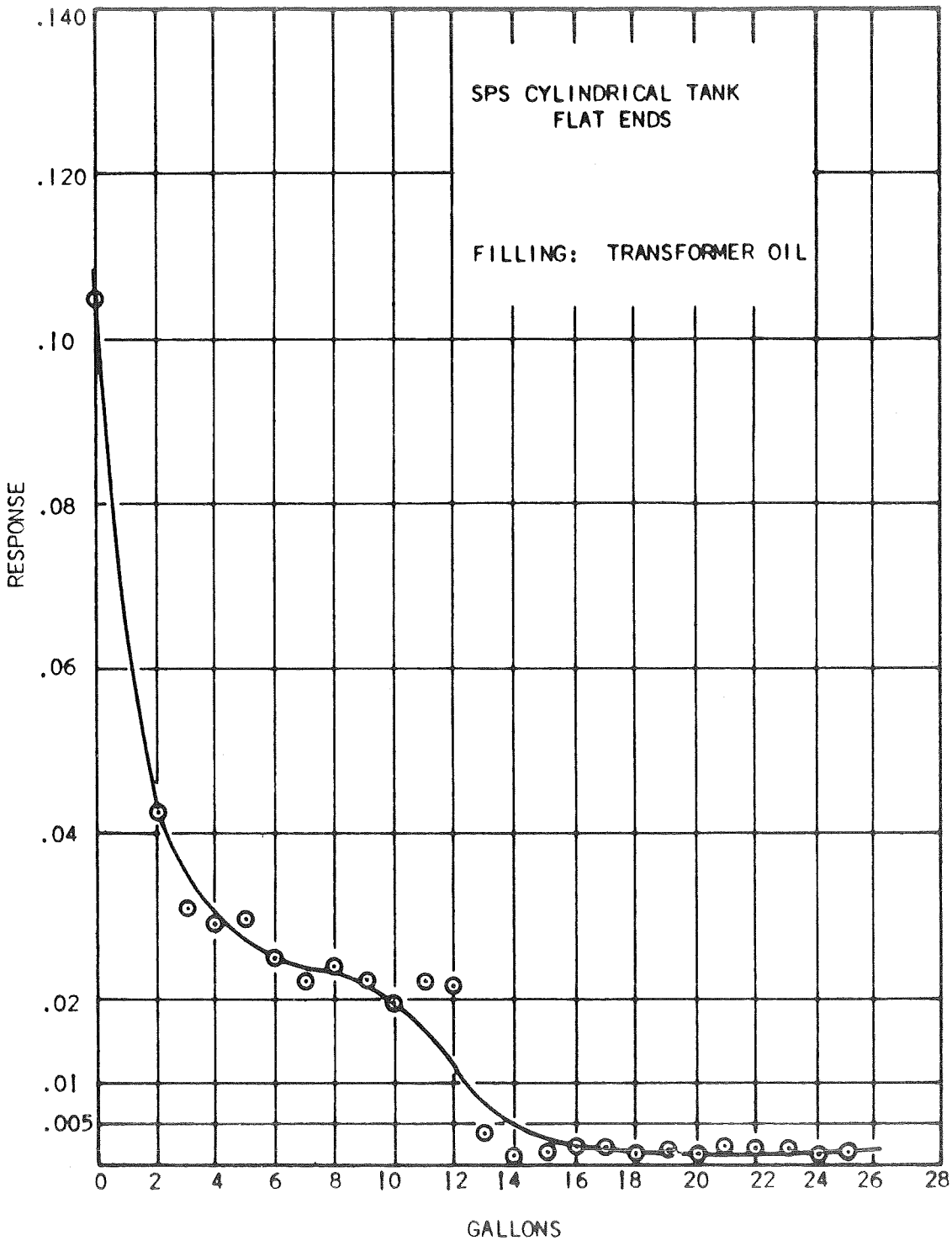

FIGURE 4-16

NP A-3914-68-264

A probe antenna was used, and the tank positioned in a manner such that the probe was out of liquid at all times. The results of the experiment are shown in Table 4-7.

TABLE 4-7

STATIC LOADING TEST-SPS TANK
TECHNIQUE B

FRACTIONAL FILLING	RESPONSE
0.0	117.0
0.1	102.0
0.2	96.0
0.3	94.4
0.4	92.8
0.5	91.3
0.6	90.5
0.7	86.4
0.8	86.4
0.9	83.2

4.4.2 Discussion

The response is shown in Figure 4-17. It is apparent from Figures 4-12 and 4-18 that the response was similar to the Technique A, with a loss of sensitivity for loadings above 30%.

The response for N_2O_4 would be of the same form with a sensitivity improved to a small extent. However, the response for MMH and Aerozine 50 would not be of any different nature than the response shown in Figure 4-17. This statement is made from a comparison of the predicted response of N_2O_4 and Aerozine 50 or MMH. If reference is made to the theory Technique B (Paragraph 3.4.3, Section III) the response for all these propellants is nearly the same. Thus, no real difference should be expected between the response of the system to these three fluids. Differences could possibly show up if a more exact analysis is made, but it is not expected that a significant difference between the more exact and approximate theory would be found. This is founded on the comparison of the general form of the approximate theory and the experimental results, which both show a decrease in system sensitivity at higher fractional fillings.

4.5 TECHNIQUE C

On the basis of the theory outlined in Paragraph 3.6, Section III, experiments were conducted to prove the feasibility of Technique C. A determination of the overall system response to fluid loading and the proper tank illumination for reorientation of the tank were the experimental goals.

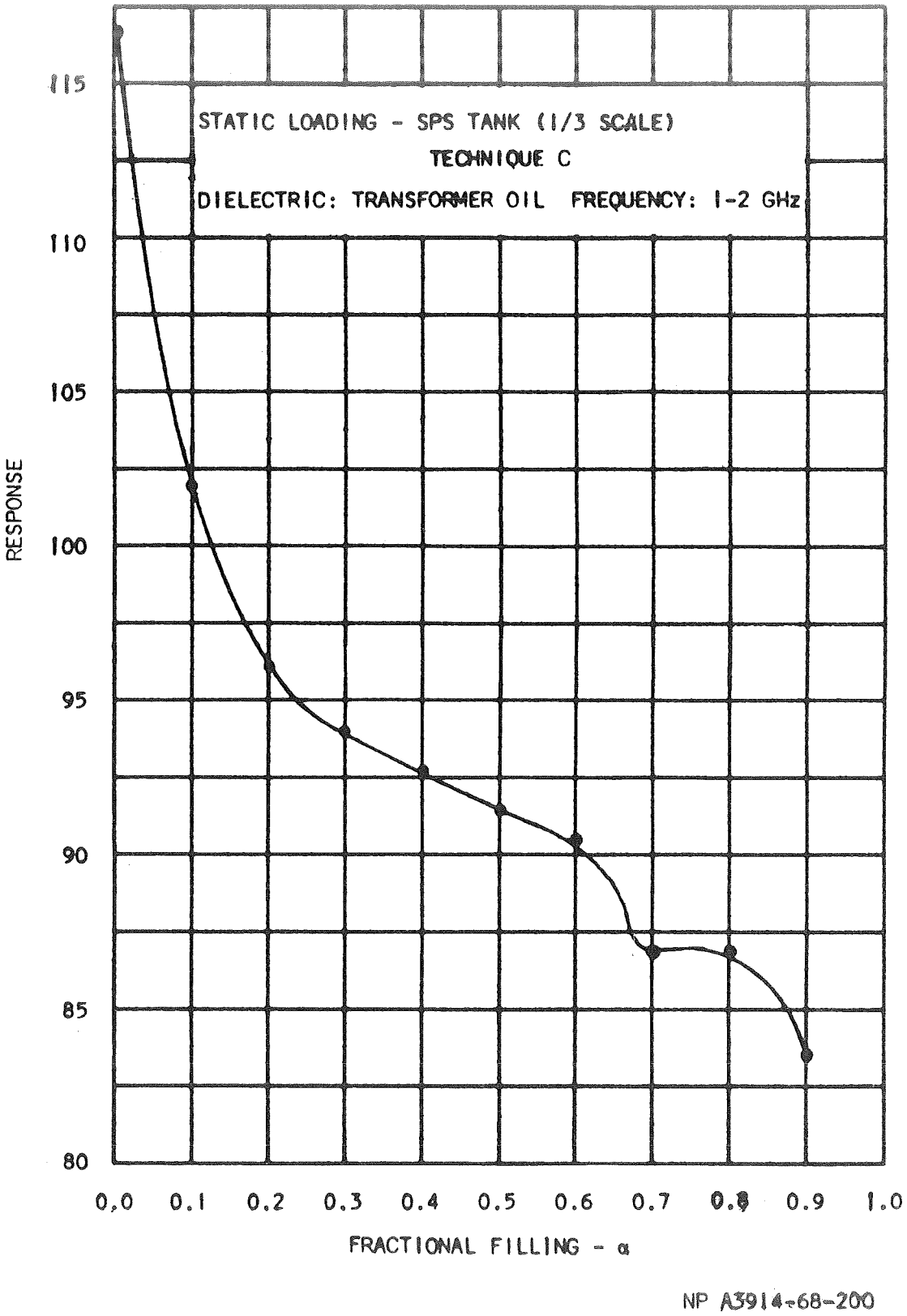
STATIC LOADING - SPS TANK (1/3 SCALE)
TECHNIQUE C
DIELECTRIC: TRANSFORMER OIL FREQUENCY: 1-2 GHz
RESPONSE
115
110
105
100
95
90
85
80
0.0
0.1
0.2
0.3
0.4
0.5
0.6
0.7
0.8
0.9
1.0
FRACTIONAL FILLING - α
NP A3914-68-200

FIGURE 4-17

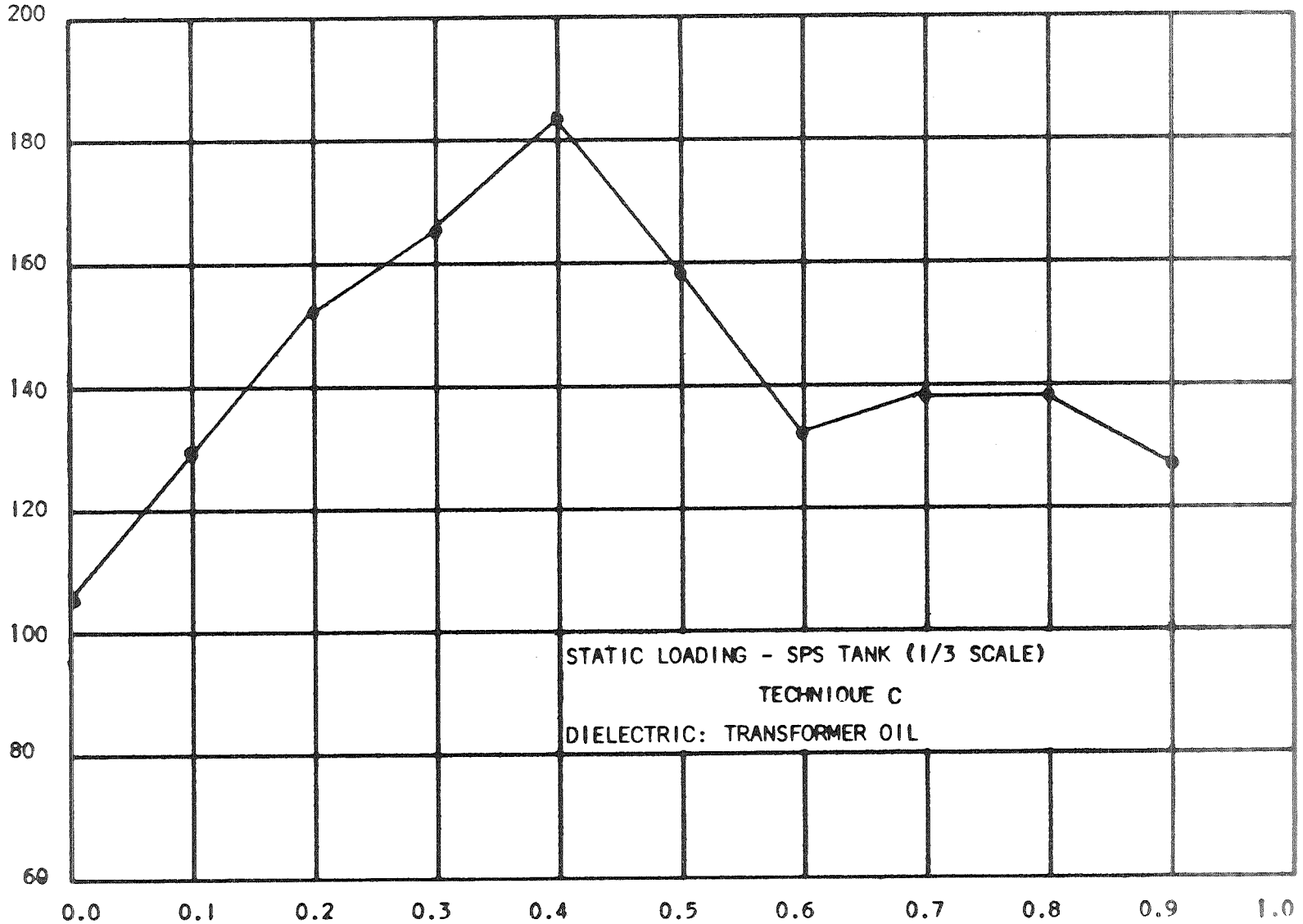

FIGURE 4-18

4.5.1 Tests Conducted

The data obtained from Technique C are shown in Table 4-8, where the cylindrical axis of the tank was vertical (tank vertical). Table 4-8 is the data for a particular decision condition in the data processor.

TABLE 4-8

LOADING DEPENDENCE - TECHNIQUE C

FRACTIONAL FILLING	VERTICAL	HORIZONTAL	INVERTED
0.00	105	105	105
0.10	131	125	130
0.20	159	145	152
0.30	166	161	169
0.40	181	171	199
0.50	189	157	137
0.60	130	123	133
0.70	142	147	124
0.80	130	135	149
0.90	125	129	126

The response is shown in Figure 4-18. The response was almost linear until the 40% loading, after which the response deteriorated. This could be attributed to either the presence of liquid around the antenna or to the characteristic response of the tank. Going to the liquid effect on the antenna, the deterioration in response was found to occur with a Teflon guard around the antenna. The Teflon antenna guard was then replaced by a Kel-F guard. As the dielectric characteristics of Kel-F are similar to Transformer Oil, no impedance change should be found as the liquid nears the antenna. The partial response is shown in Figure 4-19, showing that the non-linearity was still present. Varying the diameter of Teflon and Kel-F guards was found to have no effect on the response. It was then felt that the reason for non-linearity in the response was due to the characteristic response of the tank.

In order to check the characteristic response, the tank was put in a horizontal position such that the antenna was either out of liquid at all times, or the antenna was in liquid at all times. Loading tests were conducted for both cases.

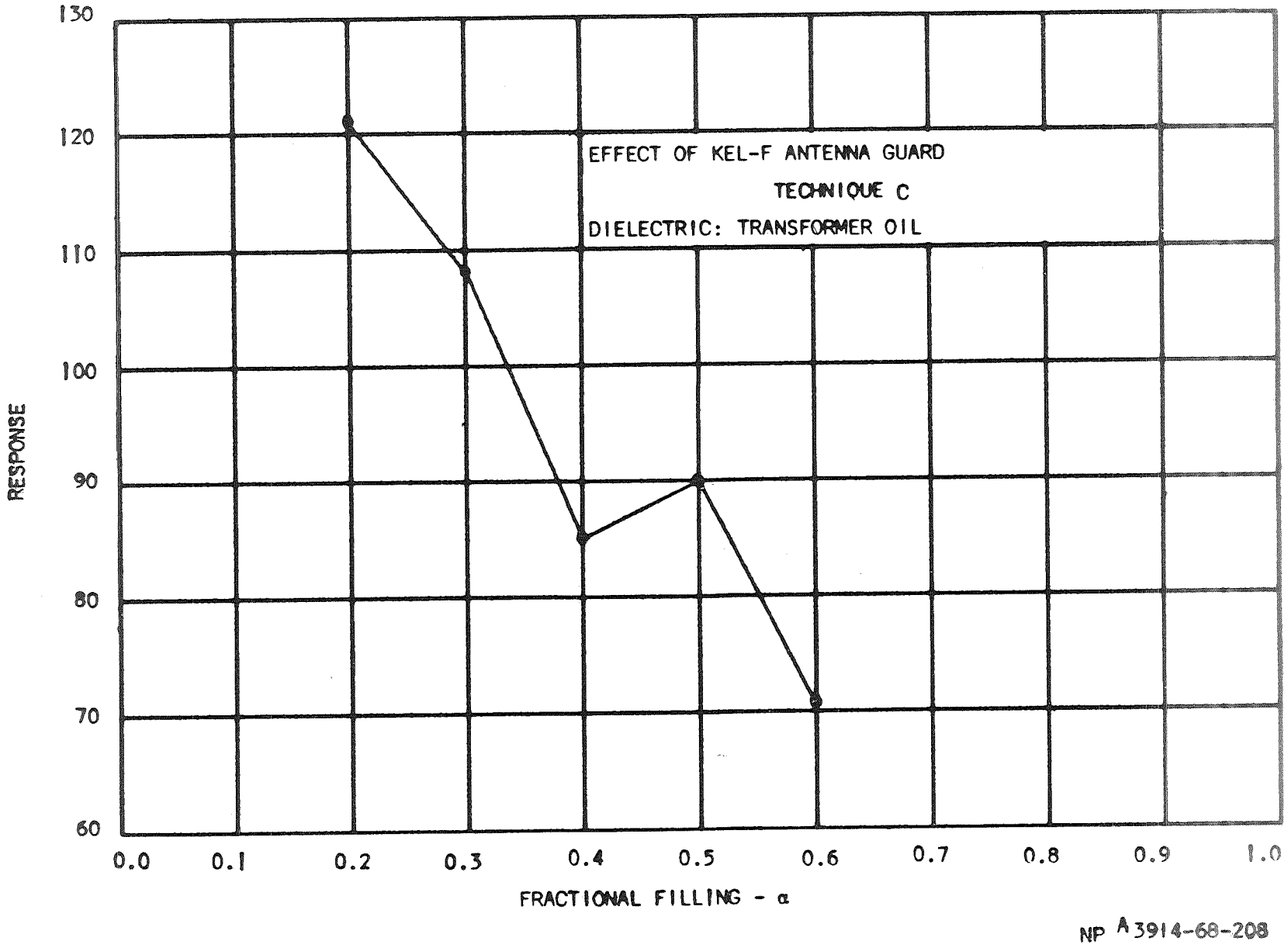

FIGURE 4-19

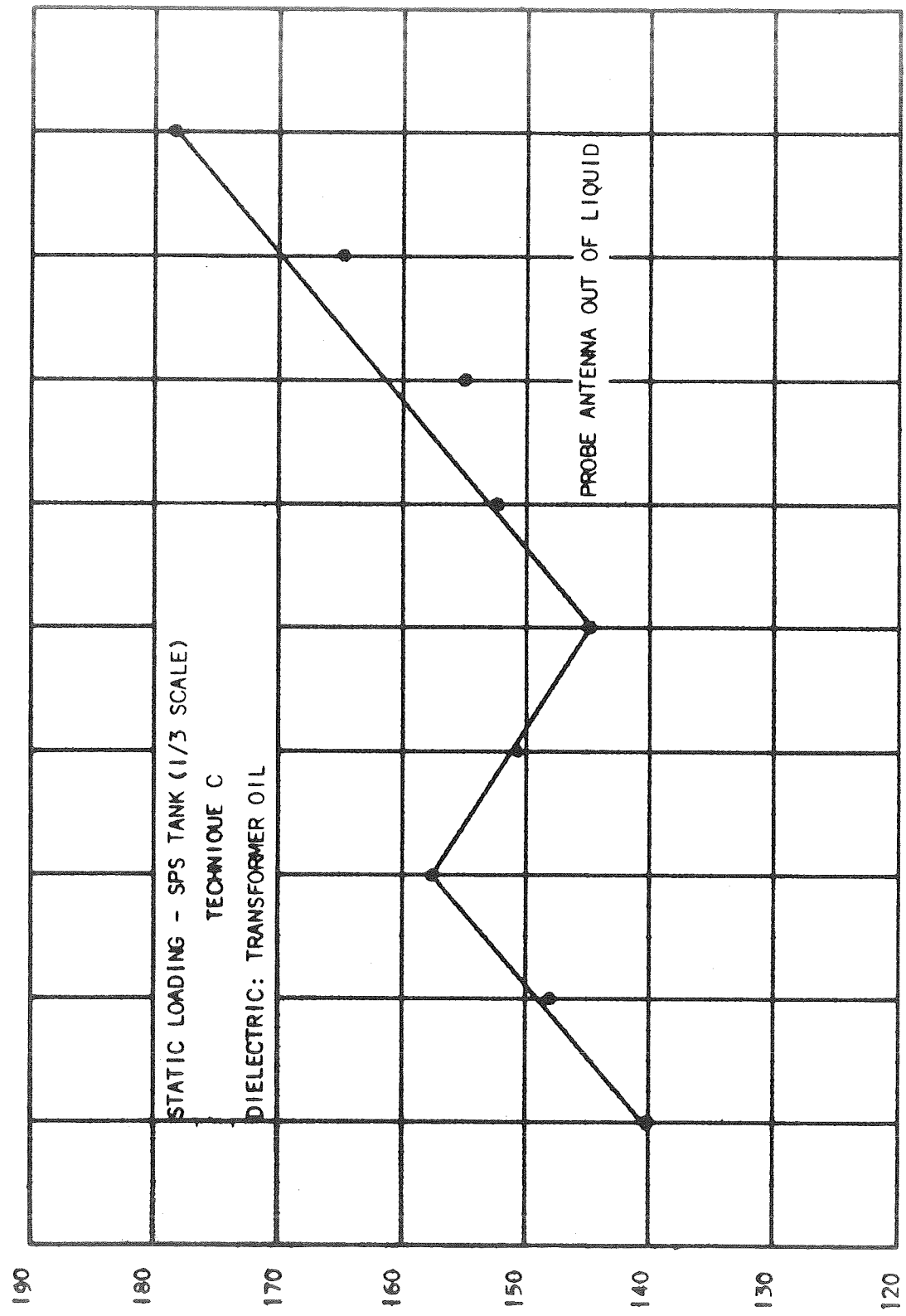

NP A3914-68-201

FIGURE 4-20

The results are shown in Table 4-9.

TABLE 4-9

STATIC LOADING TEST - SPS TANK
TECHNIQUE C

FRACTIONAL FILLING	RESPONSE	
	IN LIQUID	OUT OF LIQUID
0.1	---	140
0.2	330	146
0.3	368	158
0.4	358	151
0.5	338	145
0.6	366	153
0.7	368	155
0.8	361	165
0,9	356	179
1.0	366	---

The response obtained is shown in Figure 4-20. The non-linearity was still present around the 40% point. This suggested that it was not due wholly to the presence of the liquid. The experiment was repeated with the antenna in liquid at all times. The response obtained is shown in Figure 4-21. This response had no resemblance to the response obtained with the antenna out of liquid. Thus, the response shown earlier (Figure 4-18) could be attributed to the presence of the liquid around the antenna as well as the tank characteristic.

A response was also recorded for the antenna in and out of liquid to obtain a comparative study between the two types of responses, i.e., Technique A and Technique C. Table 4-10 shows the data obtained for Technique A in and out of liquid for an incremental loading.

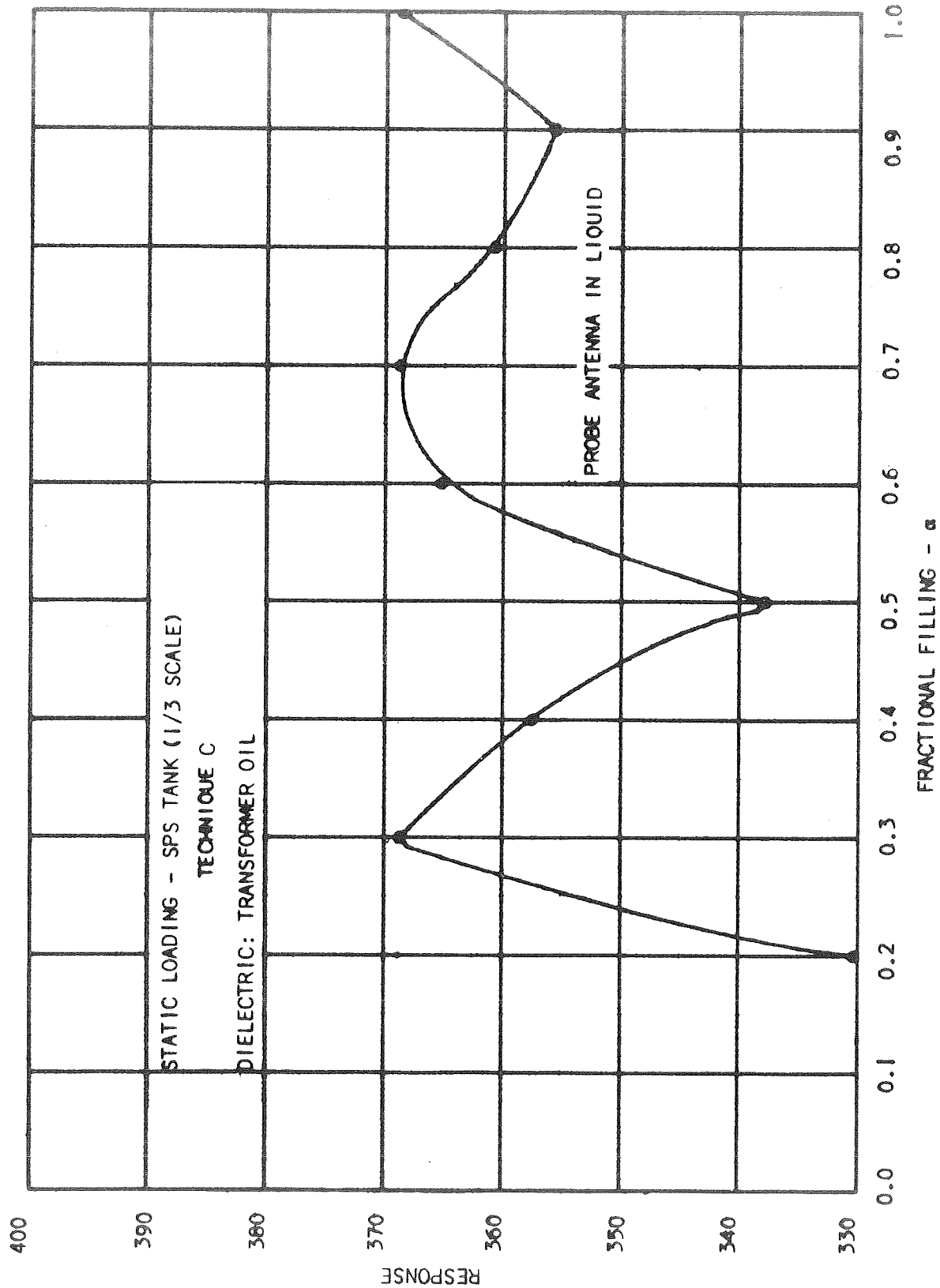
STATIC LOADING - SPS TANK (1/3 SCALE)
TECHNIQUE C
DIELECTRIC: TRANSFORMER OIL
PROBE ANTENNA IN LIQUID
RESPONSE
400
390
380
370
360
350
340
330
0.0
0.1
0.2
0.3
0.4
0.5
0.6
0.7
0.8
0.9
1.0
FRACTIONAL FILLING - α

FIGURE 4-21

TABLE 4-10

TECHNIQUE A RESPONSE FOR PROBE IN AND OUT OF LIQUID

% FILLING	RESPONSE	
	IN	OUT
10	148	140
20	112	110
30	95	86
40	102	75
50	89	73
60	87	69
70	78	67
80	85	69
90	70	65
100	78	69

The two responses are plotted in Figures 4-22 and 4-23.

The change in response due to the presence of the liquid was attributed to the disturbance of the electric field around the antenna by the dielectric.

To reduce the effect of the variance in the electric field, the probe was replaced by a loop antenna. The loop couples more strongly to the magnetic field than to the electric field, thus reducing the influence of the liquid on the antenna. A loading curve, with the loop out of liquid produced a response shown in Figure 4-24 and in Table 4-11.

It is seen that the overall system response to fluid loading is now fairly linear over the loading range, 10 to 90%.

TABLE 4-11

STATIC LOADING TEST-SPS TANK - TECHNIQUE C

FRACTIONAL FILLING	RESPONSE
0.1	130
0.2	144
0.3	149
0.4	161
0.5	158
0.6	150
0.7	165
0.8	165
0.9	177

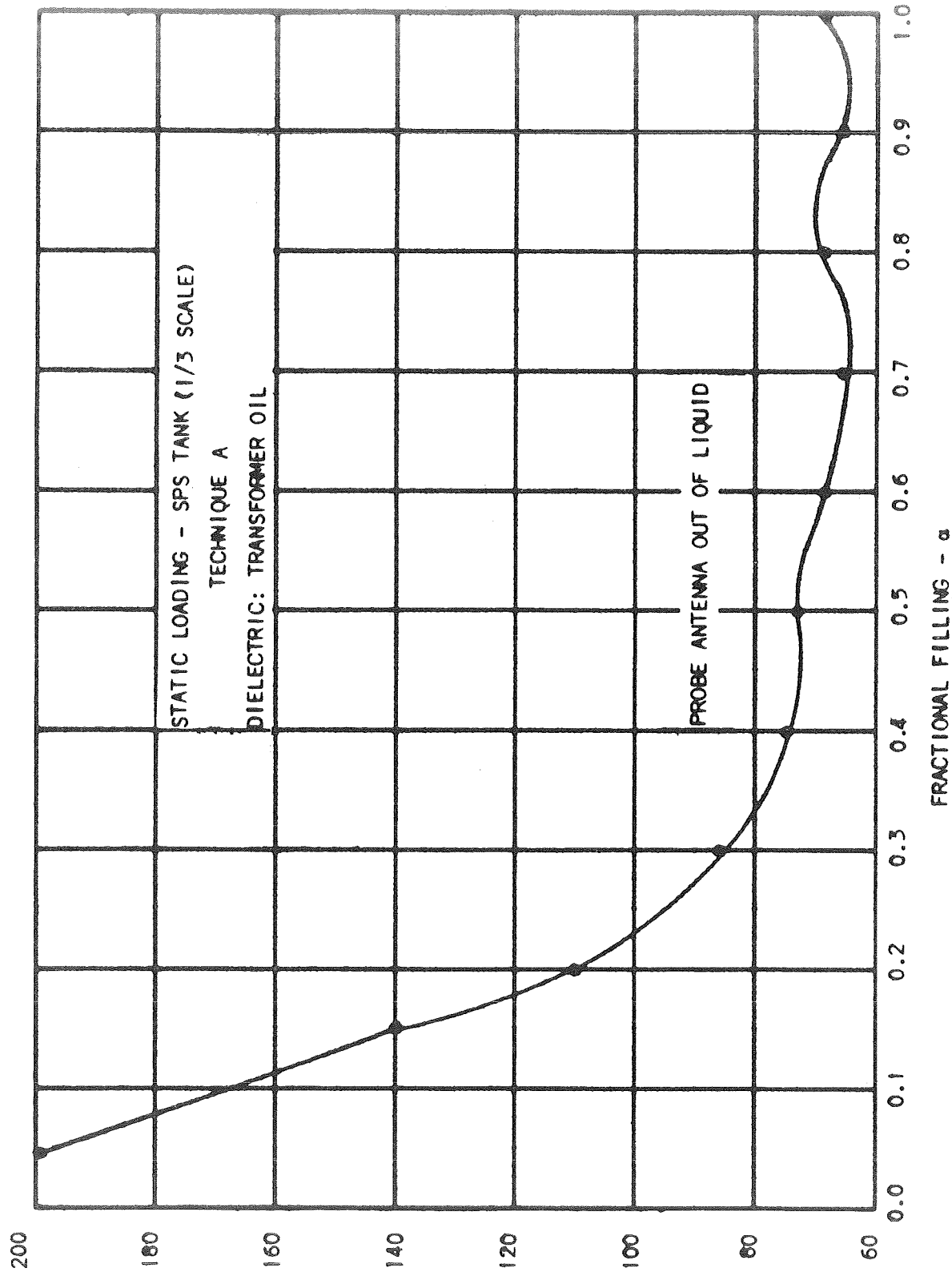
STATIC LOADING - SPS TANK (1/3 SCALE)
TECHNIQUE A
DIELECTRIC: TRANSFORMER OIL
PROBE ANTENNA OUT OF LIQUID
RESPONSE
200
180
160
140
120
100
80
60
0.0
0.1
0.2
0.3
0.4
0.5
0.6
0.7
0.8
0.9
1.0
FRACTIONAL FILLING - α

FIGURE 4-22

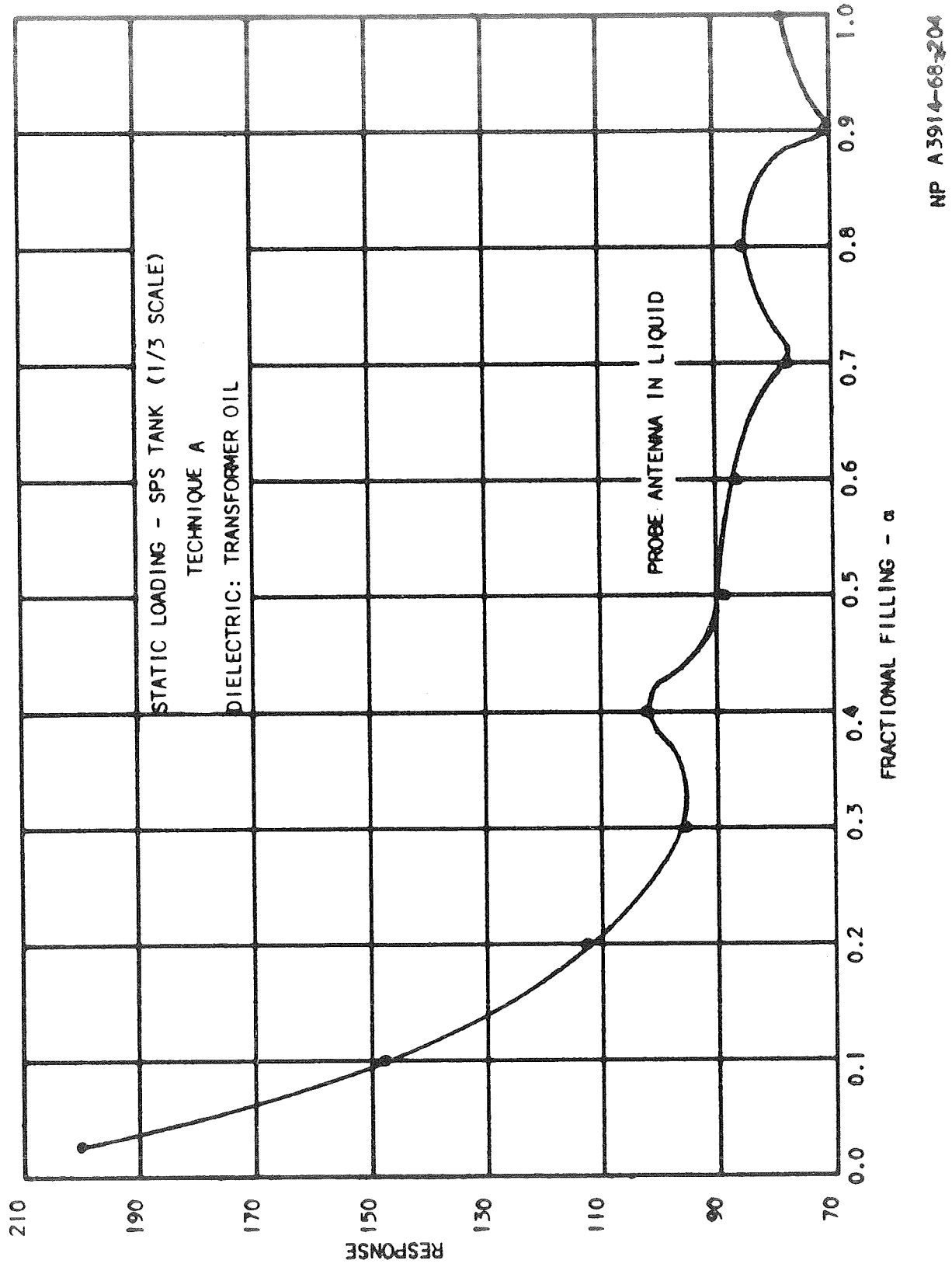
STATIC LOADING - SPS TANK (1/3 SCALE)
TECHNIQUE A
DIELECTRIC: TRANSFORMER OIL
PROBE ANTENNA IN LIQUID
RESPONSE
210
190
170
150
130
110
90
70
0.0
0.1
0.2
0.3
0.4
0.5
0.6
0.7
0.8
0.9
1.0
FRACTIONAL FILLING - α
NP A3914-68-204

FIGURE 4-23

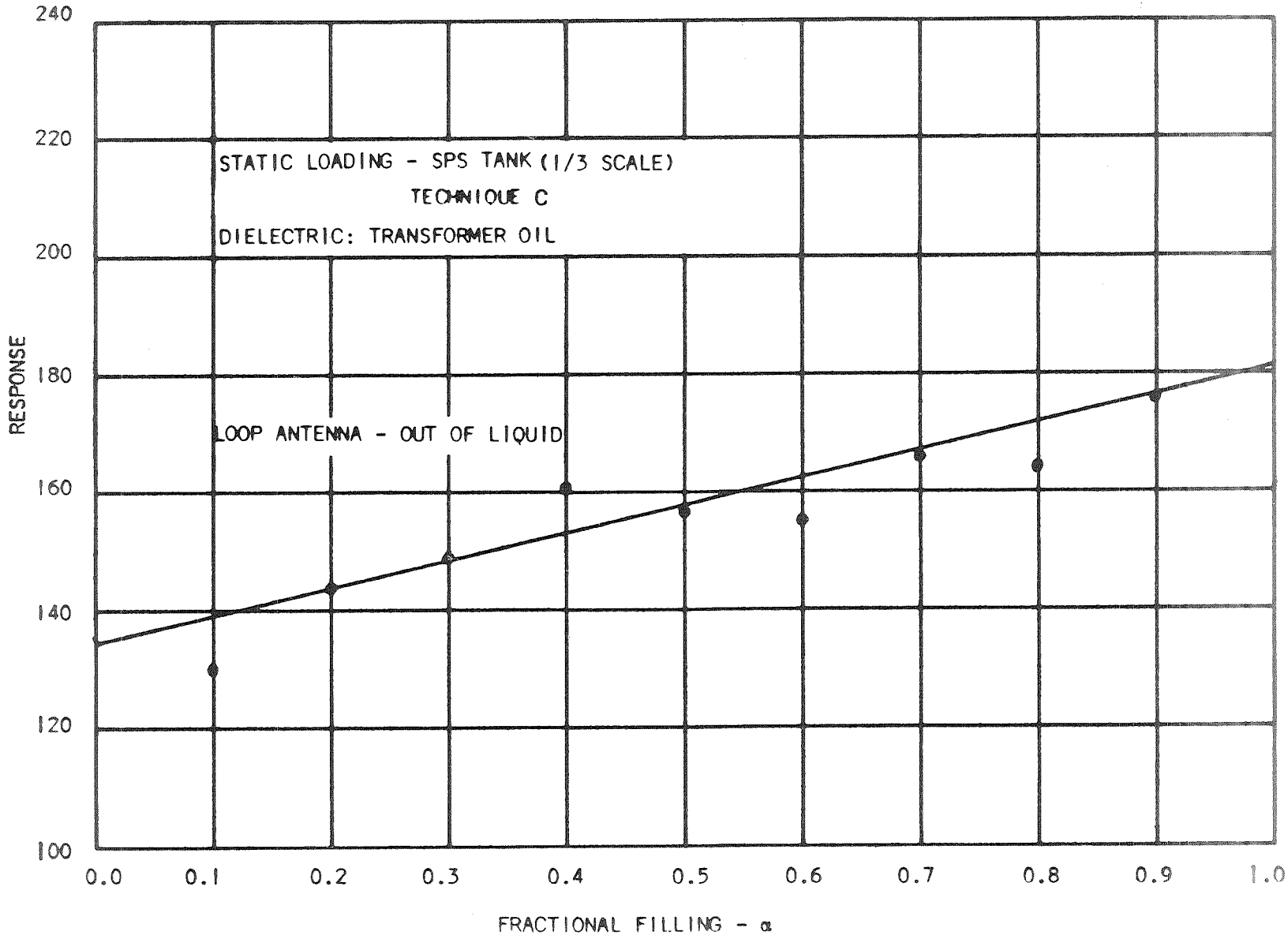

NP A3914-68-205

FIGURE 4-24

A radome then was placed over the antenna in order to reduce the effect of the fluid on the electrical field near the antenna. This altered the coupling, thus the experiments were repeated. The tank was positioned such that the antenna was in or out of liquid at all times. This produced responses shown in Figures 4-25 and 4-26, and the data is shown in Table 4-12.

TABLE 4-12

STATIC LOADING TEST-SPS TANK-RADOME PROBE GUARD

FRACTIONAL FILLING	RESPONSE	
	IN	OUT
0.1	36	36
0.2	50	40
0.3	68	53
0.4	82	70
0.5	88	79
0.6	93	83
0.7	99	81
0.8	95	77
0.9	81	76
1.0	77	--

In comparison with the response shown in Figure 4-21, which was for a probe antenna in liquid, a great improvement in response was obtained due to the change in coupling. The response does suggest that the coupling was too strong and therefore non-linear. The coupling was reduced and the experiments repeated. The responses obtained with reduced coupling are shown in Figures 4-27 and 4-28. The data is shown in Table 4-13.

TABLE 4-13

STATIC LOADING TEST-SPS TANK-LOOP ANTENNA

FRACTIONAL FILLING	RESPONSE	
	IN	OUT
0.0	10	5
0.1	42	46
0.2	54	56
0.3	74	70
0.4	85	80
0.5	90	83
0.6	93	85
0.7	97	92
0.8	96	100
0.9	84	96

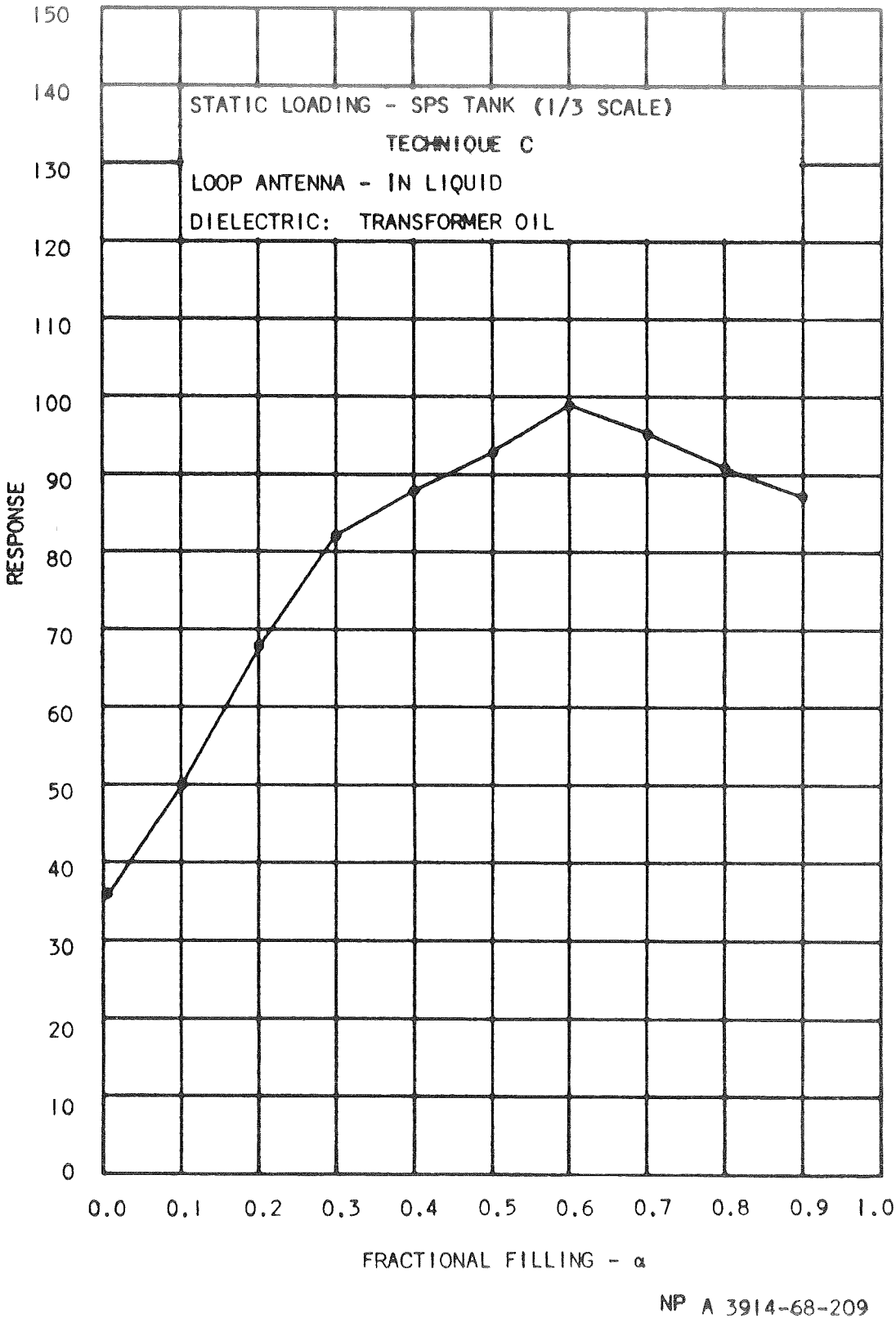
STATIC LOADING - SPS TANK (1/3 SCALE)
TECHNIQUE C
LOOP ANTENNA - IN LIQUID
DIELECTRIC: TRANSFORMER OIL
RESPONSE
150
140
130
120
110
100
90
80
70
60
50
40
30
20
10
0
0.0
0.1
0.2
0.3
0.4
0.5
0.6
0.7
0.8
0.9
1.0
FRACTIONAL FILLING - α
NP A 3914-68-209

FIGURE 4-25

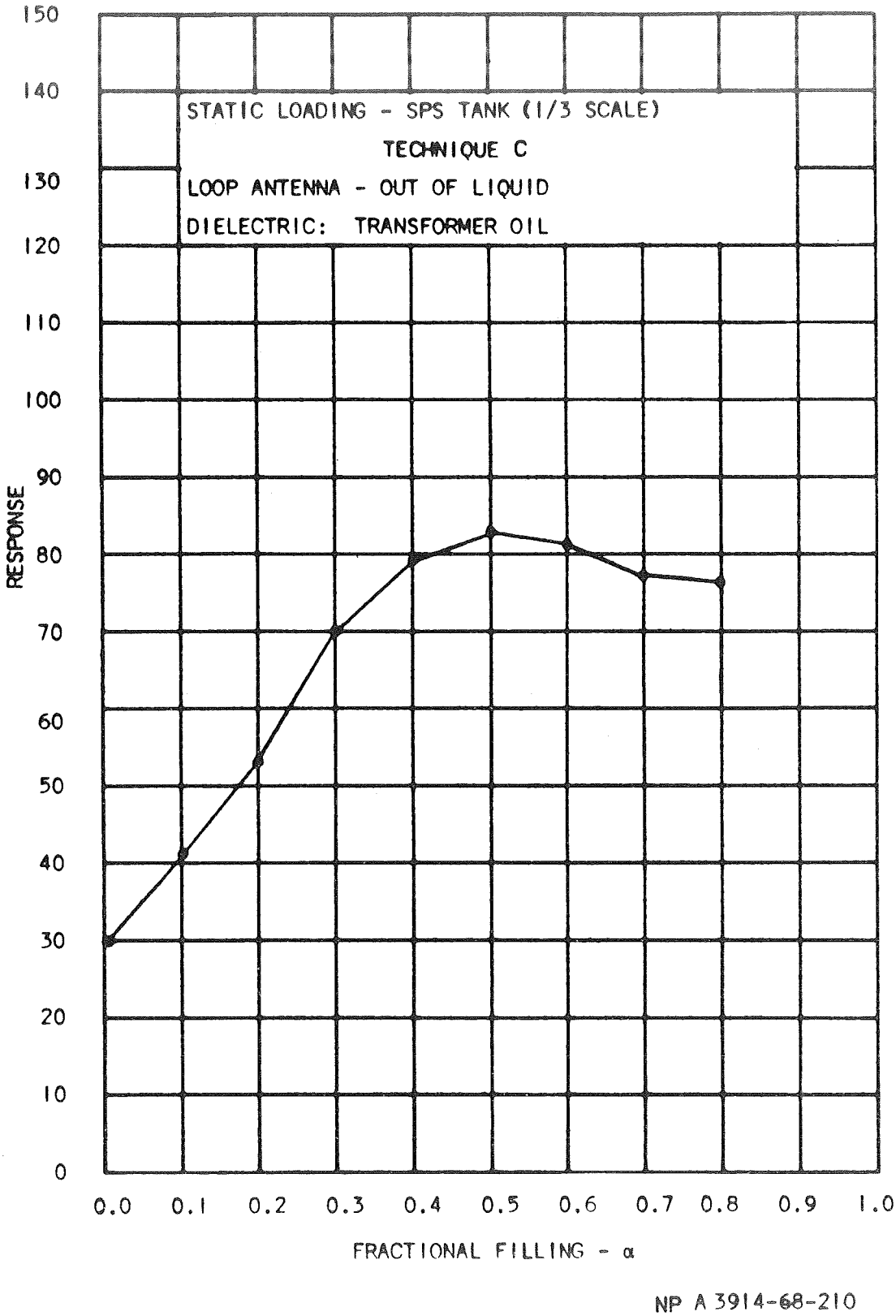
STATIC LOADING - SPS TANK (1/3 SCALE)
TECHNIQUE C
LOOP ANTENNA - OUT OF LIQUID
DIELECTRIC: TRANSFORMER OIL
RESPONSE
150
140
130
120
110
100
90
80
70
60
50
40
30
20
10
0
0.0
0.1
0.2
0.3
0.4
0.5
0.6
0.7
0.8
0.9
1.0
FRACTIONAL FILLING - α
NP A 3914-68-210

FIGURE 4-26

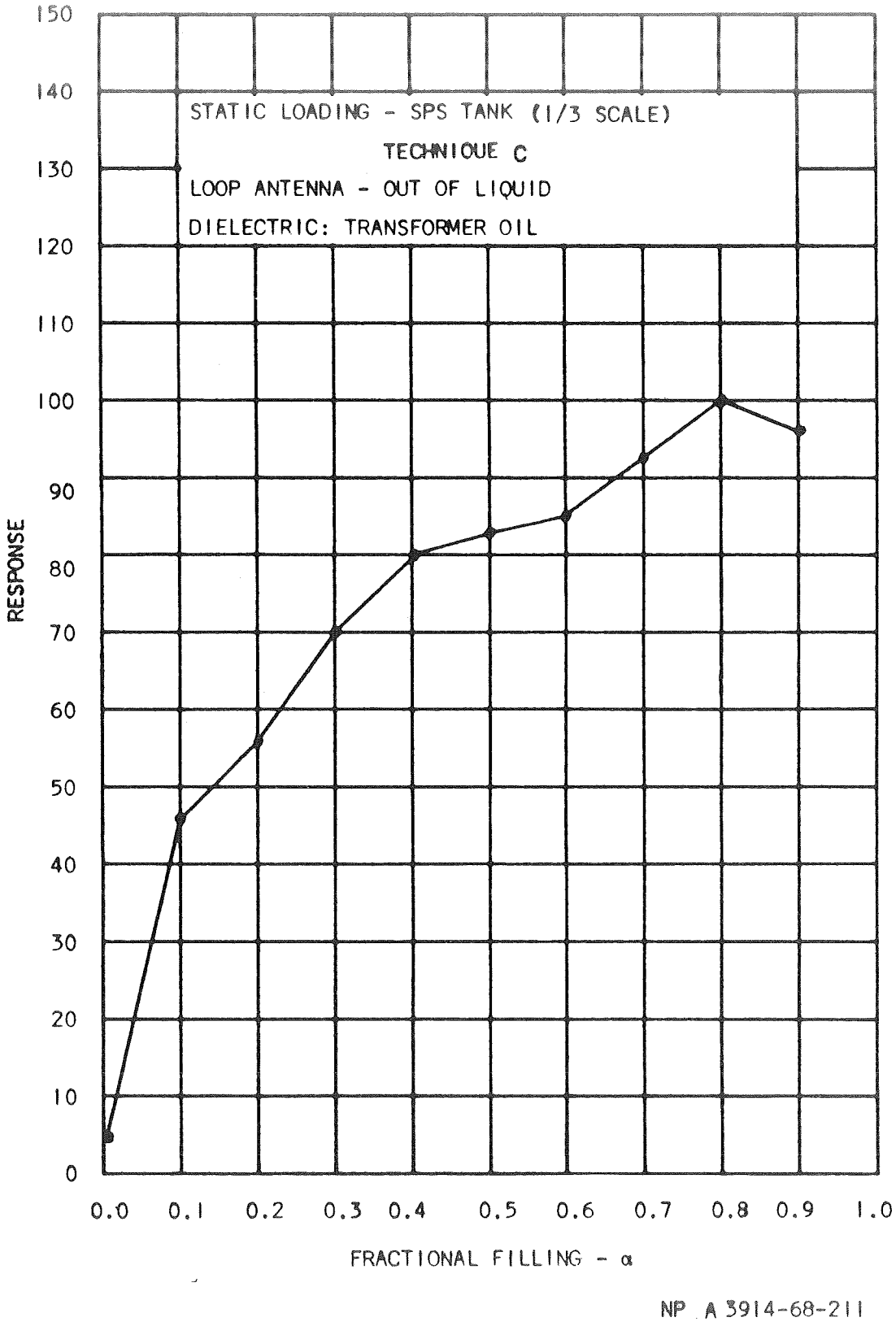
STATIC LOADING - SPS TANK (1/3 SCALE)
TECHNIQUE C
LOOP ANTENNA - OUT OF LIQUID
DIELECTRIC: TRANSFORMER OIL
RESPONSE
150
140
130
120
110
100
90
80
70
60
50
40
30
20
10
0
0.0
0.1
0.2
0.3
0.4
0.5
0.6
0.7
0.8
0.9
1.0
FRACTIONAL FILLING - α
NP A 3914-68-211

FIGURE 4-27

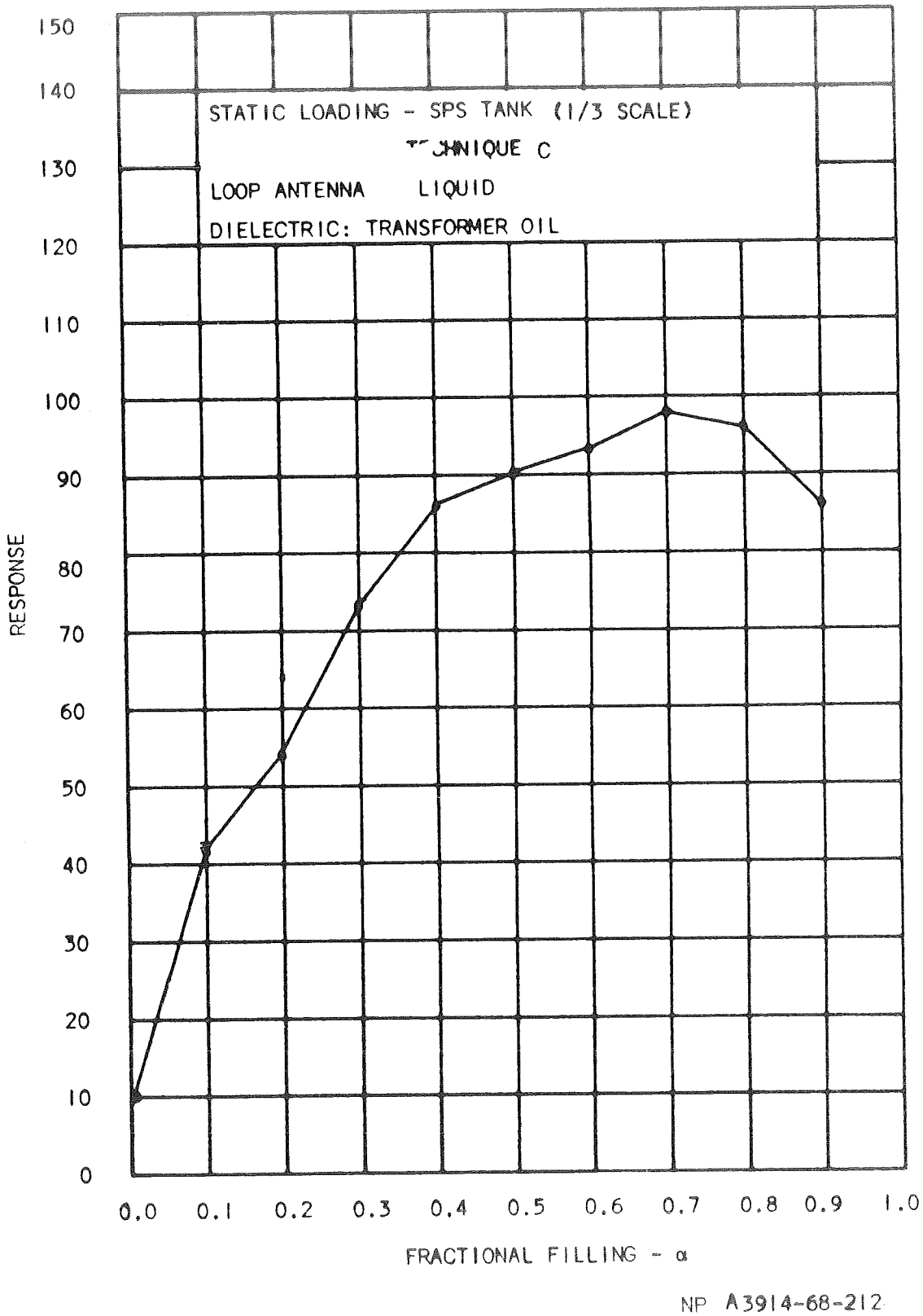
STATIC LOADING - SPS TANK (1/3 SCALE)
TECHNIQUE C
LOOP ANTENNA LIQUID
DIELECTRIC: TRANSFORMER OIL
RESPONSE
150
140
130
120
110
100
90
80
70
60
50
40
30
20
10
0
0.0
0.1
0.2
0.3
0.4
0.5
0.6
0.7
0.8
0.9
1.0
FRACTIONAL FILLING - α
NP A3914-68-212

FIGURE 4-28

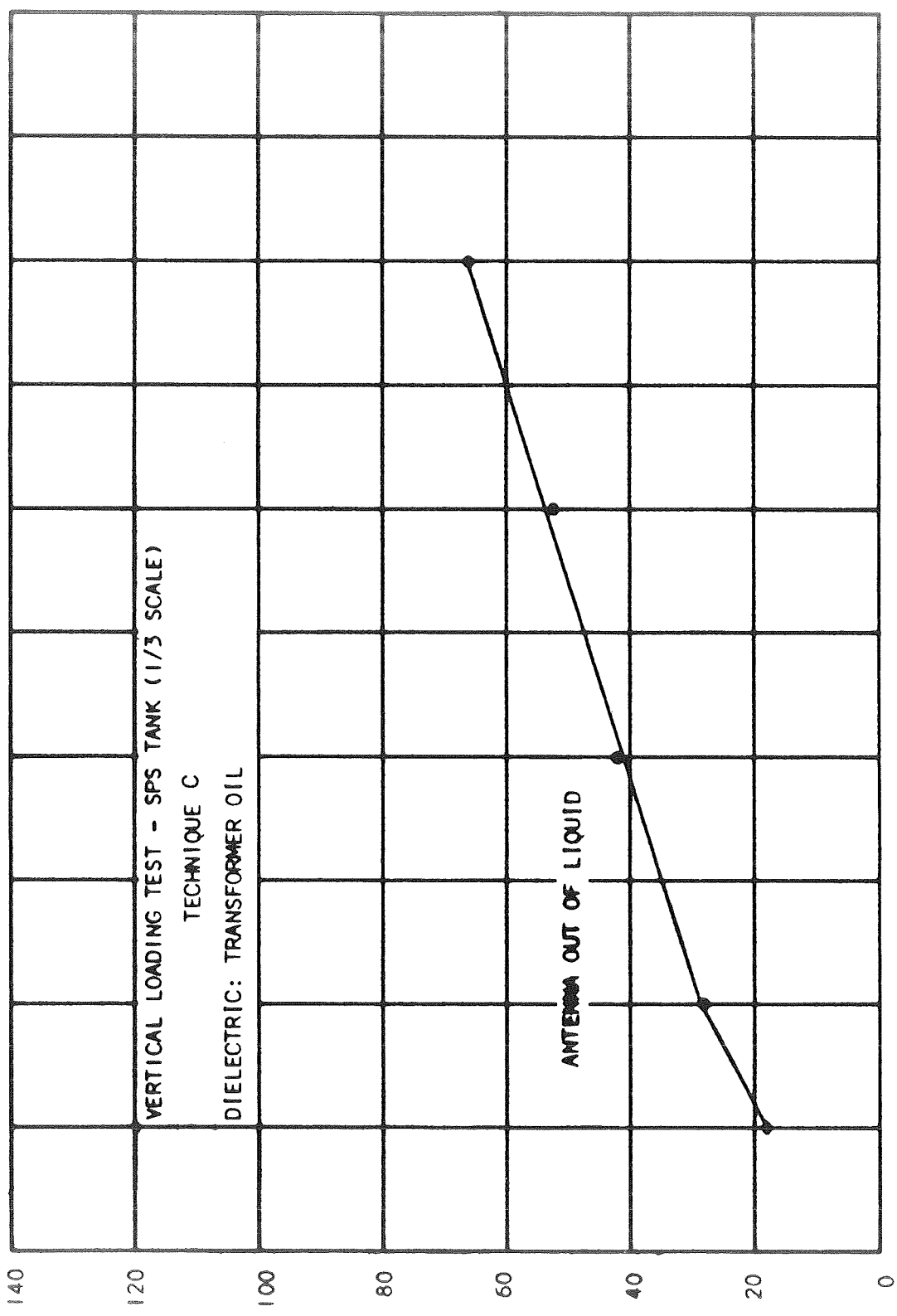

NP A3914-68-220

FIGURE 4-29

It is apparent from the similiarity of the responses that the effect of the liquid present near the probe is greatly reduced, due to the improvement in coupling and the radome shielding the loop antenna from the liquid. The non-linearity is attributed to some overcoupling still present in the system.

The coupling was altered, and a partial loading test conducted, in order to verify the expected linearization of the response. The loading tests were conducted with the cavity in the two positions, i.e., antenna out of liquid at all times, and antenna in liquid at all times. The response are shown in Figures 4-29 and 4-30.

The form of the responses were similar, but the slope obtained with the antenna out of liquid was lower than in liquid. This was still attributed to the change in coupling due to the presence of the liquid.

A vertical loading test was conducted with a change in coupling and the response obtained shown in Figure 4-31. The response was linear with a maximum deviation from linearity of 3% of the full scale readings. This deviation was present at only one filling. The remaining loadings deviated ± 1% of the full scale reading. The test was repeated with the tank at an angle to the vertical to verify repeatability. The response is shown in Figure 4-32. The deviation from linearity is more pronounced where the antenna is first immersed in the liquid.

4.5.2 Discussion

Technique C yielded the most favorable response of the three gaging techniques studied with a large degree of repeatability. The main problem to be overcome is the effect of the dielectric on the antenna. It is felt that this could be achieved by fabricating a large radome of low dielectric constant which would keep the liquid away from the antenna. This feeling is based on the fact that the response with dielectric loading was nearly linear as long as the probe did not penetrate the liquid. Since the fabrication of the radome involved changes on the tank, it was felt that this was time consuming at this stage, and thus, was not performed.

A comparison of the experimental data in Paragraph 4.5, with the predicted response for N_2O_4 shows that the experimental data was more linear than the predicted response. A good comparison of the theory and experiment though still exists, which makes it worthwhile to use the predicted response for N_2O_4 and Aerozine 50 as a guide for what to expect of this technique for those fluids. It appears that operation of the system in a tank which exhibits a fair loss over a frequency region where the dielectric constant and loss tangent of the fluids is reduced from their 100 MHz values gives some sensitivity at high loading. This is in contrast to the Technique A or Technique B which predict almost total loss of sensitivity at high fractional loadings. Again, making use of the fact that the N_2O_4 response is more linear (simulant used) than expected, the predicted Technique C response for Aerozine 50 and MMH would be expected to be more linear also. This would lead to less of a loss of sensitivity at high loadings. It would thus appear that more expectation of a useful system sensitivity over the full filling range could be made for Technique C with Aerozine 50 and N_2O_4 than with the other two techniques.

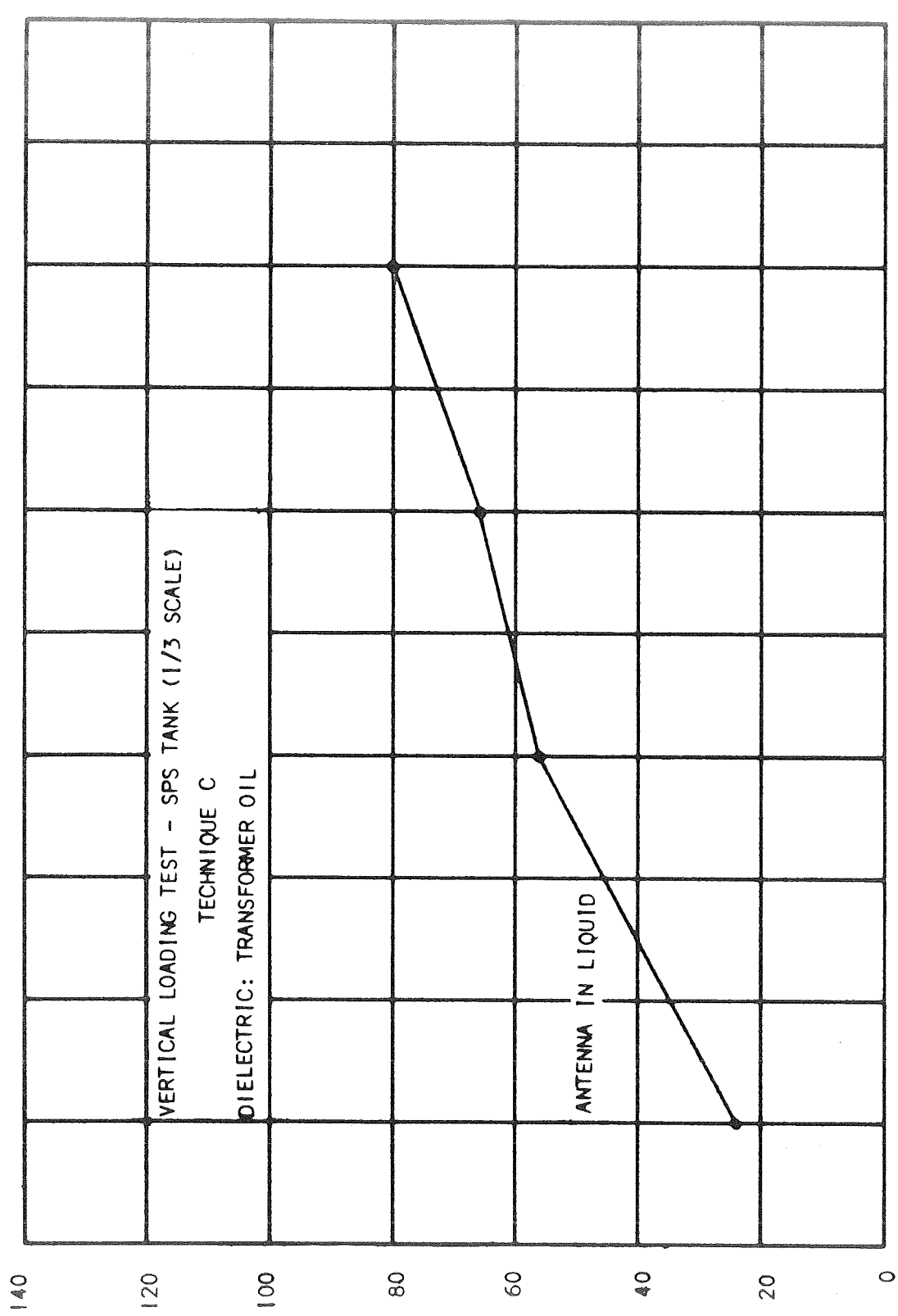
VERTICAL LOADING TEST - SPS TANK (1/3 SCALE)
TECHNIQUE C
DIELECTRIC: TRANSFORMER OIL
ANTENNA IN LIQUID
RESPONSE
FRACTIONAL FILLING - α
0
20
40
60
80
100
120
140
0.0
0.1
0.2
0.3
0.4
0.5
0.6
0.7
0.8
0.9
1.0

FIGURE 4-30

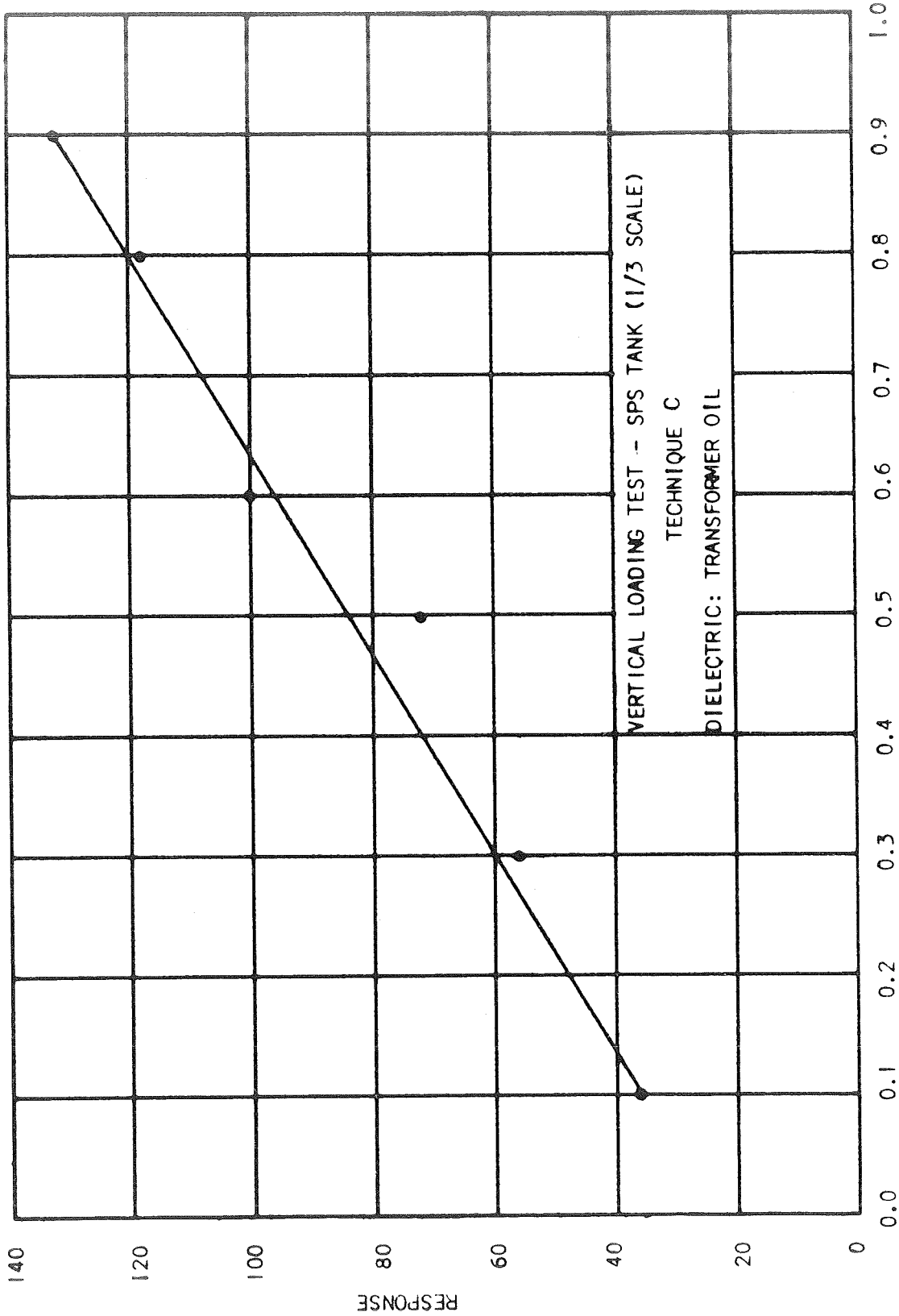

NP A3914-68-222

FIGURE 4-31

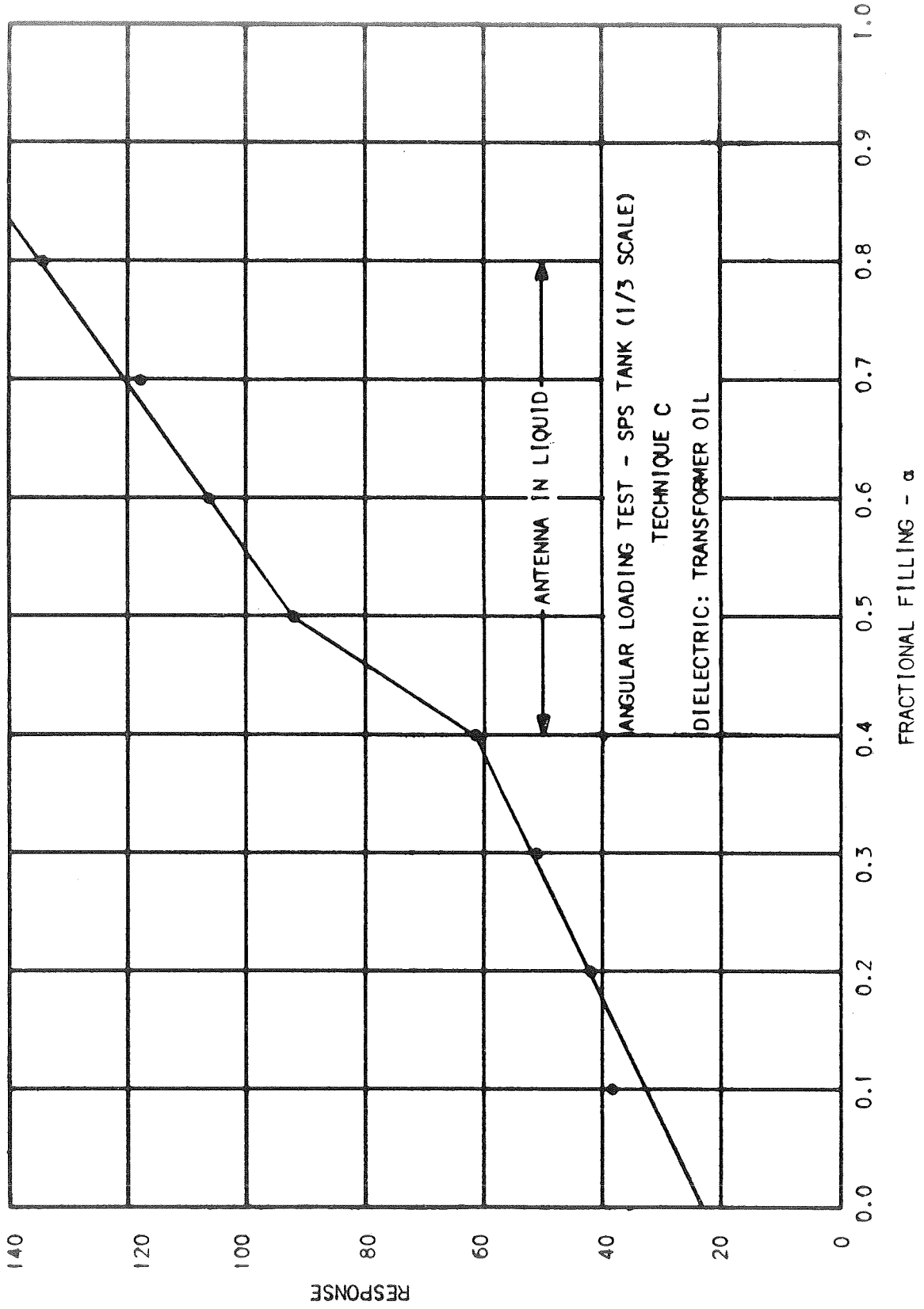
ANGULAR LOADING TEST - SPS TANK (1/3 SCALE)
TECHNIQUE C
DIELECTRIC: TRANSFORMER OIL
ANTENNA IN LIQUID
RESPONSE
140
120
100
80
60
40
20
0
0.0
0.1
0.2
0.3
0.4
0.5
0.6
0.7
0.8
0.9
1.0
FRACTIONAL FILLING - α

FIGURE 4-32

SECTION V

IMPLEMENTATION OF THE RF TECHNIQUE

5.1 INTRODUCTION

The following section gives a description of the elements required for the implementation of the RF gaging techniques as flight hardware. The elements were selected for their ability to meet both the electrical and environmental system design goals given in Section II.

In the first part of this section the system operational components, characteristic sensitivity, and accuracy are given. Next the components are detailed as to their principle of operation and ability to meet or be designed to fulfill the system goals. Because many of the components are the same in each system, they are presented as a group to avoid repetition. Where differences do exist as in the data or signal processor, they are presented relative to each system.

Some remarks on failure effects and reliability are made for critical components. These are of a preliminary nature only, though, because of the present state of the system definition. A future definition of the system components in greater detail will permit a complete failure effect and reliability analysis to be made. This definition is outlined in the recommendations, Section VII.

5 2 SYSTEM CHARACTERISTICS OF RF GAGING TECHNIQUES

From the theoretical predictions of Section III and the experimental results of Section IV an outline of the sensitivity and accuracy of the three RF gaging techniques can be presented. A block diagram of each system is presented along with its operational sequence.

These responses to propellant loading for each system are based on the accompanying block diagram and operational sequence. The components which will perform the operations are presented in the following discussion of circuit components.

5.2.1 Technique A

The implementation of a Radio Frequency Gaging System utilizing Technique A is shown in Figure 5-1.

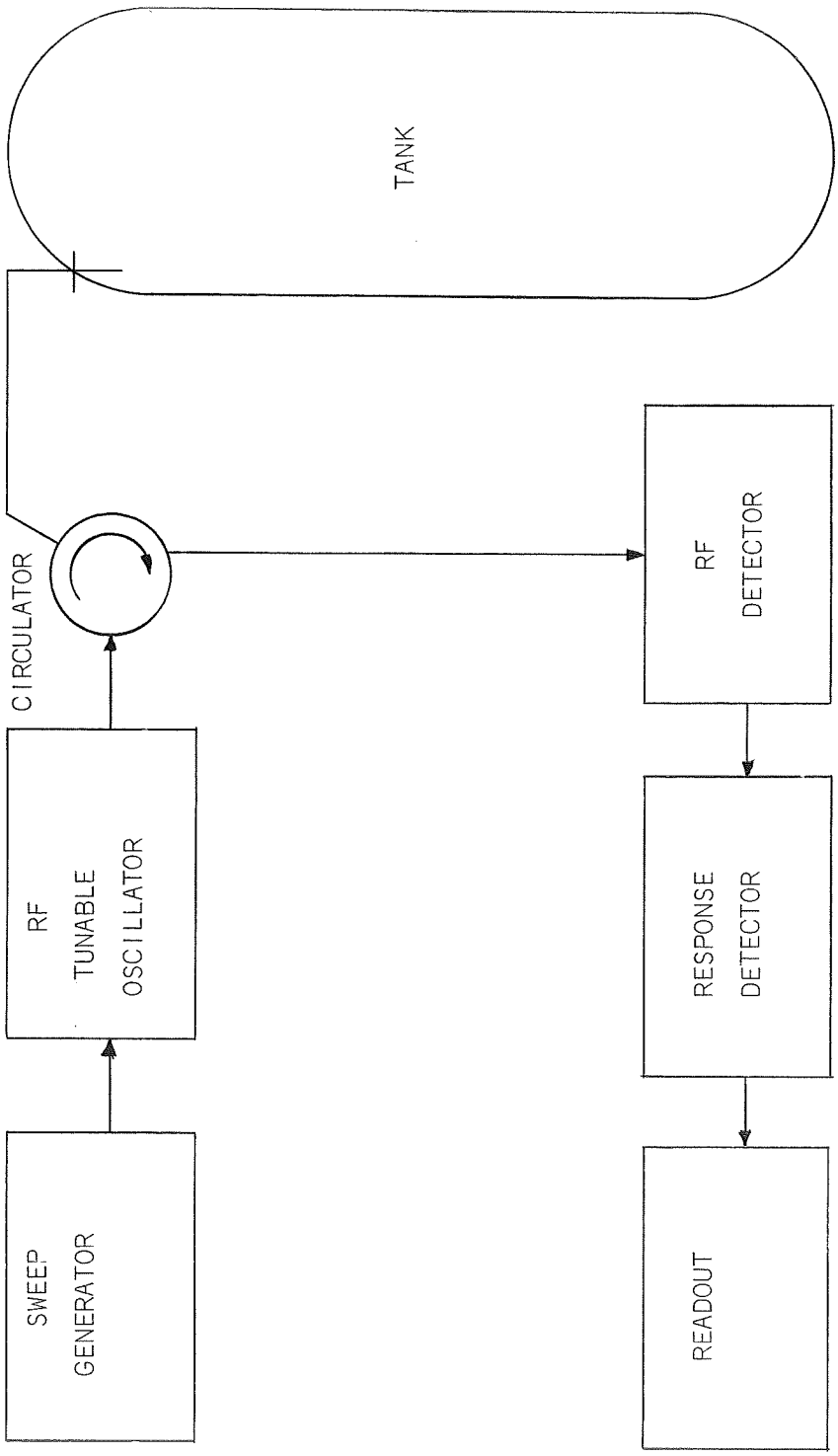

FIGURE 5-1

BLOCK DIAGRAM OF RF GAGING SYSTEM

The use of this technique or the other two for gaging a number of tanks appears feasible. To do this the output of the RF oscillator is switched to the desired tank as shown in Figure 5-2.

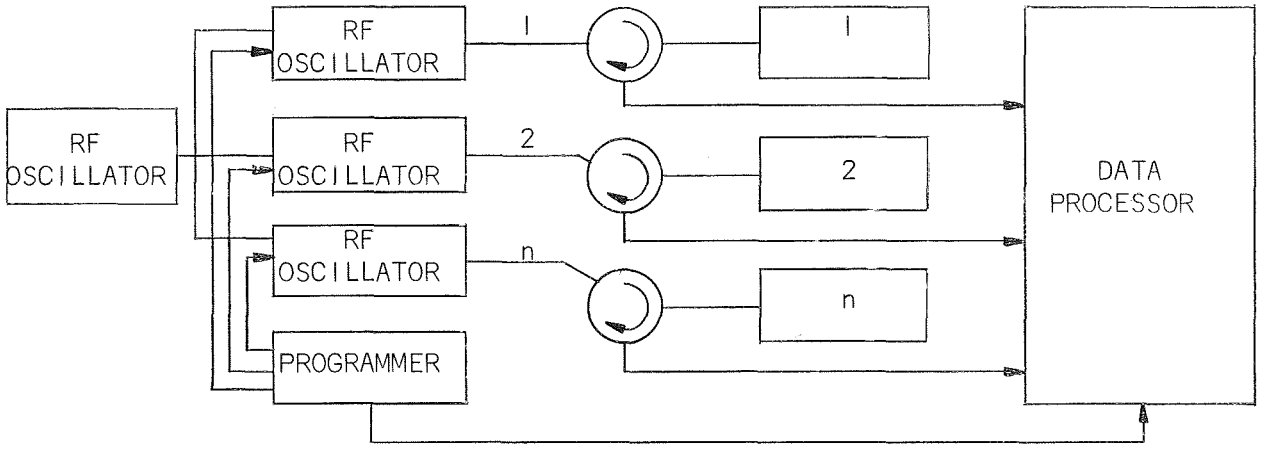

MULTIPLE TANK EXCITATION

FIGURE 5-2

The switching is carried out by the programmer sending a pulse to close the proper RF switch and a pulse to the data processor instructing it to select the response curve proper for that tank. The sequencing could be repetitive with an updated readout available for each tank once in the sequence or by command for only a given number of the tanks after some are emptied.

If the tanks have widely different excitation requirements, several RF oscillators may be needed to cover the frequency ranges required. These could be selected so that the data processing hardware would remain the same and additional switching and programming would be added. The setup of the RF oscillator switching is shown in Figure 5-3.

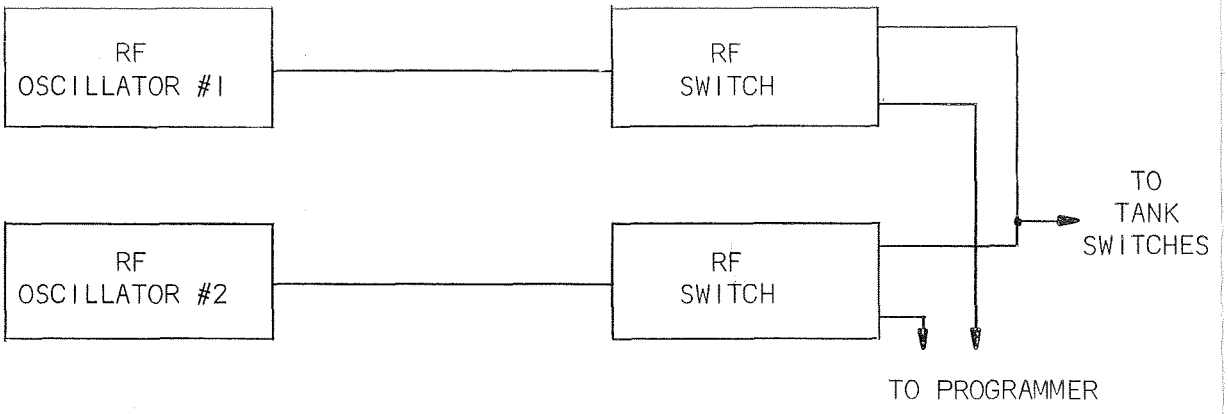

RF OSCILLATOR SWITCHING FOR MULTI-RANGING OF GAGING SYSTEMS

FIGURE 5-3

Hardware such as the switches and sequencers would be the same for all three techniques because of the similarity of the excitation. Multiple sub-units in the data processor would probably be needed to convert the processed signal to mass using the characteristic response of each tank.

The accuracy of the system can be obtained from a combination of the information on the uniformity of the RF illumination and the sensitivity wire for a particular fuel.

The accuracy curve for the three propellants for technique A is shown in Figure 5-4. It can be seen that the inaccuracy is small for low fractional filling but rapidly increases with increased loading. The predicted inaccuracy does not fall within the goals, but shows a usefulness for gaging small amounts of fuel very accurately.

5.2.2 Technique C

Paragraph 3.6, Section III, of this report, describes how the response of Technique C changes as propellant mass is loaded into the cavity. A block diagram of the Technique C of RF gaging is shown in Figure 5-5.

As before with the Technique A, an expected sensitivity and mass inaccuracy curve can be made for the system. The following curves are given for a signal processor which takes the signal from the preceding circuit and finds the difference between it and a preset constant. This is done to give an increasing output with increasing loading.

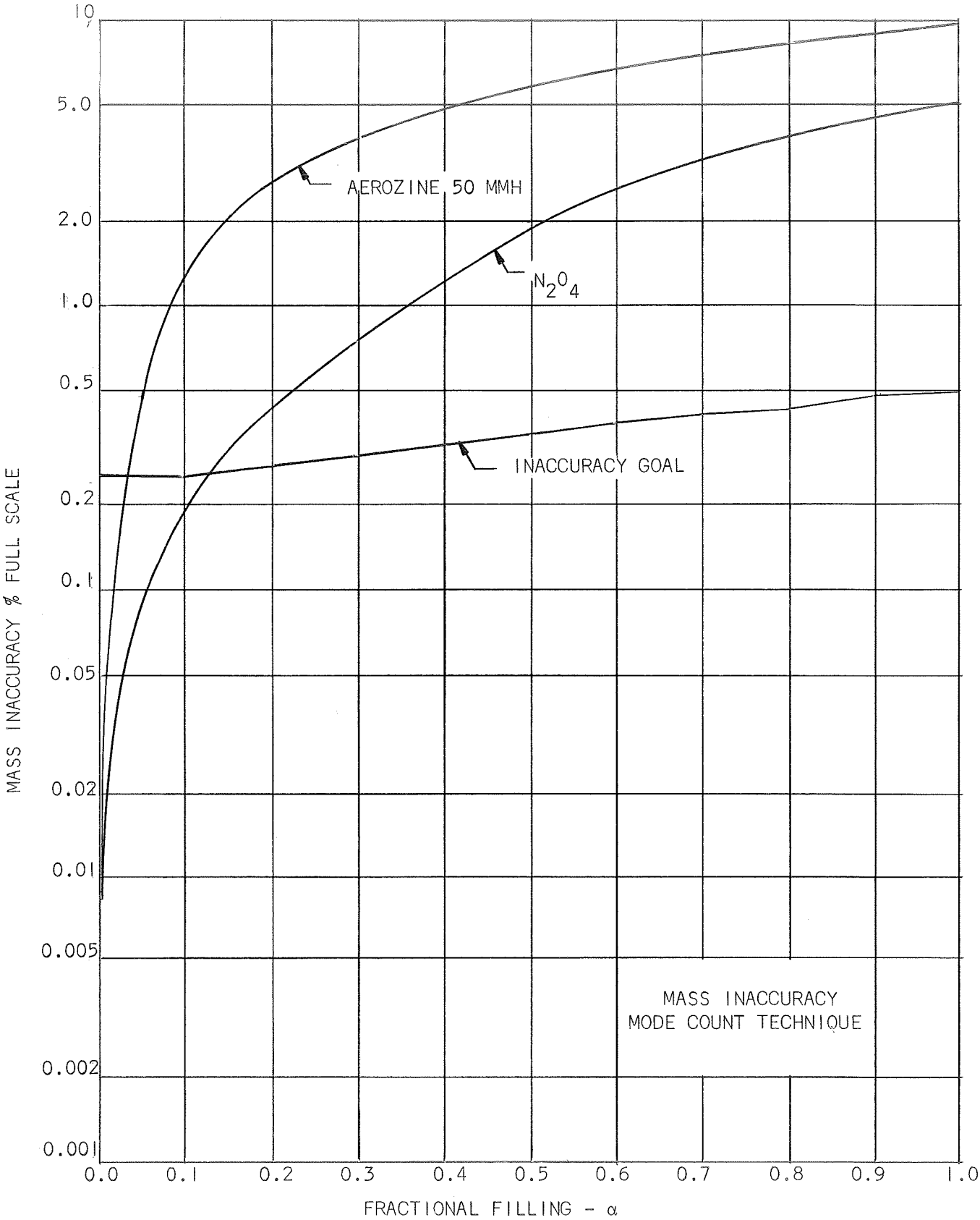
10
5.0
2.0
1.0
0.5
0.2
0.1
0.05
0.02
0.01
0.005
0.002
0.001
MASS INACCURACY % FULL SCALE
AEROZINE 50 MMH
N_2O_4
INACCURACY GOAL
MASS INACCURACY
MODE COUNT TECHNIQUE
0.0
0.1
0.2
0.3
0.4
0.5
0.6
0.7
0.8
0.9
1.0
FRACTIONAL FILLING - α

FIGURE 5-4

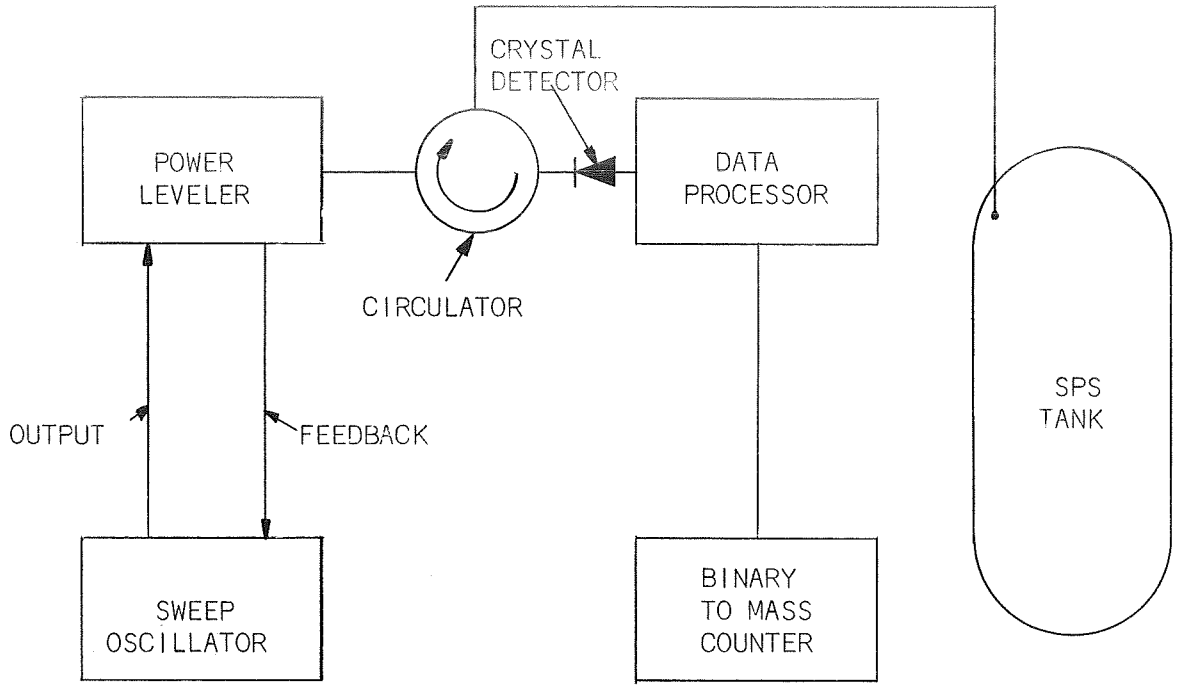

TECHNIQUE C

FIGURE 5-5

The ± 0.5% inaccuracy in response is combined with a normalized system sensitivity curve, Figure 5-6, obtained from Figures 3-23 and 3-26, Section III, and a mass accuracy obtained as in Paragraph 5.2.1. The result is shown in Figure 5-7. It can be seen that the inaccuracy is below ± 0.5% up to 25%, loading for Aerozine 50, MMH and up to 40% loading for N_2O_4. Actually the inaccuracy will probably be lowered to ± 0.5% for N_2O_4 over the entire loading range and to about ± 2% for Aerozine 50, MMH due to the linearization of the sensitivity curve indicated by the experimental data for Transformer Oil.

5.2.3 Technique B

The block diagram of the system required for the implementation of Technique B is shown in Figure 5-8.

The system response curve and mass accuracy are plotted in Figures 5-9 and 5-10. They were obtained in the manner previously outlined for Technique A. The normalized response curves are taken from Figures 3-20 and 3-21, Section III, while the response inaccuracy due to illumination non-uniformity is taken as ± 0.5%. It can be seen that the inaccuracy is above ± 0.5% for 16% loading for Aerozine 50, MMH, and for 28% loading for N_2O_4. This inaccuracy is less than that of Technique A, but still more than Technique C.

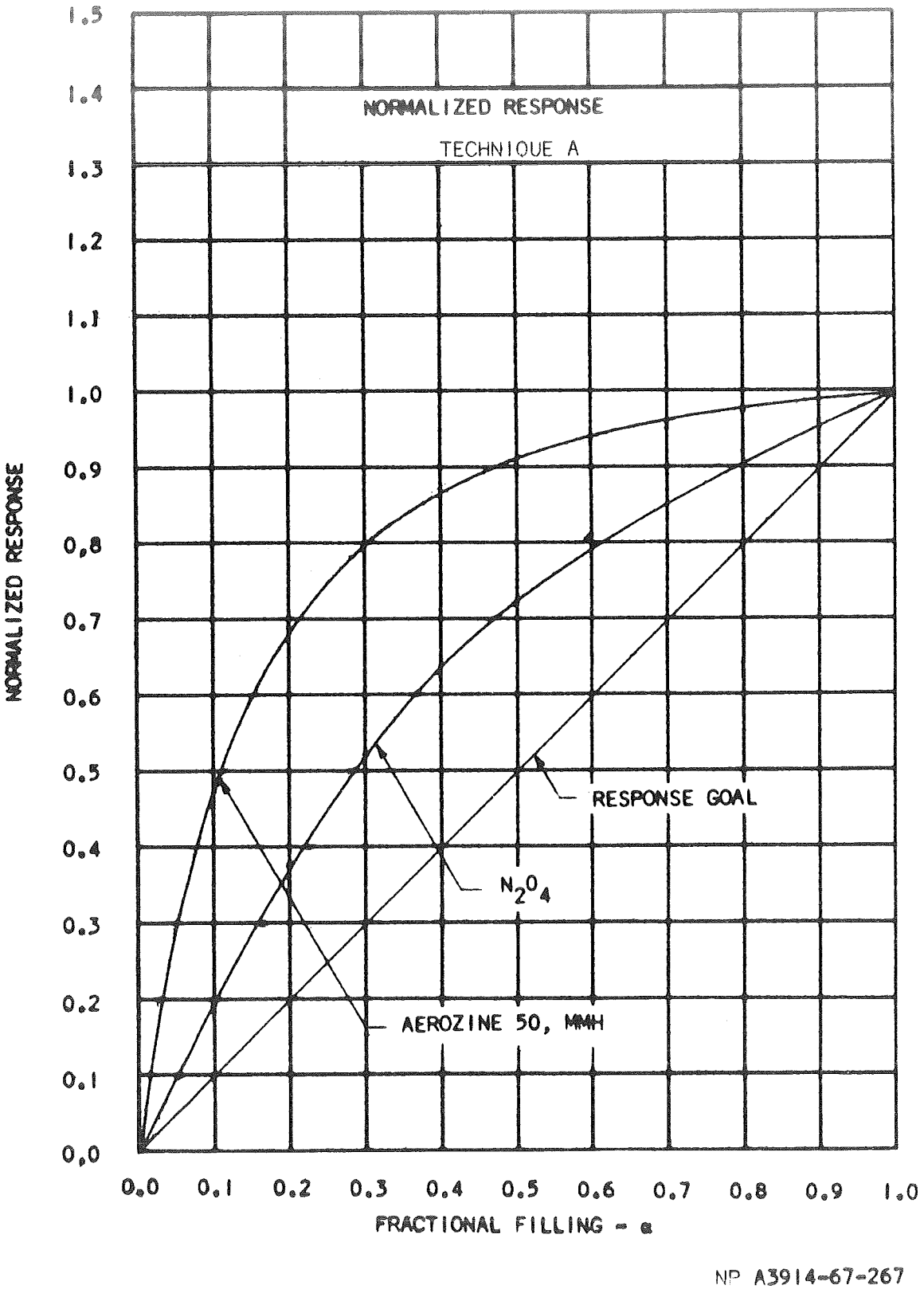
NORMALIZED RESPONSE
TECHNIQUE A
RESPONSE GOAL
N_2O_4
AEROZINE 50, MMH
NORMALIZED RESPONSE
1.5
1.4
1.3
1.2
1.1
1.0
0.9
0.8
0.7
0.6
0.5
0.4
0.3
0.2
0.1
0.0
0.0 0.1 0.2 0.3 0.4 0.5 0.6 0.7 0.8 0.9 1.0
FRACTIONAL FILLING - α
NP A3914-67-267

FIGURE 5-6

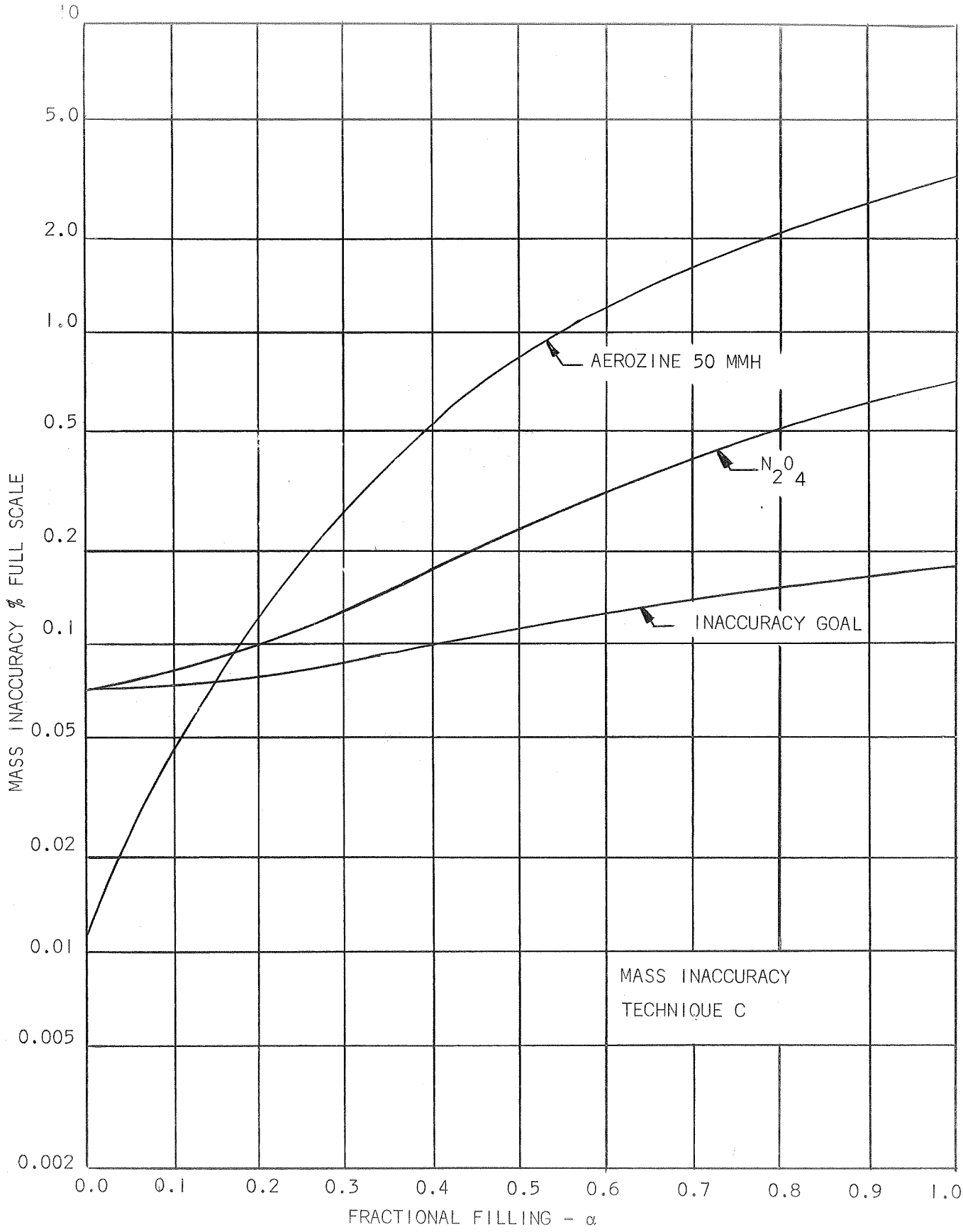
10
5.0
2.0
1.0
0.5
0.2
0.1
0.05
0.02
0.01
0.005
0.002
MASS INACCURACY % FULL SCALE
AEROZINE 50 MMH
N_2O_4
INACCURACY GOAL
MASS INACCURACY
TECHNIQUE C
0.0
0.1
0.2
0.3
0.4
0.5
0.6
0.7
0.8
0.9
1.0
FRACTIONAL FILLING - α

FIGURE 5-7

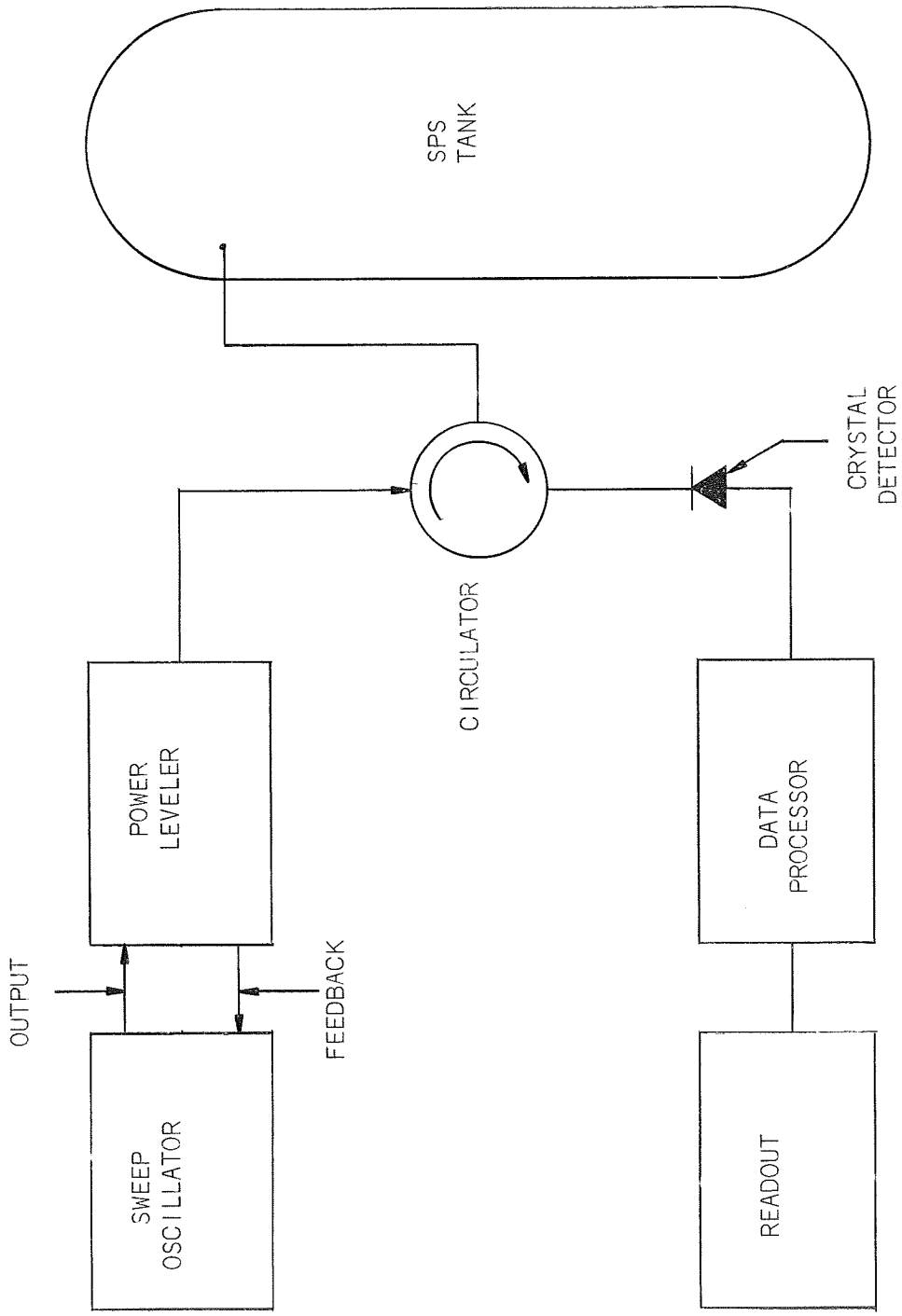

TECHNIQUE B GAGING SYSTEM

FIGURE 5-8

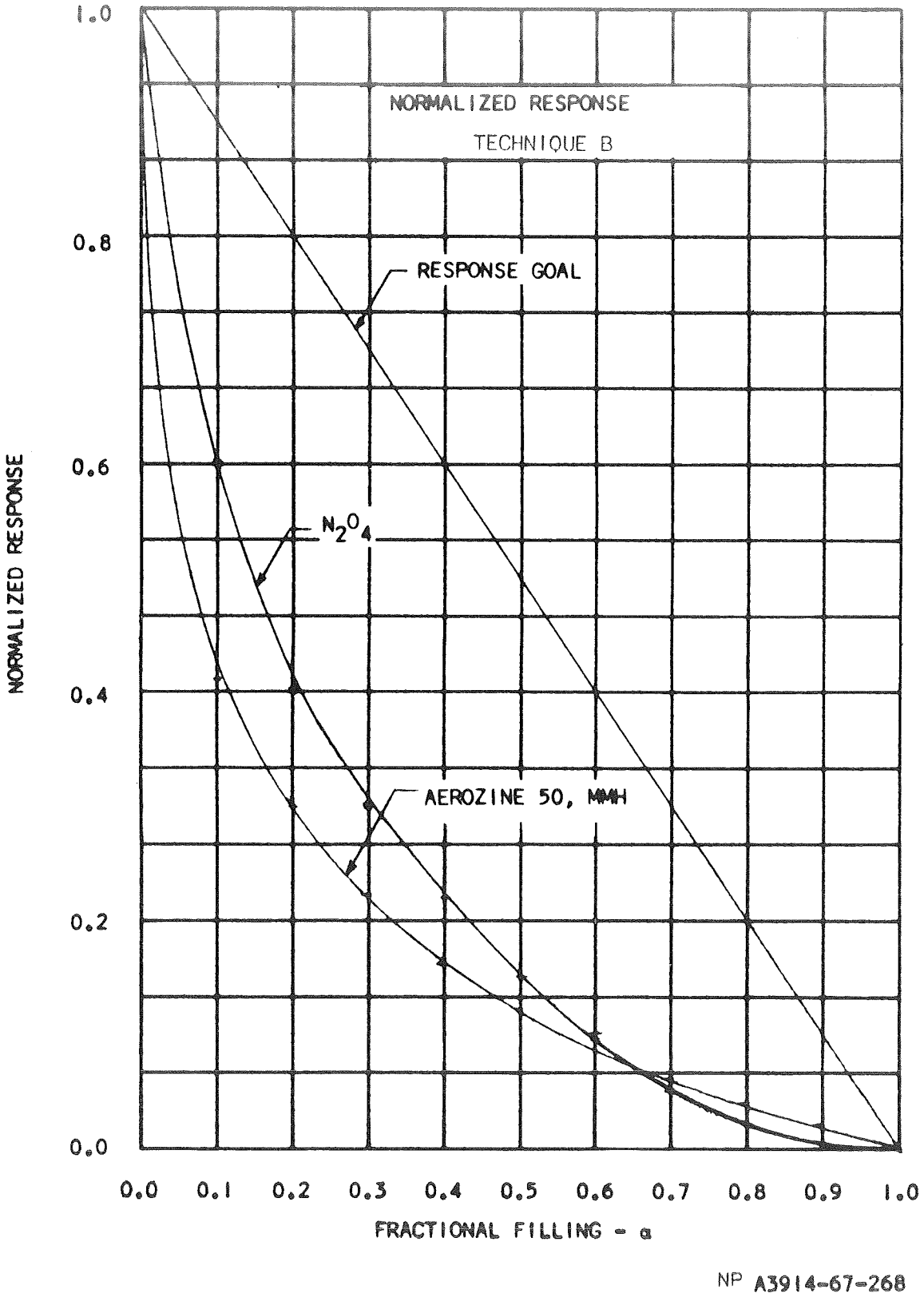
NORMALIZED RESPONSE
TECHNIQUE B
RESPONSE GOAL
N_2O_4
AEROZINE 50, MMH
NORMALIZED RESPONSE
1.0
0.8
0.6
0.4
0.2
0.0
0.0 0.1 0.2 0.3 0.4 0.5 0.6 0.7 0.8 0.9 1.0
FRACTIONAL FILLING - α
NP A3914-67-268

FIGURE 5-9

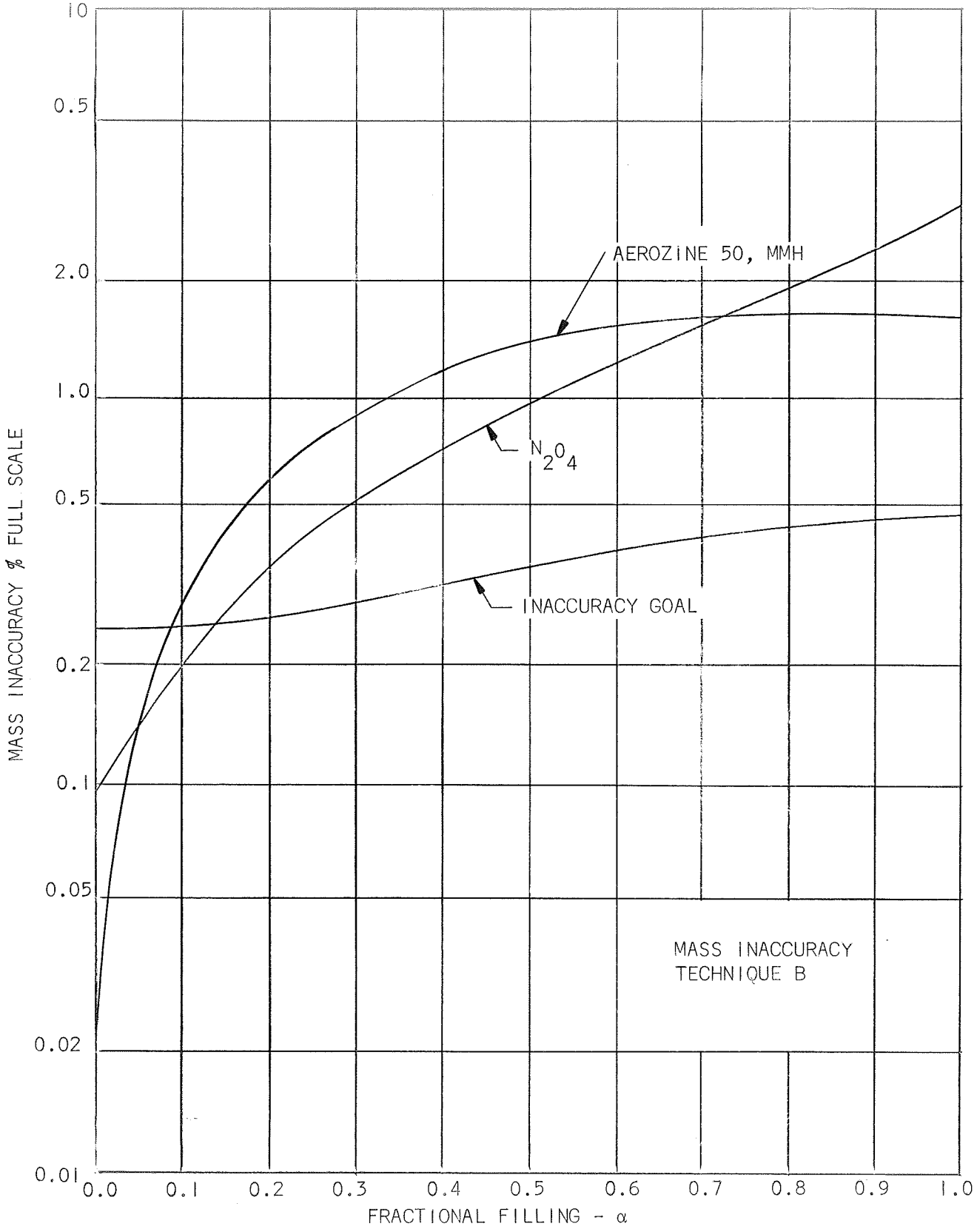
10
0.5
2.0
1.0
0.5
0.2
0.1
0.05
0.02
0.01
MASS INACCURACY % FULL SCALE
AEROZINE 50, MMH
N_2O_4
INACCURACY GOAL
MASS INACCURACY
TECHNIQUE B
0.0
0.1
0.2
0.3
0.4
0.5
0.6
0.7
0.8
0.9
1.0
FRACTIONAL FILLING - α

FIGURE 5-10

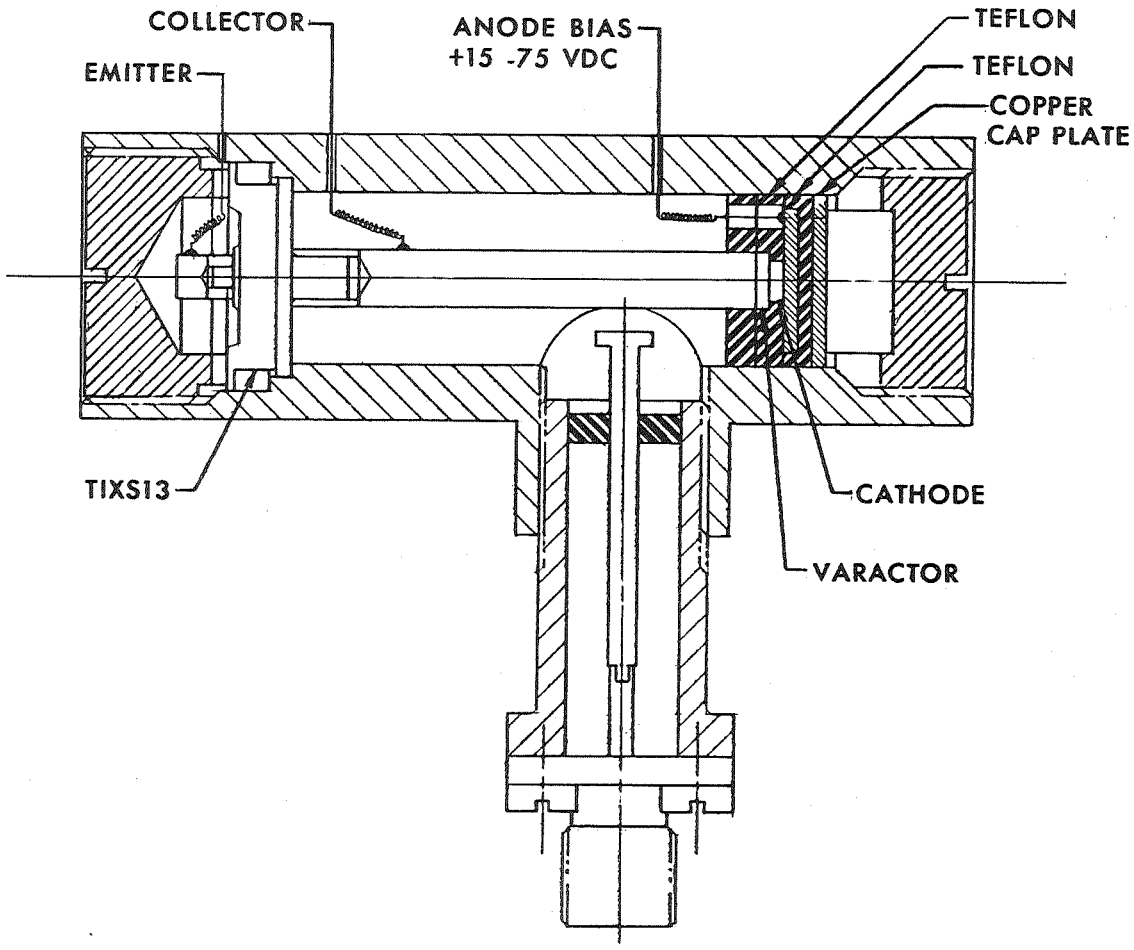

BENDIX SOLID STATE OSCILLATOR

D-3745-67-208

FIGURE 5-11

5.3 COMPONENT CHARACTERISTICS

Because many of the components are common to the three systems, they are not discussed individually for each system, except for the data processors. The data processor for the Technique A is more complex than that needed for the other two techniques.

The selection of component types for the systems was limited to those types which could meet the design goals of the system. The characteristics of the components which will allow them to meet the design goals are contained in the discussion of each component.

5.3.1 RF Oscillator and Sweep Generator

The purpose of the swept RF oscillator is to provide a signal source or excitation for the tank (resonant cavity). The importance of the swept RF source necessitates a discussion of the RF voltage-tunable oscillator.

For flight hardware systems where power and weight requirements are critical, a solid-state RF source can be used. Solid-state sources, tunable over an octave, can be used to a frequency of 2 GHz. Present technology has shown that solid-state RF oscillators with octave tuning are practical, but are generally limited to low-power applications. Due to the low RF power required to excite the tank or cavity, development of an RF solid-state oscillator is practical at this time. Since the development of a solid-state RF source is critical to the completion of the project, a prototype tunable oscillator was designed, built and tested. The oscillator uses a TIXS13 coaxial transistor, an AEL BI20040B varactor and coaxial resonating elements. A cross-sectional drawing of the oscillator is shown in Figure 5-11, and a schematic representation is shown in Figure 5-12. Coaxial rather than stripline construction was chosen because it has superior environmental immunity and greater short-term stability due to the higher Q's of the resonating elements.

The oscillator uses a common base configuration with the resonating element in the collector circuit. The resonating element consists of a length of coaxial transmission line approximately one-tenth wave length long terminated with a varactor. At the emitter terminal on the transistor, the transmission line-varactor combination is electrically equivalent to a voltage variable inductance. This inductance resonates with the collector-to-base capacitance of the transistor.

There is an optimum relationship between transmission line length, transmission line impedance, and maximum varactor capacitance to obtain maximum frequency variation for a given transistor emitter-to-base capacitance. One method of computing this relationship was developed by C. N. Herbert and J. Chernaga.[14] This method does not, however, usually result in

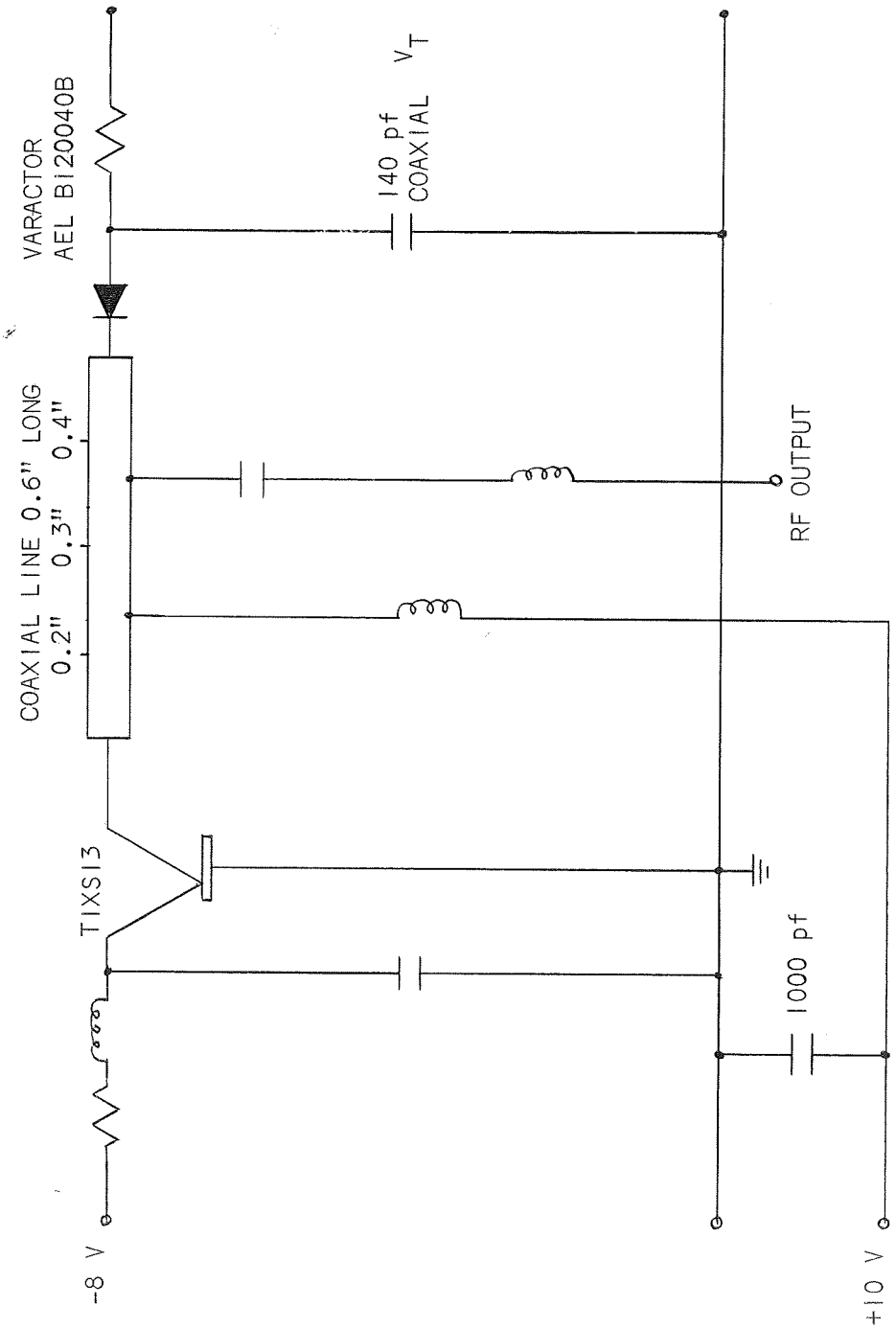

TRANSISTOR OSCILLATOR SCHEMATIC DIAGRAM

FIGURE 5-12

practical or realizable values of transmission line impedance. In developing the prototype, a varactor was selected having a reasonable compromise between Q, minimum and maximum capacitance change. The length of transmission line between the transistor and varactor was chosen on an experimental basis in order to obtain the maximum frequency variation for the total capacitance change.

The oscillator will function when the feedback is through the emitter-collector capacitance within the transistor, or through coupling between emitter and collector as a result of the common base. Either or both feedback mechanisms may be, in effect, any particular frequency. Significant output power was not obtained from this structure until a small 4-picofarad capacitor was added from the emitter to ground. This additional capacitance apparently altered the emitter circuit impedance to achieve a more optimum phase condition for feedback.

The output is AC coupled from the collector circuit by adjusting a flat-ended pickup probe near the center conductor. The axial location of the connection was determined experimentally by obtaining maximum flatness of output power versus frequency. Typical plots of output power versus frequency for two locations are given in Figure 5-13. In the best location, the output power was 16 ± 2 dBm from 1.1 to 2.0 GHz.

The tuning characteristic, i.e., the output frequency versus varactor voltage is given in Figure 5-14. No attempt has been made in the prototype to lineate this tuning characteristic since a nonlinear sweep may be desired.

The results obtained with the prototype clearly demonstrate the feasibility of an octave bandwidth, solid-state, voltage tunable, RF oscillator. The prototype is voltage tunable, with a power output of at least 12 dBm, over a range from 1.1 to 2.0 GHz. The overall package is compact, electrically efficient and could be made rugged enough to withstand extreme environmental conditions.

The present specifications for the oscillator are given below:

RF Performance	Typical
Nominal Frequency Band	1.0 to 2.0 GHz
Power Output into Load VSWR - 1.25	40 mw
Power Output Variation	4 dB
Fine Gain, Variation	1.5 dB/50 MHz max.

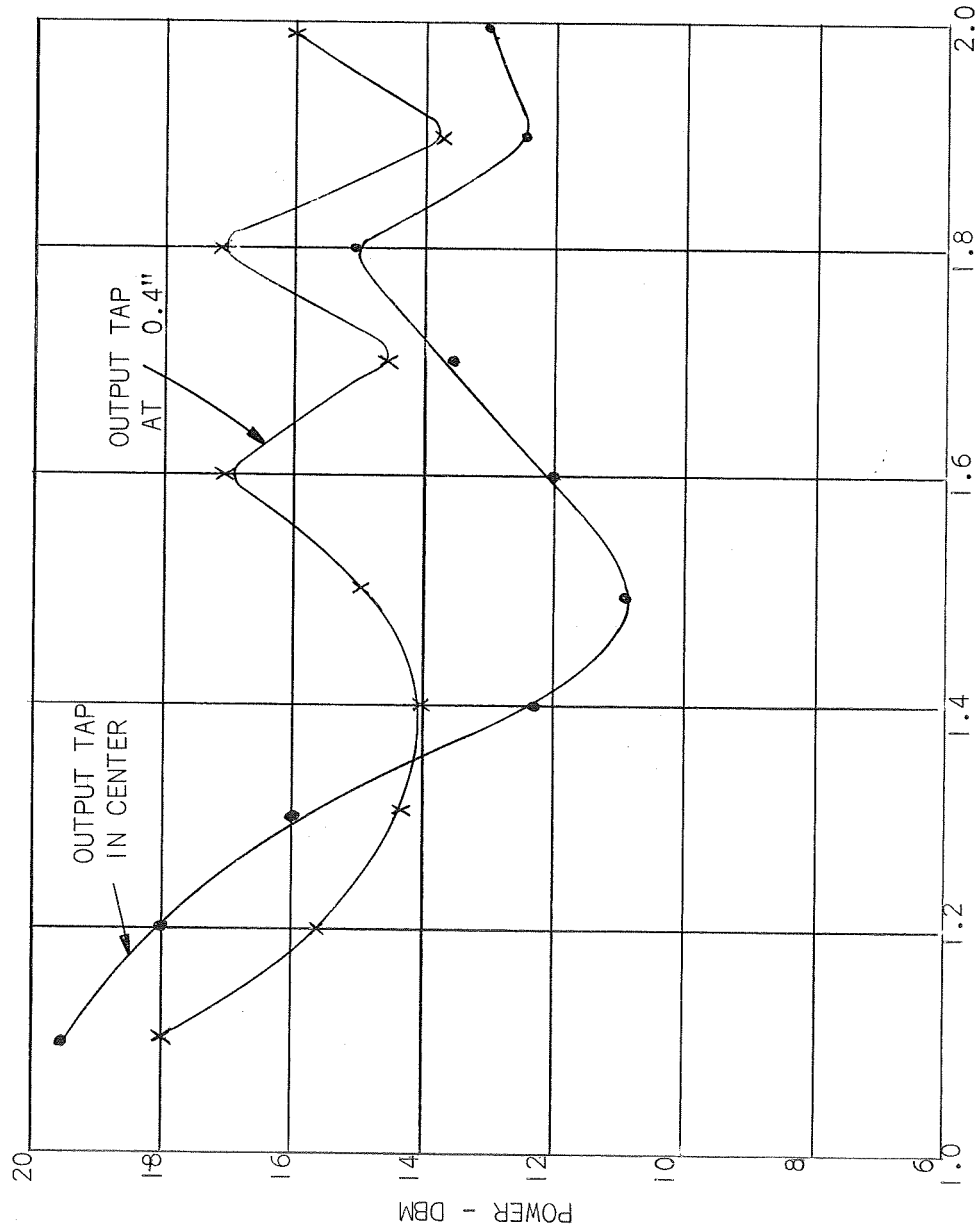

TYPICAL VARIATIONS IN OUTPUT POWER FOR TWO TAP POSITIONS

FIGURE 5-13

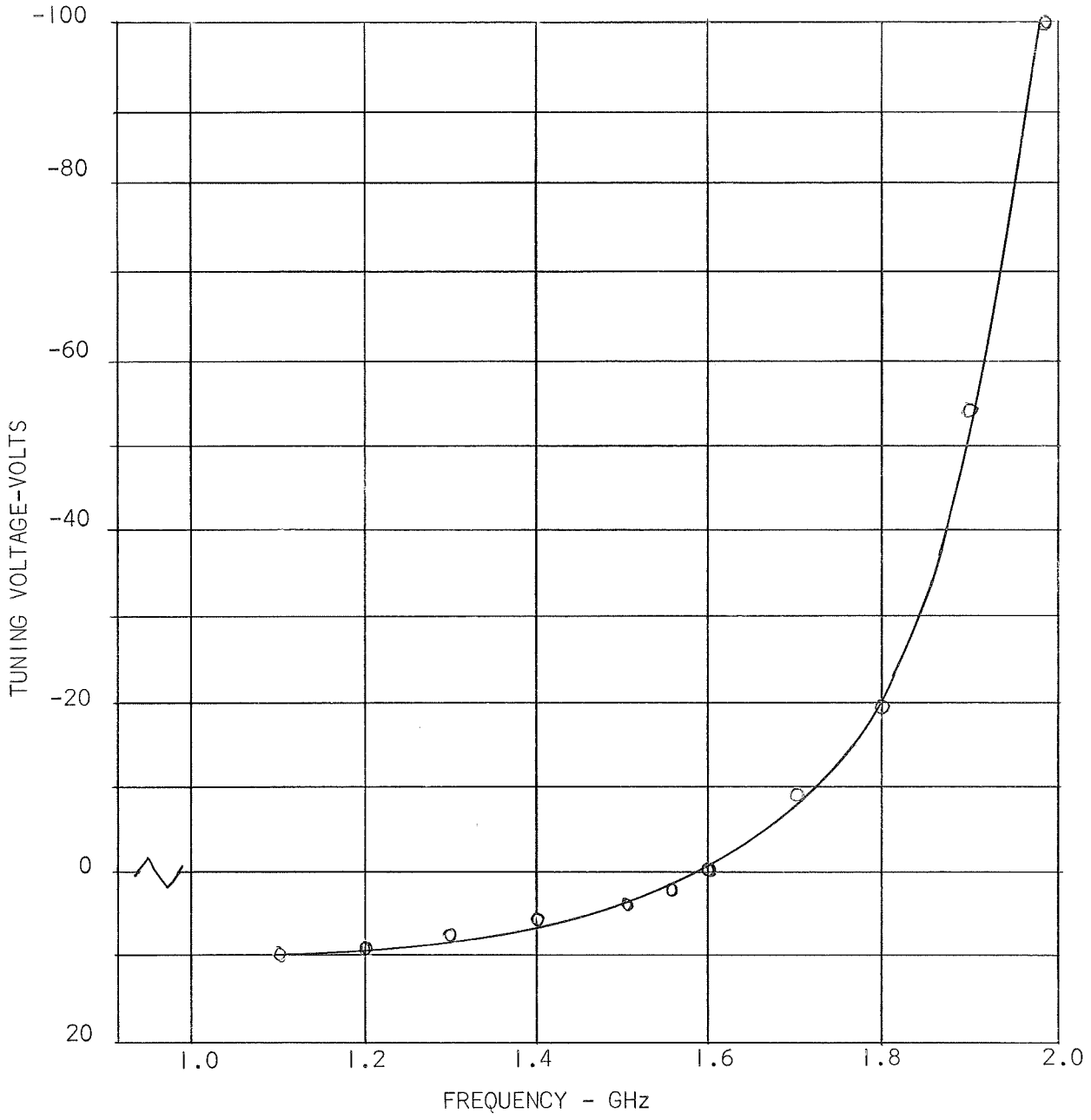

OSCILLATOR TUNING CURVE

FIGURE 5-14

Specifications (Con't)

Spurious Oscillation

Ratio of Signal to 2nd Harmonic Output	30 dB
Ratio of Signal to all other Spurious Outputs	60 dB
Output Impedance	50 ohms
Sensitivity to Supply Voltage	0.3 MHz/v
Residual FM, Peak to Peak	5 KHz
Frequency Drift, -30°C to +65°C	5 MHz
Pulling Figure, VSWR 1.5:1 at any phase	5 MHz

5.3.2 RF Cables

A large number of designs of flexible coaxial cables are now available for RF use. High frequency cables have the common feature of a solid dielectric of stabilized polyethylene separating the inner and outer conductors. The inner conductor may be solid or stranded, and is usually copper. The outer conductor is a single or double layer of braid, usually copper, which may or may not be tinned. The outer protective cover is usually vinyl, and in some cases armored for additional protection.

At low frequencies, the attenuation in a cable is primarily the result of conductor losses; and, therefore, increases as the square root of the frequency. Dielectric losses increase linearly with the frequency, and become increasingly important at high frequencies. When these losses are appreciable, the cable attenuation is highly sensitive to frequency. Consequently, the cabling required for instrumenting a system should be minimized to avoid excessive power loss.

Experience has shown that repeated flexing of RF cables may cause the center conductor to shift in the dielectric insulating material, causing variations in the characteristic impedance of the cable. The use of armored cables, with mechanical supports, is recommended to prevent this occurrence.

Cables used in the RF system should have low attenuation characteristics as well as low VSWR ratings. The use of semi-rigid cable in the system

will insure that additional modes will not be generated due to the movement of the cable. Specifications for the proposed cables are given below:

Mechanical	
Outer Conductor Diameter	0.141"
Inner Conductor Diameter	0.036"
Minimum Bending Radius	0.125"
Electrical	
Characteristic Impedance	50 ohms
Capacitance	30 pF/ft
VSWR	1.05 or less @ 0-106 Hz
Attenuation	11.5 dB/100 ft @ 1 GHz. 21.1 dB/100 ft @ 3 GHz.

5.3.3 Circulator

A circulator is a ferrite device with more than two terminals with a characteristic that the input to the Nth port appears as the output from the (Nth + 1) port, and theoretically gives a zero output from any other port. A circulator can be used in the measurement of the reflected RF energy that is not transmitted or coupled into a termination. For the proposed systems, the circulator will be used to isolate the RF input from the output, and to pass the reflected power as shown in Figure 5-15.

5.3.4 Probes

The radio frequency probe, or antenna, is used as a means of coupling energy into and out of the tank or cavity. Basically, the possible antenna configurations are of two types, the loop and the monopole.

The monopole antenna is best suited for coupling electric fields into a cavity. To provide electric field coupling, the center conductor of a coaxial cable is extended, as a probe, into the cavity and will couple to

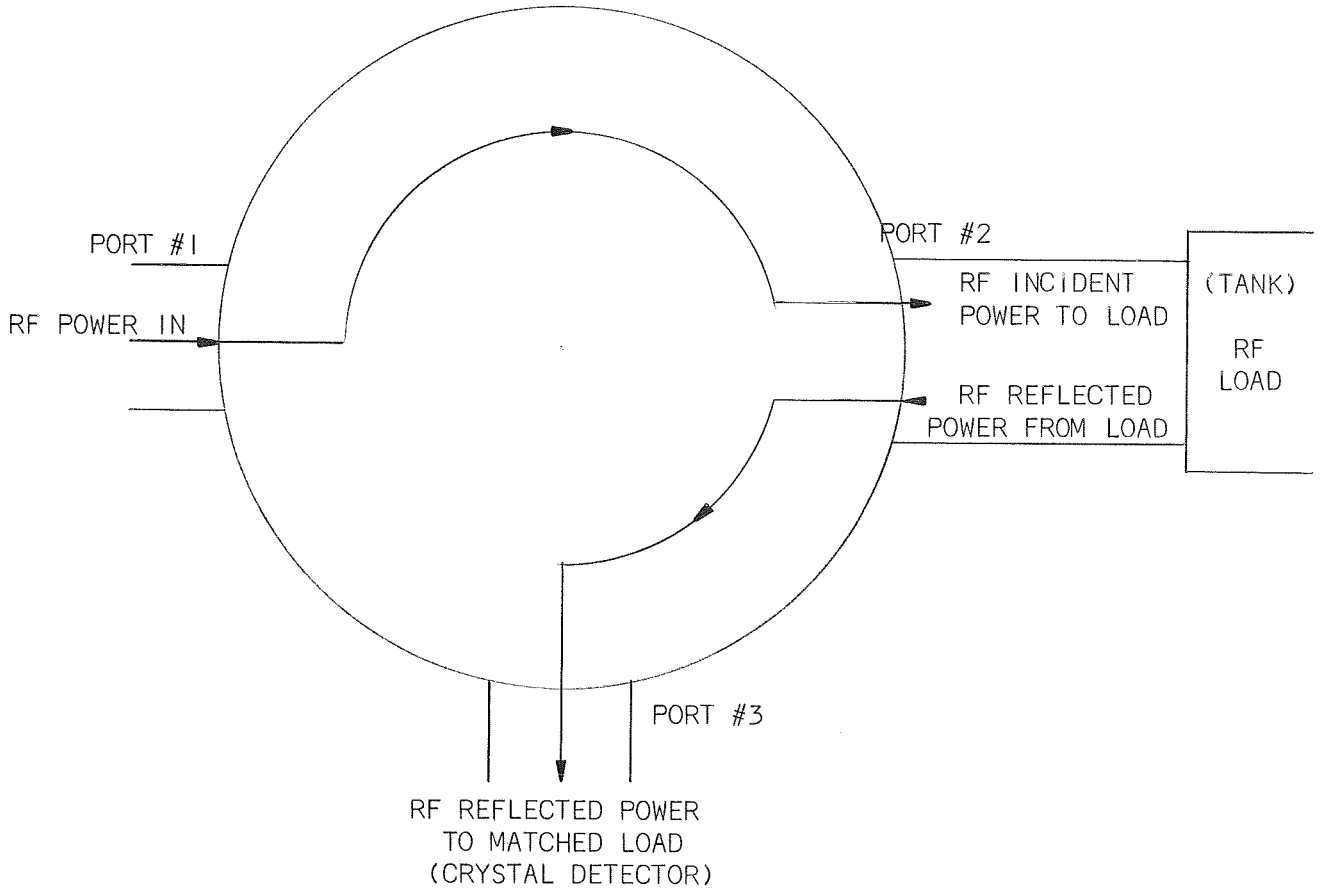

BASIC CIRCULATOR

FIGURE 5-15

the cavity if it is orientated with a component of the electric field within the cavity. In coupling to a cavity with a monopole, the electric field of a mode terminates on the probe, inducing a current in it. Conversely, a voltage applied to the probe produces electric fields inside the cavity that may excite oscillations. This is a form of capacitance coupling, the magnitude of which is determined by: 1) The surface that the monopole exposes to the electric field, and 2) The intensity of the electric field at the position of the probe in the cavity. Thus, (for example) the maximum coupling is obtained in a cylindrical cavity operating in the TM_{010} mode when the excitation probe is located on the end plates of the cylinder. However, the coupling to this mode will be zero if the probe projects into the cavity from the side wall instead of the end wall.

Magnetic coupling to the cavity (tank) may be provided by terminating the center conductor of a coaxial cable in a loop so that magnetic flux within the cavity will be coupled to the cable. A current passing through such a loop will excite oscillations within the tank. Conversely, oscillations within the tank will induce a voltage in the coupling loop. The magnitude of the coupling can be readily controlled by the orientation of the loop and its location with respect to the magnetic field.

From the above discussion, it can be seen that the location, type and length of antenna used in the RF gaging system is important. The probe and cable could be made to be compatible with the fuels and the pressure and temperature environment within the tanks by proper selection of materials and method of instruction. The probe will be protected by a teflon radome housing so that only the far field of the probe is affected by the material within the tank.

5.3.5 RF Signal Detector

Detection of the RF energy coupled through a tank is accomplished through the use of a crystal or diode detector. Detection of RF energy is accomplished by recovering from a modulated wave, a voltage or current which varies in accordance with the modulation present on the wave.

Detection of amplitude-modulated waves is ordinarily accomplished by means of a diode rectifier. A simple circuit for a diode detector is shown in Figure 5-16.

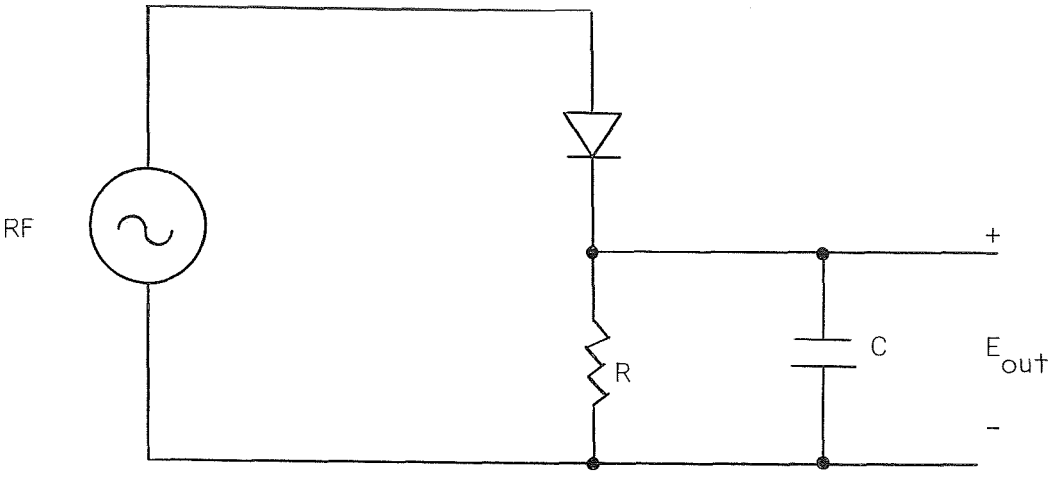

DIODE DETECTOR CIRCUIT

FIGURE 5-16

At each positive peak of excited voltage, the capacitor charges up to a potential equal to the peak of applied voltage. Between peaks, the charge in the capacitor discharges through resistor R. The result is that the detector follows the envelope of the RF signal produced by the tank. At frequencies above 1,000 MHz, a silicon crystal diode rectifier (crystal detector) is most commonly used.

The RF signal detector that will be used will be a low-power crystal detector. It will have a signal-to-noise ratio of approximately 60 dB. The specifications for a suitable crystal detector are shown below:

Maximum input	100 milliwatts peak or average
Impedance	50 ohms
VSWR	1.2: 1 maximum
Frequency Response	$\pm$ 0.2 dB maximum
Frequency Range	1.0 GHz to 2.0 GHz
Sensitivity	0.4 µV/µW minimum
Dynamic Range	40 dB
Square Law	$\pm$ 0.5 dB variation from square law up to 50 mV peak
Detector Element	Diode

SECTION VI

CONCLUSIONS

The basic program covered herein was set up to evaluate the feasibility of using the RF technique to measure the mass content of the SPS tanks in the LEM System, and to relate the results of this study to other similar applications. On the basis of the theoretical predictions, experimental data and hardware study, given earlier in this report, the following conclusions can be made:

1) An electromagnetic field can set up within the tank for all conditions of propellant filling and distribution which is uniformly influenced by the presence of the propellant. The non-uniformity is less than ± 0.5% of the measurement range.

2) Three RF-based mass measurement techniques can be postulated, using this uniform-illumination theory.

3) Sensitivities of greater than ± 0.1% could be realized using Technique A for propellant loadings of up to 10%. However, in Technique A, the sensitivity of the measurement parameter is limited as propellant content is increased for propellants, such as Aerozine 50 and MMH.

   The sensitivity of the measurement parameter is not similarly limited if Techniques B and C are used. Basic sensitivities of ± 0.1% are theoretically possible, using these techniques. The sensitivity of the proposed systems for a given propellant, will be dependent on the tank content.

4) The accuracy of the three techniques is limited by the non-uniformity of the influence of the propellant on the electromagnetic field and the sensitivity of the measured parameter. The non-uniformity is essentially constant over the entire loading range for all propellants while the sensitivity is a decreasing function of loading. The overall result is an accuracy which decreases with increased loading for all propellants. Technique C shows the most promise of meeting the ± 0.5% accuracy goal with all propellants, while Techniques A and B could have an inaccuracy less than ± 0.5% for a low tank content, but not for a high tank content.

5) The maximum response time for a gaging system operating on each of the three techniques explored can be 0.2 second or less. Sweep sources for tank excitation and signal processing components are available which can provide a measurement in less than 0.2 second.

6) The system can be made compatible with the Apollo or LEM propellants; N_2O_4-Oxidizer, Aerozine 50 and MMH fuels.

7) Installation of the proposed gaging systems into propulsion system tanks will require minimal modification of existing tank structures. This installation will consist of a probe which can be mounted through the tank walls or on the center stand pipe.

8) Gaging system accuracy can be maintained independent of tank pressure. Temperature effects on the fuels can be compensated for in the gaging system design.

9) Theoretically, the vibration and acceleration goals should be met by such a gaging system, but they were not verified experimentally.

10) The maximum system weight should be below 20 pounds, exclusive of cabling, with the use of transistorized microwave sources and integrated circuits in the data processor.

11) The system power requirements can meet the 28 volts, 1 ampere, continuous current with limited 5-second, 5-ampere current surge requirements.

12) The system output can be made available as parallel and serial binary signals, or 0 - 5 VDC analog.

13) The system can be adapted to a variety of tanks because of the ability of the RF technique to uniformly illuminate tanks of arbitrary geometrical shape.

14) The systems are capable of providing mass gaging for a quantity of separate tanks. A minimum of additional hardware would be needed to cover more than one tank if the other tanks are similar to the first.

15) The dielectric properties of the propellants are not satisfactorily known over the frequency range of interest. A method is available to make the necessary measurements, and a program to measure these properties should be followed to assure adequate gaging system design.

SECTION VII

RECOMMENDATIONS

7.1 INTRODUCTION

On the basis of the study program accomplished by Bendix, the use of Radio Frequency techniques to gage propellant mass aboard orbiting space vehicles has been proven feasible. The Bendix Corporation recommends that a hardware development program be initiated, which will result in the implementation of Technique C as a breadboard system.

The development of a breadboard system is recommended in order to assure that a physically realizable RF Gaging System can be implemented. Although subassemblies have been fabricated and tested during the feasibility study, a complete system has not been fabricated. Fabrication and test of a complete breadboard system will allow adequate definition of a flight prototype, and will provide a test bed for the solution of any unforeseen problem areas.

7.2 HARDWARE DEVELOPMENT PROGRAM

The following tasks are recommended in order to provide further development of a RF Gaging System for orbiting space vehicles:

Task I - DESIGN BREADBOARD SYSTEM

The design of a breadboard RF Gaging System will be based on the design parameters established from the feasibility study. The breadboard system will use all of the components, or their functional equivalent, required for a prototype system. The breadboard system will not include packaging to a final configuration; however, it will be packaged to a level sufficient to allow testing with scale model propellant tanks. The following tasks will be performed in the design phase:

a) Design

The tank probes, electronic circuits, mechanical parts, and interconnecting elements required for signal conditioning and data processing will be designed. Any mechanical parts required for the system will be selected to meet the environmental requirements. Special attention to compatibility requirements will be given to any components which will come into contact with the propellant. All mounting hardware required will be defined.

b) Propellant Measurements

The Roberts-Von Hippel technique should be perfected for measuring the properties of liquids such as glycol, benzene, etc., before being applied to the propellants in question. The properties of the propellants N_2O_4, Aerozine 50 and MMH should then be measured over the frequency range of interest. This should include the determination of the effects of temperature on the propellants in order to decide whether temperature compensation methods are needed for the gaging systems.

c) Theoretical & Experimental Studies

Further study will be made to better define the theoretical basis for Technique C as a means of mass measurement with respect to the propellants in question. Experiments, up to date, have not indicated any further problems besides the liquid effect on the antenna. The theoretical study should also be used to determine whether any major hardware problems will be encountered in implementing the techniques. Methods of overcoming these problems will be outlined which may be evaluated by experimentation.

Task 2 - FABRICATE EXPERIMENTAL HARDWARE

On the basis of the design studies, the necessary hardware will be fabricated for experimentation. These experiments will be conducted in order to verify the system characteristics predicted by the design studies. These characteristics would include sensitivity, accuracy and response time under the expected environmental conditions. These experiments will be conducted with and without tank internal perturbations in order to study their effect on the accuracy and sensitivity of Technique C.

Task 3 - EVALUATE SIGNAL PROCESSING DESIGN

The electronic means of signal processing necessary to achieve a mass readout will be evaluated on the basis of system accuracy and sensitivity. Invariance to propellant position will be verified by experimentation with scale model propellant tanks.

Task 4 - SPECIFY SYSTEM COMPONENTS

A specification of the system components required for a total mass gaging system will be made. This specification will include system operational characteristics relative to the worst tank, propellant and environmental conditions. Components will be chosen that are suitable for flight hardware.

SECTION VIII

REFERENCES

1. Bell Aerosystems Company, Storable Propellant - Data for the Titan II Program, Air Force Ballistic Systems Division, Report No. AFBSO-TR-61-351, November, 1961.

2. Aerojet-General Corporation, Storable Liquid Propellants; Nitrogen Tetroxide/ Aerozine-50, Liquid Rocket Plant, Report LRP 198, 2nd Edition, 1962.

3. Meirbachtol, C. J., and Burns, G.A., Electrical Properties of Propellants at Radio Frequencies as Required for RF Resonance Propellant Gaging, Technical Report, AFFDL-TR-40, Air Force Flight Dynamics Laboratory, Research and Technology Division, Air Force Systems Command, Wright-Patterson Air Force Base, Ohio, April, 1966.

4. Montgomery, C. J., Technique of Microwave Measurements, Boston Technical Press, Inc., Lexington, Mass. 02173, 1964.

5. Roberts, S., and Von Hippel, A., Journal of Applied Physics 17,610, 1946. 66

6. Von Hippel, A., Dielectric Materials and Applications, The M.I.T. Press, Cambridge, Massachusetts, August, 1966.

7. Harrington, R.F., Time Harmonic Electromagnetic Fields, McGraw-Hill Book Co., New York, New York, 1961.

8. Smyth, C. P., Dielectric Behavior and Structure, McGraw-Hill Book Co., New York, New York, 1955.

9. Johnson, Field and Wave Electrodynamics, McGraw-Hill Book Co., Chapter 6.

10. Atwater, Introduction to Microwave Theory, McGraw-Hill Book Co., Chapter 1, 5.

11. Jackson, Wiley, Classical Electrodynamics, Chapter 8.

12. Moreno, T., Microwave Transmission Design Data, Dover Publications, New York, 1958.

13. VanBladel, Electromagnetic Fields, McGraw-Hill Book Co., Chapter 14.